HYBRID IMAGING GUIDANCE SYSTEM FOR BIOPSY OF THE BREAST

by

Cameron A. Piron

A thesis submitted in conformity with the requirements
for the degree of Master of Science,
Graduate Department of Medical Biophysics
University of Toronto

Hybrid Imaging Guidance System For Biopsy of the Breast

Cameron Piron
Masters of Science 2001
Department of Medical Biophysics
University of Toronto

Abstract

A novel system for obtaining biopsy samples of lesions detected using contrast-enhanced magnetic resonance imaging (MRI) is presented. Contrast-enhanced MRI is used to detect the lesion, while the real-time ultrasound information is used to monitor the progression of a biopsy needle into the lesion. By accurately registering these two imaging modalities, the high sensitivity of MRI and real-time imaging capabilities of ultrasound are combined to improve the accuracy of lesion biopsy.

The accuracy of this system and implementation of the biopsy techniques in pre-clinical trials are presented in this thesis. Targeting experiments were performed to evaluate the accuracy of MR-guided needle positioning and US image registration. Tissue-equivalent phantom experiments were performed to test the accuracy of the system in a more realistic model of a lesion within breast tissue. It was determined that the addition of ultrasound to guide needle placement provided substantial benefit in accuracy over MR-guided biopsy alone.

Acknowledgments

I would like to thank the many people who have inspired, encouraged, and assisted me during my graduate work.

I would like to first thank my supervisor, Dr. Don Plewes, for challenging me and allowing me to grow within this department. He has encouraged me to look at things from different perspectives and to use those perspectives to solve problems in novel ways. I would also like to thank the members of my supervisory committee for their guidance and countless suggestions to which I am indebted.

I would further like to thank Dr. Rene Shumak for her patience, direction, trust and inspiration during the development of this work. She has been essential in bringing this research from the lab to the clinic and has inspired me to venture further into a career in medicine.

I would like to thank the fellow members of the Plewes' team, and my fellow graduate students for their assistance and friendship.

Finally, I would like to thank my mother, father and sister who were a constant source of love and support. Your belief in me made a world of difference.

Table of Contents

List of Figures

List of Tables

Chapter 1

Introduction

1.1 Motivation

Early detection of breast cancer is critical for successful treatment and survival [1,2]. Currently, x-ray mammography is the primary imaging modality used to detect breast cancer [3]. Mammography has proven to be successful in the general population, but it is less effective in woman with dense breasts [4]. The development of a new breast imaging technique, contrast-enhanced magnetic resonance imaging (MRI), has proven to be a very sensitive imaging tool for breast cancer detection, which is not limited in dense breasts [5,6]. This technique has demonstrated the capability to detect lesions that are occult to traditional imaging modalities in various clinical trials throughout the world [7,8,9,10,11]. Wide application has been hampered by the lack of a compatible and accurate biopsy system. Such a biopsy system is necessary to obtain tissue samples to confirm the malignancy status of lesions detected with MRI.

In this thesis, a novel technique to biopsy lesions detected using MRI and occult to other screening modalities is presented. Although many groups have developed functioning MRI biopsy systems, there still remain many unresolved issues. The approach explained in this thesis, merges MRI and ultrasound (US) in an attempt to solve the problems encountered with current biopsy systems.

1.2 Breast Cancer in the Population

In Western society, breast cancer is the most frequent cancer occurring in women, and second only to lung cancer in mortality. It is responsible for an estimated 5,500 deaths each year in Canada, and 43,700 in the United States [12,13]. Incidence of breast cancer has been increasing over the last 10 years, but the death rate has reduced. This has been primarily attributed to the successful early detection of breast cancer in women and subsequent treatment of the disease [13].

The advent of genetic testing has resulted in the identification of the breast cancer susceptibility genes BRCA1 and BRCA2. It has been shown that lifetime risk of developing breast cancer is 80-90% and 60-80% in these respective mutation carrier populations [14,15,16]. These incidence rates are exceptionally high relative to the general population lifetime risk of 11% [13]. Furthermore, the mutation carriers have been shown to develop breast cancer at a younger age relative to the normal population [17]. Providing a breast-screening program to detect cancer in this population of women can potentially reduce their breast cancer mortality rates substantially [1,2]. Mammography has been demonstrated to be an ineffective screening modality for these women [11]. This is believed to be due to the limited effectiveness of this modality in the denser breasts associated with this younger population [2,18].

1.3 Treatment

Breast cancer that is detected at an early enough stage can be successfully managed with current treatment strategies [19]. These cancers are treated using various methods including surgery, radiotherapy, chemotherapy, and hormone therapy, with usually two or more in conjunction [20]. Current trends towards reduced patient morbidity have promoted breast conservation strategies such as lumpectomy or partial mastectomy. Systemic therapy after surgical and radiation therapy such as chemotherapy and hormonal therapy are used if the tumour type indicates a chance of recurrence [20]. Continuing improvement in the treatment of breast cancer depends on effective

detection techniques and accurate classification of the tumour type. The detection of a small tumour in the biologically active breast of a young woman is a daunting task.

1.4 Breast Biology

1.4.1 Breast Anatomy

In the simplest of terms, the breast is a highly differentiated sweat gland, which has evolved to produce and secrete milk during lactation. It is composed of a varying mixture of fatty tissue, glandular components, lymphatic and blood vessels. The glandular tissue or "parenchyma" consists of between 15 to 20 ductular units, which radiate from the nipple. Each of these units consists of a large duct that branches out to form lobules. One can think of each of these ductular units as a bunch of grapes. The grapes or lobules consist of terminal ducts and their supportive tissue. The stems of the bunch consist of subsegmental and segmental ducts, which empty into the sinus behind the nipple. The terminal ducts form into the terminal duct lobular units (TDLU), which are the most biologically active components of the breast. These units are responsible for milk production, are often the sites of breast carcinomas. These components are demonstrated in Figure 1.1 [21,22].

1.4.2 Progression of Breast Cancer

Each duct in the TDLU has a lining of mammary epithelium, which is composed of an inner layer of epithelial cells and an outer myoepithelial layer. The majority of breast neoplasms occur in the epithelial cells of the TDLU's. The process starts with epithelial hyperplasia, or increase in the number of cells. This is typically a normal process that is related to hormonal changes in the breast, but it may progress to atypical hyperplasia, which is an abnormal overgrowth of cells. At this stage it is believed that the movement towards a cancerous condition is still reversible. The next step is the development into carcinoma-in-situ, which is considered a proliferative neoplasm which remains confined to the ducts. This stage is considered irreversible and is capable of progressing to be infiltrating or invasive carcinoma. When the cancer breaks out of the ductal

walls and invades the lymph and stroma of the breast, it is classified as infiltrating duct carcinoma. The most common type of mammary carcinoma is infiltrating ductal carcinoma (approximately 72% of total types), while the related version, in which the lesion originates in the intralobular ducts is infiltrating lobular carcinoma (12%) [23][24].

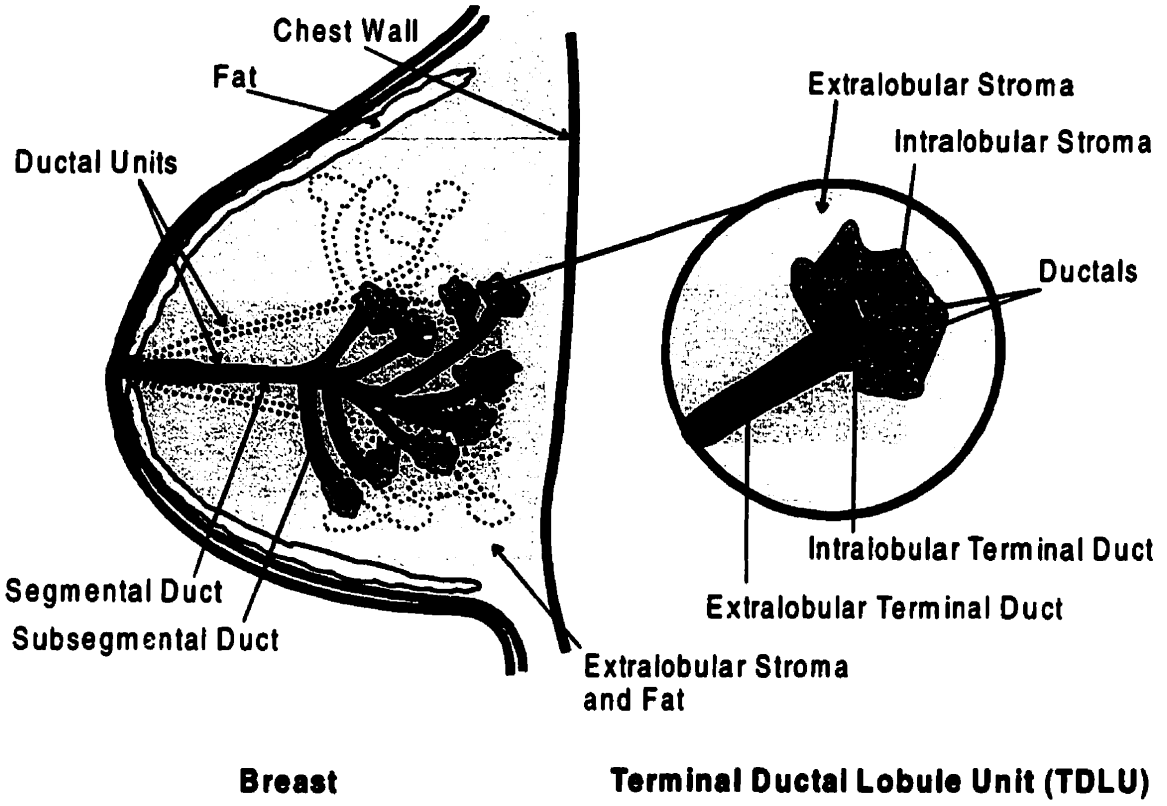

Figure 1.1: Anatomy of the Female Breast. The diagram on the left demonstrates the ductal units radiating from the nipple. The structure is often said to resemble a bunch of grapes, with the lobules of the breast described as the grapes. The ducts of the breast terminate in the lobules, and form the terminal ductal lobules units as demonstrated in the diagram on the right at a greater scale.

Tumour growth is strongly dependent on angiogenesis for delivery of nutrients and oxygen required for cell proliferation [25]. The degree of angiogenesis and extent of tumour vascularity play a role in the aggressiveness of early breast cancer [26]. In general, malignant lesions in a breast take on a very different pathological form from benign lesions. As a basic guideline, malignant tumours tend to be dense due to epithelial cell and fibroglandular overgrowth, and exhibit indistinct shape and heterogeneity due to stromal invasion. These tumours further differ

from surrounding healthy tissue based on the increased permeability and density of capillaries due to tumour angiogenesis [21,27]. It is on this basis of differing neovascularization and angiogenesis in particular, that MRI is capable of imaging tumours [28].

1.5 Breast Cancer Detection

As mentioned previously, the success of breast cancer treatment depends on detection of cancer at the earliest stage. The method of detection used can range widely from self-examination of the breast to the application of advanced imaging technology. Historically, self, and clinical examination of the breast were the standard breast tumour detection technique. The increased density of the tumour relative to the surrounding breast tissue allows detection by simple palpation. This technique is a cheap and reliable method, but it can only detect tumours at advanced stages and it is not effective in breasts with large amounts of dense parenchyma. Medical imaging is now routinely used and has provided substantial benefit in detection of non-palpable breast tumours. This was demonstrated with an initial study done by the Health Insurance Plan of New York (HIP) conducted from 1960 to 1970, which compared the effectiveness of mammography to physical examination. The results showed a 40% reduction in mortality for women in the 50-year old age group with the use of screening mammography [29]. Since that study, various imaging technologies have been developed and are applied to address two clinical breast cancer detection problems:

- *screening* of asymptomatic patients
- *diagnostic* imaging of patients with suspicious findings

The function of screening is detection of lesions in asymptomatic women, in the hope of detecting cancerous lesions at their earliest stage. The role of diagnostic imaging is somewhat different. Lesions that are detected by screening modalities, or indicated by suspicious clinical findings, require an imaging procedure designed to determine whether the lesion is cancerous or benign. The detection and diagnosis of lesions is currently done using three fundamental imaging modalities:

- mammography
- ultrasound (US)
- contrast-enhanced magnetic resonance imaging (MRI)

1.5.1 Mammography

The primary imaging modality used for breast cancer screening is mammography. The application of this imaging technique requires the breast to be rigorously compressed and positioned in an orientation allowing craniocaudal or mediolateral views. The signal variations in a mammogram arise from differences in the relative amount of X-ray attenuation in different tissues in the breast [30].

The radiographically dense parenchyma of the breast appears as a region of bright signal while the less attenuating fat appears dark. The lesions are identified in mammograms due to their increased attenuation and elevated brightness relative to the surrounding glandular tissue. Detected lesions can be determined to be malignant or benign based upon their borders and architectural features. Very small calcifications have been found to be indicative of breast lesions. These micro-calcifications form when calcium precipitates from the secretions of the breast in areas of breast epithelial pathology [22].

Mammography has a sensitivity of detecting breast cancer estimated to be between 80-90% in the general North American population [31,32,33]. Although mammography has a high sensitivity in older women, it has been found to have sensitivity as low as 54% in women younger than 40 years [4,33]. These younger women tend to have denser breasts where lesions can often be obscured by the large amount fibroglandular tissue, which appears bright on mammograms. Recent technological advancements such as digital mammography are designed to improve lesion visualization in these regions of dense tissue [34].

1.5.2 Breast Ultrasound

The ability of ultrasound to obtain good image soft tissue contrast has made it a valuable technology for breast cancer detection. It is generally agreed upon that major roles for ultrasound breast imaging are for the differentiation of malignant and benign lesions, detection of lesions in dense breasts, evaluation of lesions inaccessible to mammography and as a guide for interventional procedures [35]. The following sections describe the basic principals of ultrasound image formation and the clinical application of ultrasound for breast cancer detection to a level necessary to comprehend the issues discussed in this thesis.

1.5.2.1 US Imaging

Ultrasound imaging is able to differentiate soft tissue based upon acoustical properties. The "pulse-echo" principal allows these properties to be probed by emitting short pulses of ultrasound energy into tissue and detecting an echo a short time later. These pulses reflect back to the transducer a short period of time after acoustical interactions with the tissue as demonstrated in Figure 1.2. The lapse of time until detection of echo indicates the depth from which it came and the amplitude of the echo indicates the degree of physical difference between two tissues at that point.

The tissue property effecting the propagation of an acoustical wave is the tissue acoustical impedance. The acoustical impedance (Z) is a mechanical property defined by the product of the density (ρ) and the speed of sound (c) through that material (Equation 1.1).

$$Z = c\rho \tag{1.1}$$

Generally, variations in the acoustical impedance are due to changes in the compressibility, or stiffness of the tissue. The speed of sound through a tissue is a function of its bulk modulus (B) and equilibrium density (ρ_o) (Equation 1.2).

$$c = \sqrt{\frac{B}{\rho_o}} \tag{1.2}$$

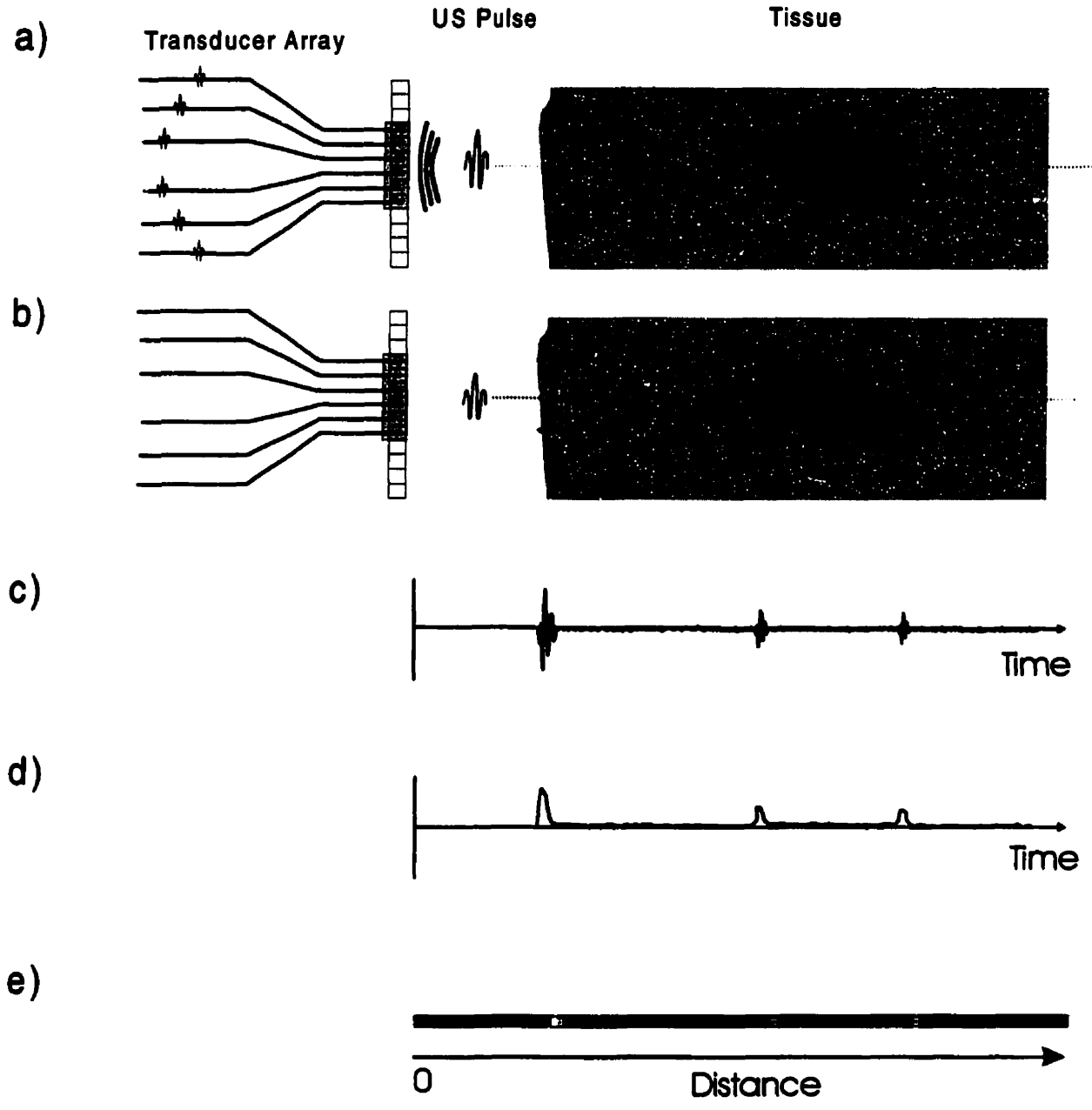

Figure 1.2: Ultrasound Image Formation. a) An ultrasound waveform is generated by phased activation of a set of 6 transducer elements. This pulse is focused into the tissue b) The pulse interacts at the tissue interfaces producing echoes c) these echoes return to the transducer where they are detected and converted into an electrical signal d) envelope detection of this signal is performed e) each detected echo is converted into a pixel intensity forming an A-scan image.

The speed of sound typically only varies by a few percent for most soft tissues, which is an important assumption used to determine the echo time of flight. This information is then used to determine the depth at which an echo was generated. In breast tissue however, the variation

between the speed of sound in the two main constituents of the breast varies considerably [36]. This difference results in tissue interfaces appearing at distorted positions in the US image [37,38]. Ordinarily this issue is not a major concern in clinical US studies where the absolute position of structures in the image is of less importance than the relative position of structures, however in the scope of this thesis, consideration of this phenomena is relevant. This issue is addressed in greater detail throughout the progression of this thesis.

Acoustic waves interact with tissue exhibiting both attenuation and reflective properties. The attenuation due to absorption and scattering causes the beam to lose energy as it moves through the tissue. The amount of attenuation of the ultrasound beam is frequency dependent resulting in a reduction of the beam intensity exponentially with depth [38]. Reflection of the ultrasound beam back to the transducer occurs when the beam hits a discontinuity in the interface between tissues with different acoustical impedance. A wave incident to an interface of acoustic impedance mismatch will reflect a portion of energy, and transmit the rest. If the angle of incidence of the echo is equal to zero, then the echo will reflect back to the transducer. When there is a variation in acoustical impedance over an irregular interface then the echo will reflect back at various angles. The echoes that reflect back to the transducer give rise to a signal known as a scatter signal. In tissue with microscopic fluctuations in acoustical impedance, a small amount of the beam is scattered in all directions, giving rise to a backscatter signal. The backscatter signal is dependent on the wavelength of the ultrasound wave relative to the size of the scattering targets and, therefore, depends on the transducer frequency and the tissue imaged. Generally, the echoes resulting from specular reflections tend to be very strong and distinct, while the signals arising from backscatter tend to appear as a low-level distinct texture. This texture is due to the constructive and destructive interference created by summation of the reflected waves from the many scattering point sources. [39,40,41]

An ultrasound pulse is emitted into tissue and subsequently detected to create an ultrasound image using a transducer. The transducer converts an electrical signal into a mechanical vibration forming an ultrasound pulse. A number of separate transducer elements can be used in a linear one-dimensional array for the purpose linear array imaging. The principals for the formation of an

ultrasound image are shown in Figure 1.2. Here the individual array elements may be excited independently or in phase with one another. By timing the activation of subgroups of these elements, a wavefront can be generated. Depending on the timing of these elements, this wavefront can be focused at a particular depth, or steered in a particular direction. When a wave is generated, it will propagate through the tissue, reflecting at tissue interfaces and attenuating along the depth. The reflected signals will be detected by the transducer element and register as a radiofrequency signal. The peaks of this radiofrequency signal are detected, and by making assumptions about the speed of sound in the tissue the depth the interfaces can be calculated. This information can be displayed as a single line in which the echo strength is shown as pixel intensity. Imaging in this manner is known as A-scan imaging. If the array was shifted, this process is repeated and another A-scan line could be acquired. By repeating this process for different array positions or groups of transducer elements, a set of lines could be acquired to form a 2-dimensional image. This type of imaging is known as B-scan, or B-mode imaging. This 2-D image can be acquired many times per second resulting in "real-time" imaging. The ability to change the phasing of the transducer elements allows the flexibility of focusing the beam at many depths in the tissue. [39,40,41].

Shown in Figure 1.3 is a diagram of a linear array US transducer. The beam profile of an individual transducer element is illustrated, as well as the imaging volume of the entire transducer. The individual elements are pulsed as a phased array to scan in the transverse direction and focus at various depths in the axial direction [40]. The resolution of the ultrasound image in the three planes defined by the scan plane of the transducer, as seen in Figure 1.3, is defined by the frequency of the transducer, the length of the ultrasound pulse, the number of transducer elements and the focus of the transducer.

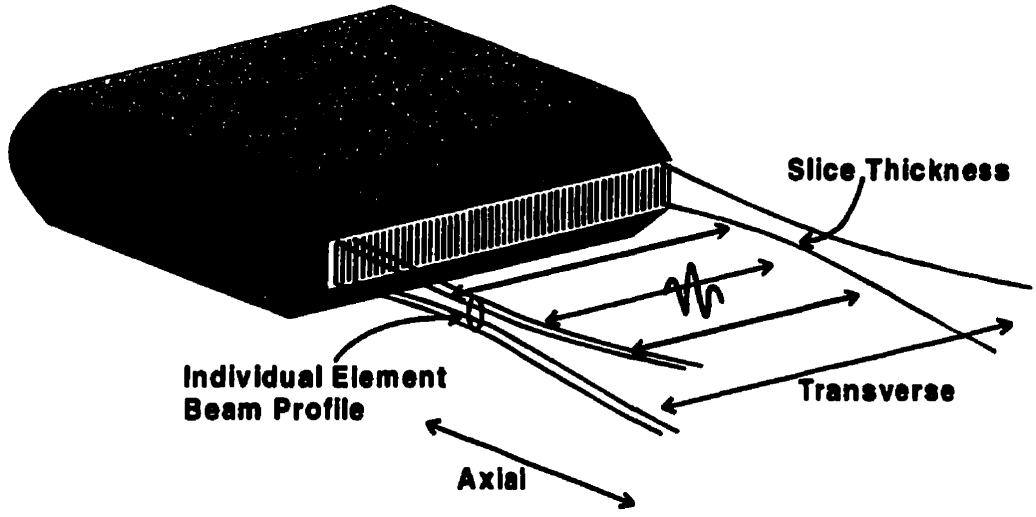

Figure 1.3: Linear array ultrasound transducer: An array of individual transducer elements operate as a phased-array to allow imaging over volume. The two imaging planes and imaging slice thickness are demonstrated relative to the transducer element face.

1.5.2.2 Clinical US Imaging

For breast imaging applications, a linear array transducer in the frequency range of 7.5-10.0 MHz is typically used. The imaging procedure is done with the patient in the semi-supine position with their breast compressed against their chest wall. This orientation enables access to all areas of the breast, as well as minimizing the amount of tissue imaged. The breast is imaged by moving the transducer in radial and anti-radial scans relative to the nipple following the ducts of the breast [43,44].

The anatomical components of the breast such as fat, parenchyma, ducts and blood vessels have characteristic ultrasonic features. Fat lobules (FL) appear slightly hypoechoic relative to the fibroglandular tissue (G) as seen in Figure 1.4 a) and b). The homogeneous structure of adipose tissue tends to generate little detectable scatter. The fibroglandular tissue appears homogeneously echoic compared to fat. This bright signal is due to the specular reflections generated at the many interfaces within the dense and heterogeneous glandular tissue and the inherent backscatter signal of the parenchyma. The interfaces between the fat and fibroglandular tissue also generate strong echoes due to specular reflection caused by their mismatching acoustic impedance. The

attenuation due to the two tissue types differs substantially; the fat tends to have a low attenuation whereas the fibroglandular tissue is highly attenuating [41].

1.5.2.3 Diagnostic Indicators

Ultrasound is most clinically useful for distinguishing cysts from solid lesions, and malignant lesions from benign lesions. It has been demonstrated that the echogenicity of the lesion, attenuation of the US beam, and morphology of the border are the primary indicators differentiating cysts from cancers. Cysts tend to appear hypoechoic, with little to no echogenicity [44]. They tend to demonstrate posterior enhancement with well-defined borders appearing round or oval in shape. The accuracy with which US can distinguish cysts from solid lesions has been reported to be 95-100% [43]. The use of certain sonographic features to classify lesions as either malignant or benign has been demonstrated to be accurate and may avoid biopsy of benign lesions, although it is a technique that is highly dependent on operator skill. One study determined the three most reliable criteria to characterize whether a lesion is malignant or benign are the appearance of the lesion borders, general shape of the lesion and width-to-height ratio [45]. Diagnosis made using these features would have increased the overall cancer biopsy yield from 23% to 39%. The most important predictors of benign or malignant tumour status are the borders of and shape of the mass. They differ in that malignant tumours tend to demonstrate irregular borders indicative of invasion of the surrounding stroma. Posterior shadowing and hypoechoic appearance of the lesion tend to be indications of malignancy [44,45,46]. This is clearly depicted in Figure 1.4 a and 1.4 b where an ultrasound image of a cyst is compared to a breast carcinoma.

Extensions to basic B-mode ultrasound imaging such as Doppler imaging and the use of microbubble contrast agents have demonstrated improved detection and specification of tumours in clinical studies. A full review of these technologies is found in Chapter 4.

The ability to image lesions in real-time and the option to use different imaging orientations are strengths of conventional US imaging. This thesis will explore a novel technique that exploits these strengths to achieve accurate breast biopsy samples.

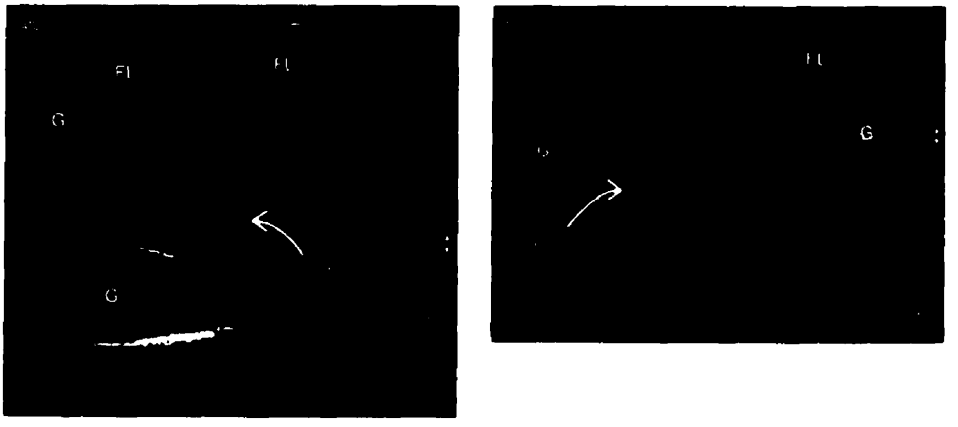

a) b)

Figure 1.4: Comparison of cyst and carcinoma in US images: a) Typical cyst with well defined border and posterior enhancement b) Invasive carcinoma as hypoechoic region demonstrating irregular shape, poor margins, and posterior shadowing. In both images fat lobules (FL) and fibroglandular tissue (G) are identified.

1.5.3 Contrast-Enhanced MRI

The first attempts to use MRI to detect breast cancer began in the mid 1980's [47,48,49]. The results from these studies were discouraging, finding that cancer could not be detected using the traditional T1 and T2 contrast mechanisms. It was not until later that same decade that the use of contrast agents provided a major breakthrough in breast MRI. Two groups in Germany discovered that paramagnetic contrast agents could be used to visualize the increased blood flow characteristics of breast tumours [10,50]. Since then many different groups around the world have implemented contrast-enhanced MRI of the breast for both screening and diagnostic purposes [3, 5-9,11,28,51,52-56]. The following sections describe the basic principals of MRI and its application to breast imaging only to a level necessary to understand the phenomena that are important in the context of the development of this thesis.

1.5.3.1 General Theory

Magnetic resonance imaging (MRI) is an imaging technique based on nuclear magnetic resonance (NMR). Atomic nuclei with an odd number of protons and/or neutrons possess a property known

as spin angular momentum S, or simply spin. Associated with this spin is a magnetic dipole moment, u. In biological tissues, the hydrogen proton (mainly found in H_2O) is the most abundant atom possessing this property. [1]

When these spins are placed in an external magnetic field (B_0) a fraction align with the magnetic field creating a net magnetic moment (M). This can be viewed as a classical ensemble average of the dipole moments, $M = \sum u$. Another effect of the magnetic field is that the nuclear spins act as spinning gyroscopes if perturbed from the longitudinal axis. They will precess about the longitudinal axis with a frequency known as the Larmor frequency. This frequency is related to the strength of the magnetic field through the Larmor equation:

$$w = \gamma B_o \tag{1.3}$$

This rotation about the longitudinal axis can be viewed classically as M precessing about the static magnetic field as a top rotates in a gravitational field. At a magnetic field strength of 1.5 T, the Larmor frequency for a hydrogen proton is approximately 63.9 MHz. In Figure 1.5, we see a representation of the magnetization vector (M) in a static magnetic field. The longitudinal component of the vector, or longitudinal magnetization (M_Z), and transverse component, or transverse magnetization (M_{XY}), are illustrated relative to the static magnetic field (B_o).

In order to measure the NMR signal from a sample, the magnetization vector must be tipped into the transverse plane. This is done using a pulsed electromagnetic field (B_1) applied at the Larmor frequency. The amount the vector is tipped depends on the strength and duration of the applied B_1 field. The magnetization vector in the transverse plane generates a time-varying magnetic field that can be detected by a receiver coil tuned to the Larmor frequency, as an induced voltage.

---

1 Material from this Section is drawn from "Introduction to Magnetic Resonance Imaging" by Nishimura [57] and "Magnetic Resonance Imaging", second edition by Stark and Bradley [58].

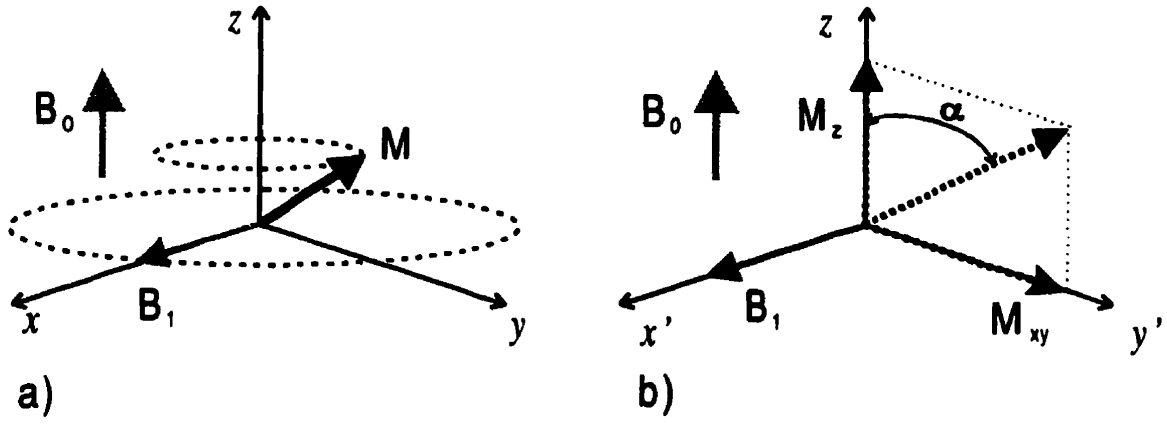

Figure 1.5: Orientation of M relative to B_0, B_1 and the defined axis: a) The application of B_1 causes the longitudinal magnetization, M to tip into the transverse plane where both vectors rotate at the Larmor frequency. b) With a rotating reference frame, (i.e. x'-y' plane rotating at the Larmor frequency), The M and B_1 are stationary. The transverse (M_Z) and longitudinal (M_{XY}) components of the magnetization as well as the tip angle (α) are demonstrated.

When the magnetization vector is initially tipped, all the dipole moments are coherent, or in-phase. As time progresses, two relaxation phenomenon occur which cause the decay of the transverse magnetization and the return of the longitudinal magnetization. The longitudinal relaxation is an exponential growth with a time constant T1 and is known as spin-lattice relaxation. The T1 relaxation mechanism involves the exchange of the energy absorbed by the nuclei and the surrounding lattice. The transverse relaxation is approximated as exponential decay with a time constant T2, and is known as spin-spin relaxation. The spin-spin relaxation results in non-reversible dephasing of the transverse magnetization resulting in signal loss. The T1 and T2 relaxation constants differ according to the tissue being imaged and its molecular environment. In most biological tissues the T1 values vary from 100-1500 ms, while T2 values range from 20-300 ms (at 1.5T). Differences in T1 and T2 values provide a major source of contrast in MR images.

In addition to the native T2 relaxation effects, variations in the magnetic field of the tissue environment are responsible for phase dispersion resulting in an apparently reduced T2. This effective T2, or T2* is responsible for rapid signal lose due to dephasing of the MR signal. Generating a spin echo can reduce this effect.

1.5.3.2 MR Imaging

The formation of a signal due to interactions of a spin, a static magnetic field, and excitation rf field is the fundamental mechanism for generation of the detectable MR signal. It is the goal of MR imaging to determine the positions of these signals over 3 dimensions and generate an image. Given a volume of spins within a static magnetic field, they will all precess at the same resonant frequency, w, and will produce a measurable signal, $S(t)$, in the transverse plane after application of a B_1 pulse given by:

$$S(t) = \int_x \int_y \int_z M_{xy}(x,y,z) e^{-iwt} dxdydz \tag{1.4}$$

From this received signal the spatial distribution of spins within this volume cannot be determined. A method to encode the spatial positions of the spins is accomplished using the resonant frequency dependence of the spins on the magnetic field strength. The use of linear gradients to superimpose a magnetic field on the main magnetic field results in the frequency of the spins being a function of spatial position as defined by:

$$w(x,y,z) = w_0 + \gamma(G_x x + G_y y + G_z z) \tag{1.5}$$

This spatial encoding strategy is accomplished with gradients in the x, y and z directions (G_x, G_y, G_z). These gradients can be turned on for various durations and amplitudes. For example, the magnetic field strength along the x-axis can be modified by the application of the G_x in a spatially dependent manner, such that the product $G_x x$ is added to the main magnetic field. If we were to include the effects of these gradients in Equation 1.4 and assume that we have only excited a single slice of the volume of spins restricting the signal to only the x and y direction, then we would have the following signal equation:

$$S(t) = \int_x \int_y M_{xy}(x,y) e^{-i2\pi[k_x(t)x + k_y(t)y]} dxdy \tag{1.6}$$

The $M_{XY}(r)$ is a function of the NMR parameters of proton density, T1and T2 tissue relaxation. The equation has been simplified by demodulating the signal by the Larmor frequency and we replacing the frequency terms with the spatial encoding parameters:

$$kx(t) = \frac{\gamma}{2\pi}\int_0^t Gx(\tau)d\tau \tag{1.7}$$

$$ky(t) = \frac{\gamma}{2\pi}\int_0^t Gy(\tau)d\tau \tag{1.8}$$

The form of the signal equation (Equation 1.7) shows the transverse magnetization signal as a set of discrete samples in 2D Fourier transform space, also known as k-space. The values for kx, ky in Equation 1.8 are the MR spatial encoding parameters. The transverse magnetization is sampled discretely using the gradients to "Fourier encode" the signals. Sampling of the correct frequency components results in filling the k-space for the region being imaged. The imaging problem becomes one of acquiring the complete set of signals from k-space to enable an inverse Fourier transform (Equation 1.7) to determine $M_{XY}(r)$. This is done by varying the strength and duration of the gradients so different k values can be obtained (Equation 1.8). The timing of the excitation pulses and the gradients form the basic components of the pulse sequences used in MRI.

In order to encode in three dimensions, a combination of gradient encoding schemes and selective slice excitation is used. The detectable MR signals arise from the transverse magnetization formed using either gradient echo, or spin echo techniques. These signals, or echoes are sampled digitally during the application of the frequency encode gradient (G_X). This gradient defines the location of the echoes in one dimension. The use of a phase encoding gradient (G_Y), allows determination of the location of the echoes in another dimension. By successively phase encoding a set of echoes, and sampling them during the frequency-encoding gradient, successive lines of k-space can be acquired. This is the basis for 2D MR imaging. The determination of the third dimension is defined by selective excitation of a slab of the imaging volume. By application of a slice selection gradient in concert with an excitation pulse, a thin slice of spins can be selected for imaging. A

pulse sequence timing diagram in Figure 1.6 demonstrates these spatial encoding principals for a gradient-echo sequence. The echo time (TE) and pulse repetition time (TR) are indicated on the pulse sequence. The echo time designates time from the initial rf excitation pulse to the detected echo, whereas the repetition time indicates the duration between successive rf excitation pulses. Modification of these pulse sequence parameters allows various aspects of contrast of the spin system to be elucidated. Various imaging strategies can be implemented to probe NMR properties of tissue using various pulse-sequences resulting in images with differing SNR, contrast mechanisms, and resolution.

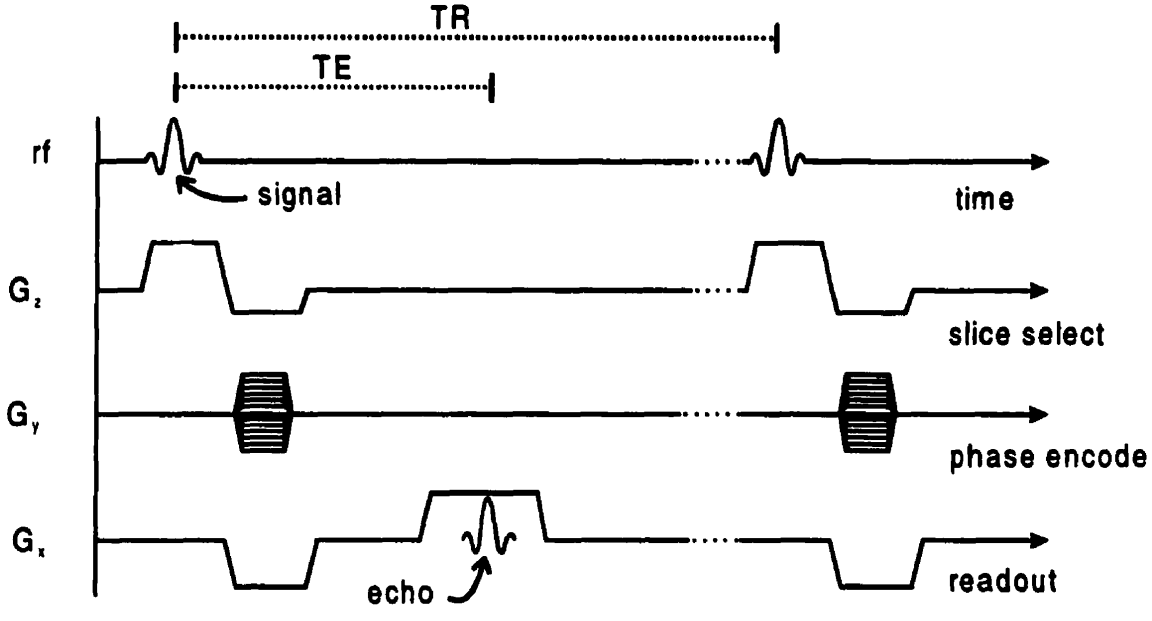

Figure 1.6: Pulse sequence diagram for gradient recalled echo (GRE) sequence. Typical values for TE and TR for a T1 weighted GRE sequence would typically range from 5-15 ms and 350-500 ms respectively.

1.5.3.3 Clinical Breast MR Imaging

The detection of breast cancer using MRI is based upon tumour angiogenesis. Tumour neo-vascularization and the associated increase in capillary permeability and leakage space can be used to differentiate tumours from normal breast parenchymal tissue [21,27,28]. These features can be probed with the use of contrast agents. The contrast agent used for breast imaging studies is an intravenously injected paramagnetic agent. Paramagnetism arises in atoms that have unpaired

electrons, which demonstrate significant net magnetization in an external magnetic field. Gadolinium is typically used due to its strong paramagnetic character [58].

After intravenous injection, gadolinium-based contrast agents distribute in the blood. Small contrast agent particles will leak through permeable sections of the capillary walls and distribute into the surrounding interstitial space. The contrast agent accumulates in tissues with rich, and highly permeable microvasculature. The gadolinium interacts with the water molecules in the interstitial space and within the microvasculature effectively shortening its T1 relaxation time constant. This reduction in T1 relaxation rate results in an increase in the associated MR signal. [10,58]

Breast cancers accumulate contrast agent more quickly than surrounding parenchyma tissue due to the tendency of tumours to have an increased number of vessels, expanded interstitial space and increased capillary permeability [10,50]. This leads to a time-dependent increase in the MRI signal of a cancer relative to the surrounding tissue. The dynamics of the MRI signal enhancement associated with a bolus injection of contrast agent usually enables differentiation of lesions and normal breast tissue. This enhancement as a function of time has been determined to be an important factor in the differentiation of malignant and benign lesions as will be discussed in Section 1.5.3.4.

One technique to capture the contrast enhancement of the breast over time, involves obtaining multiple, full volume MR images of the breast in concert with injection of contrast agent. Various imaging strategies are implemented in order to examine the contrast agent kinetics and morphology of the lesion. Contrast-enhanced MRI techniques are currently used for both screening of asymptotic women as a bilateral procedure, and follow-up imaging procedures for symptomatic women.

1.5.3.3.1 MRI Breast Screening Protocols

The standard imaging sequences used for MR breast studies are fast T1-weighted sequences.

Two-dimensional, or three-dimensional gradient recalled echo (GRE), dynamic imaging sequences are often used [6,59]. These sequences allow fast imaging of a whole volume of breast tissue (2.5 – 5.0 minutes/acquisition). The volume of the breast is imaged multiple times, once before contrast agent injection, and then multiple times afterwards for a total imaging duration between 10-15 minutes. The information of interest in these images is the dynamic contrast agent uptake. In order to visualize this uptake better, the high-intensity signals that exhibit no uptake, such as fat, are removed. Two such methods are 1) image subtraction and 2) fat-suppression. Image subtraction is accomplished by simply subtracting the pre-contrast image from each of the post-contrast images. Fat-suppression techniques take advantage of the fact that fat resonates at a frequency slightly lower than water. The proton signals from fat will precess at a frequency 3.5 parts per million slower than water signals [6,58]. The application of a saturation pulse centred at the frequency of the fat allows suppression of the fat signal. Both of these techniques have demonstrated effective elimination of fat signal in the dynamic images.

1.5.3.3.2 Sunnybrook Breast Screening Protocol

Throughout this thesis, particular attention will be paid to a breast screening study, which began in 1997 and is still in progress at Sunnybrook and Women's College Health Sciences Centre (SWCHSC). One of the main objectives of this study is to determine the effectiveness of contrast enhanced MRI as a screening tool for women carrying the BRCA genetic mutation. The MRI screening protocol used is based on the concepts previously discussed. The specific imaging technique is outlined in second column of Table 1.1 and is illustrated in Figure 1.7. The protocol requires the patient to lie prone in a specially designed apparatus in which their breasts hang pendant. The breasts are gently immobilized in a medial-lateral configuration by two pairs of compression plates which each contain a receiver coil. These 4 coils are used to image the breast in a phased array configuration. The schematic of the apparatus is shown in Figure 1.7a, superimposed on an axial image of a patient. Once the patient is lying comfortably with both breasts compressed, they are positioned inside the closed-bore of the MR magnet. The imaging sequence requires an initial axial and coronal spin-echo imaging series to identify the position of the breast.

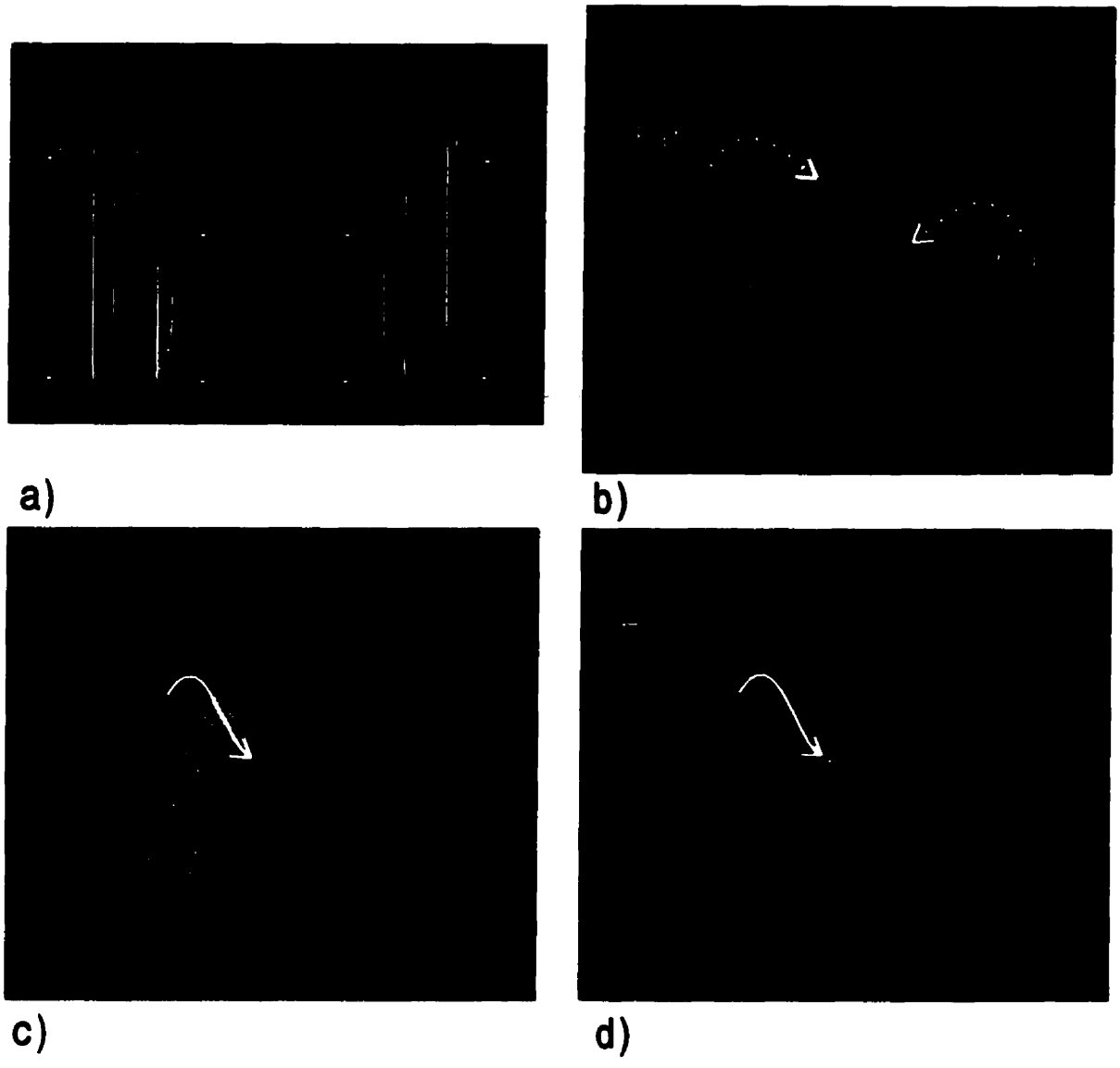

Figure 1.7: Contrast-Enhanced MRI of the Breast. a) Axial view through the torso of a woman. Compression plates and coils superimposed on image as well as white lines indicating sagittal scan plane orientation. b) Sagittal T1-weighted image of the breast, pre-contrast. Bright fat signal (F) and fibroglandular signal (FG) contrast due to different T1 values. c) Image acquired 2.5 minutes after contrast injection. Focal enhancement indicated by white arrow d) Subtracted image, depicts focal enhancement clearly.

The first set of 3D, Spoiled gradient (SPGR) T1-weighted sagittal images are obtained over both breast volumes as an initial pre-contrast image set of the breast (Figure 7b). Bilateral imaging is accomplished with 3D interleaved volume imaging in which software and hardware modifications allow switching between multiple receive coil arrays using a technique based upon the work of Greenman et al [60]. The contrast agent is then injected and the sagittal imaging sequence is

repeated every 2.5 minutes for a total of 10 minutes. The image in Figure 7c shows an image taken 2.5 minutes after contrast agent injection. The image in Figure 7d demonstrates the resulting image when the pre-contrast image in Figure 7b is subtracted from the image in Figure 7c. These images effectively demonstrate the change in contrast agent uptake over time. The lesion indicated on Figure 7c is clearly depicted after subtraction of the pre-contrast image.

A second imaging protocol has been developed for the SWCHSC high-risk study for use in conjunction with the screening protocol. This "follow-up" procedure is done for lesions that have been previously identified by MRI and demonstrate characteristics suspicious of a carcinoma. This imaging protocol focuses upon on a single breast where the imaging sequence probes the morphology and kinetics of the lesion with improved resolution. The imaging sequences used for this "follow-up" protocol are outline in the third, forth and fifth columns of Table 1.1. The sequence is broken up into three series. The first series is a T2-weighted spin echo sequence, which demonstrates the fluid regions of the breast. The second series is a fast-SPGR T1-weighted sequence where the entire breast is imaged every 20 seconds. The third series is a high -resolution 3D-spoiled gradient series, which results in high-resolution images of the breast. The improved temporal and spatial resolution obtained with this protocol provides an opportunity for improved diagnosis ability of the lesions.

Imaging Parameters	Screening Protocol	Follow-up Protocol T2-weighted Series	Follow-up Protocol Dynamic Series	Follow-up Protocol High Resolution Series
Pulse Sequence	3D SPGR	2D Fast Spin Echo	2D SPGR	3D SPGR
Acquisition Matrix	256 x 256	256x128	256 x 128	512 x 256
Field of View	18 cm x 18 cm	18 cm x18 cm	18 cm x 18 cm	18 cm x 18 cm
Pixel Size (freq,phase)	0.7x0.7 mm	0.7x1.4 mm	0.7x1.4 mm	0.4x0.7 mm
Slice Thickness	2.0 – 3.0 mm	3.0 – 5.0 mm	5.0 – 6.0 mm	1.0 - 1.5 mm
Time per Acquisition	2.5 min	5 min	20 sec	7 min
Fat Suppression	Subtraction	Fat Saturation	Fat Saturation	Fat Saturation

Table 1.1: MR Imaging parameters for SWCHSC High Risk Screening Study

1.5.3.4 Diagnostic Indicators

Contrast enhanced MRI of the breast has proven to be a highly sensitive modality for detecting breast cancers. It has demonstrated sensitivities between 90-100% in various clinical screening studies [5-11,49]. This is slightly higher than the sensitivity of mammography in the general population that has been quoted as being between 80-90%. This is expected to be substantially higher than US for which a consensus has been reached that US is not an appropriate screening modality [3,31-33,41,61]. Although the sensitivity of breast MRI is relatively high, there still remains potential to improve the specificity. Using spatial and temporal information from the images, specificity measures have been shown to range from 37% to 97% [5-11,51,52]. The two fundamental criteria used to characterize lesions detected with breast MRI are the contrast enhancement kinetics and lesion morphology. These properties have been demonstrated to be useful in characterizing the lesion's malignancy status, however the inherent histologic variability of benign and malignant lesions, and investigator's differing image interpretation criteria results in widely ranging specificity values. The contrast enhancement time course of cancerous verses benign lesions differs substantially. Typically a cancer will demonstrate fast enhancement relative to the surrounding structures due to the increased capillary permeability and leakage space associated with tumour neo-vascularization. The contrast agent has a tendency to leak out of the tumour vasculature into the surrounding extra cellular space resulting in accumulation of contrast agent. Consequently, there is an increase in the MR signal relative to the surrounding tissue due to the interaction of the contrast agent with the water molecules as previously discussed. The MR signal associated with most malignant or benign lesions tends to rise and peak quickly relative to surrounding tissue in this early contrast enhancement phase.

At later phases, contrast agent will either tend to accumulate into larger concentrations, or diffuse out into the leakage space and back into the capillaries resulting in lower concentrations of contrast agent depending on the nature of the tumour microvasculature. The resulting change in MR signal due to the contrast accumulation or depletion can be plotted over time to generate a time-signal intensity curve. Time-signal intensity curves that plateau or decrease in the late phases of contrast enhancement tend to be associated with malignant lesions, whereas continued gradual

enhancement is generally associated with benign lesions and normal fibroglandular tissue [28,52,53,56].

The information from these time-signal intensity curves is used to characterize whether a lesion is malignant or benign. In one study examining the effectiveness of the signal time intensity curves for differential diagnosis, the use of the rate of enhancement as an indication for malignancy was shown to result in a sensitivity of 91% and a specificity of 37%. Whereas the shape of the enhancement curve alone proved to be a strong indicator of malignancy, demonstrating a sensitivity of 91% and a specificity of 83% [52].

There still remains overlap in distinguishing benign from malignant tumours based on the enhancement kinetics, especially between benign fibroadenomas and invasive carcinomas. The enhancement curves are not specific enough to characterize lesions, thus the morphology of a lesion is used in parallel with the lesion enhancement information. Features similar to those used in mammography and US are used to characterize lesions. Lesions demonstrating rim-enhancement and diffuse boarders are indicative of carcinoma, while benign lesions tend to demonstrate internal septa and a lobulated appearance [54,55]. Even with the rich temporal and spatial information in MR images, the specificity of the technique continues to be an aspect of breast MRI that has the potential to improve.

Comparison of Imaging Techniques

Mammography has proven to be a cost effective and sensitive imaging modality for screening the general population, although its effectiveness is substantially reduced in women with dense breasts. Ultrasound has demonstrated its utility in specific breast imaging functions, such as distinguishing malignant tumours from benign and guidance of interventional procedures. Ultrasound has not proven to be an effective screening modality. Contrast-enhanced MRI, on the other hand, has proven to be a highly sensitive imaging modality independent of the density of a women's breast. The use of this imaging technique for breast imaging is still relatively new compared to US and mammography, but has already demonstrated its utility in the detection of

aggressive cancers that are occult to traditional imaging modalities. In one study comparing the effectiveness of MRI, mammography and US as a screening tool in a population of women who were suspected carriers of the breast cancer susceptibility gene, it was found that MRI has a sensitivity of 100% compared to mammography and US, both with sensitivities of 33% [11]. MRI may be very sensitive, but it is not specific in distinguishing malignant from benign tumours. In fact, none of these modalities is capable of 100% specificity. In order to diagnosis a lesion definitively as cancerous, or benign, a tissue sample must be obtained. These tissue-sampling techniques are explained in the following section.

1.6 Tissue examination

Breast tissue samples are acquired using three general biopsy techniques:

1) fine needle aspiration.
2) wire localization with open surgical excision
3) large needle core biopsy

The first technique acquires fluid suspensions of cells from the lesion, which is examined using cytological analysis, whereas the second and third techniques acquire a solid sample of the tumour, which is sectioned and examined under histopathological analysis.

The least invasive approach, fine needle aspiration (FNA), involves using a fine (20-23 gauge), puncture needle with a syringe. The needle is positioned into the lesion and with the use of negative pressure on the syringe; fluid is aspired and preserved on slides, which are used for cytological examination.

The gold standard for lesion biopsy is considered to be surgical excision. The first step of this procedure involves localizing the detected lesion, typically by placing a fine needle (20 gauge) through the lesion and threading a fine hook wire through the centre. These needles are shown in

Figure 1.8 i) and ii). When the wire is in place, and the hook catches the tissue, the needle is removed leaving the wire in place. The patient then goes to surgery where the surgeon uses the wire as a guide and cuts until the end of the wire is reached when a large section of tissue is removed. A specimen radiograph is then obtained to determine if the lesion removed is actually contained within the excised tissue, and then sent for analysis.

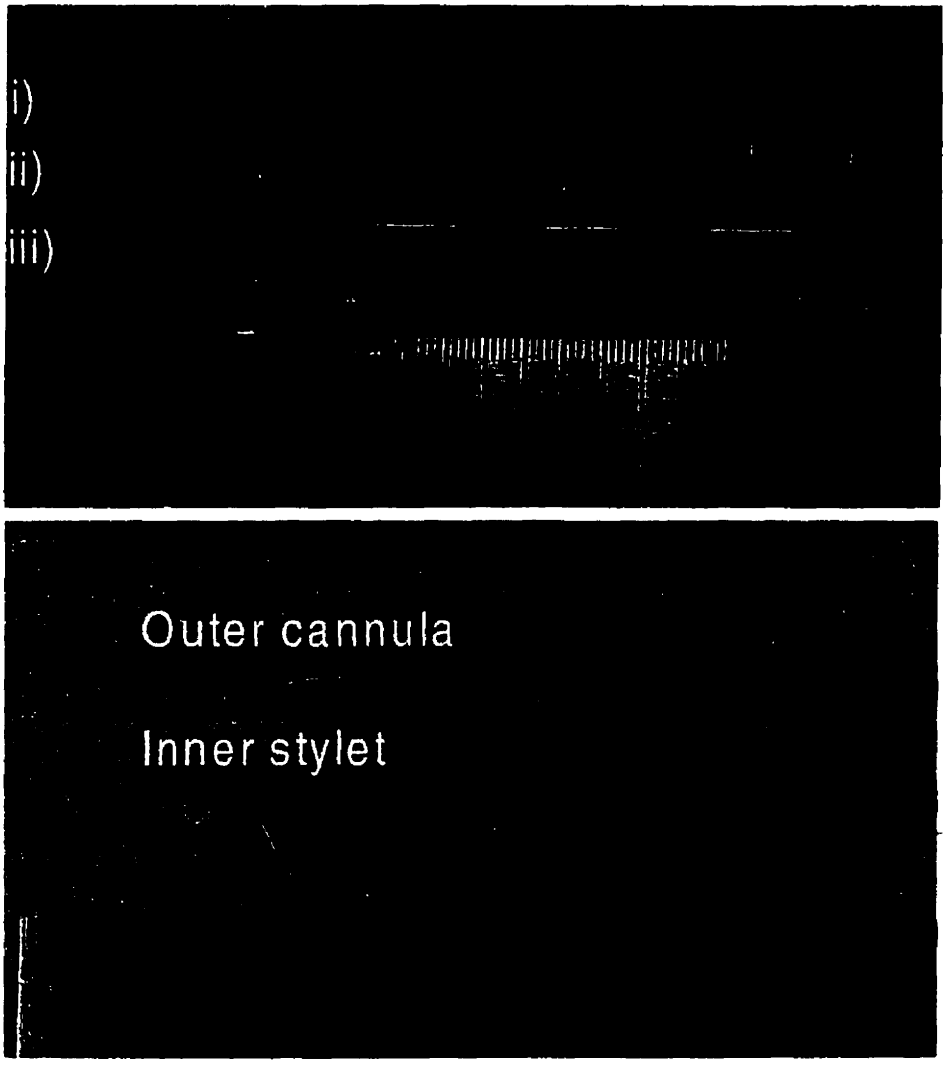

Figure 1.8: Comparison of different biopsy needles: i) Localization wire ii) Localization Needle (20 gauge) iii) Core biopsy needle (14 gauge). The localization wire can be threaded though the centre of the localization needle until the hook at the front is deployed. The lower image shows the two components of a biopsy needle; the outer cannula and the inner stylet. Note the sample notch in the inner stylet.

Large core biopsy is an option for obtaining a tissue sample suitable for histological analysis

without resorting to excisional surgery. A large (14-18 gauge), needle is used in conjunction with a rapid-fire automated biopsy device, or otherwise known as a biopsy gun. The needle consists of two parts - an inner stylet, cut with a sample notch for acquiring the sample and an outer cutting cannula as demonstrated in Figure 1.9. The biopsy needle is held in the spring- loaded blocks of the biopsy device, which fires in two stages. The posterior block fires first, advancing the inner stylet, containing the sample notch, into the lesion. The anterior hub is fired causing any material in the sample notch to be cut by the outer cannula allowing the tissue to fall into the notch for subsequent resection. After the device is fired, the needle is removed from the breast and the sample in the notch sent for analysis.

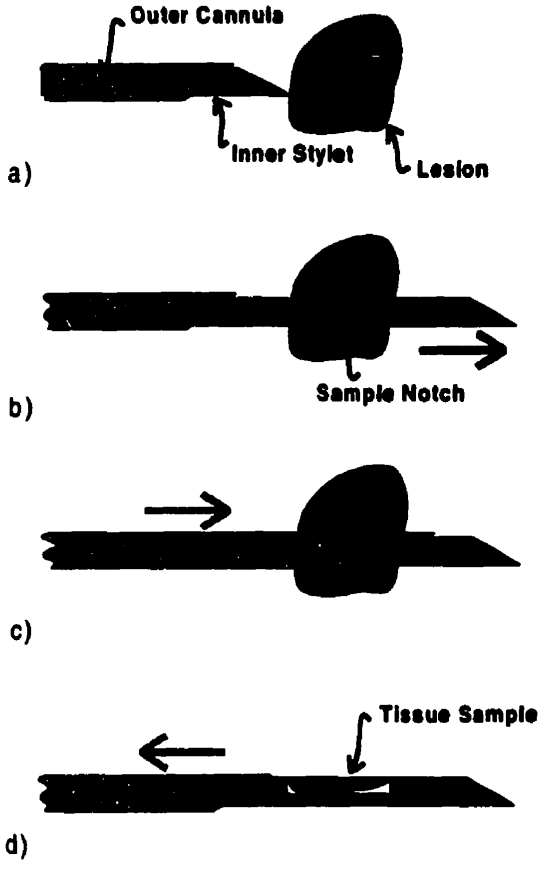

Figure 1.9: Tumour sampling with a biopsy needle: a) The shaft of a biopsy needle consists of two components; the outer cannula and inner stylet. In this first series we see the needle in the pre-fire position. b) The two components are fired independently by a spring loaded firing mechanism in the biopsy device. In this series we see the inner stylet fired forward through the lesion. Tissue from the lesion will fall into the sample notch of the stylet. c) The outer cannula is then fired, cutting the tissue specimen contained in the notch. d) The needle is removed from the breast, and the outer cannula is pulled back revealing the biopsy specimen.

Although surgical excision is the most accurate tissue examination technique, it is also the most expensive, time consuming and invasive. There has been interest in using needle biopsy techniques (core biopsy or FNA) due to the minimal impact on the appearance of the breast and substantially reduced cost. Institutions have reported sensitivity and specificity of over 90% for both FNA and core biopsy techniques [62]; however, FNA is not widely used in North America due to the difficulty in obtaining adequate cytologic material [63]. The agreement between core biopsy and surgical excision has been demonstrated to range from 87% to 100% [64].

The accuracy of all the tissue examination techniques is contingent on whether the tissue in question is actually sampled. Sampling of the incorrect region in the breast can result in an incorrect diagnosis. The ability to remove the lesion in a surgical excision requires accurate placement of the wire into the lesion, while the sampling of lesions with FNA and core biopsy requires the needle to be positioned precisely. The strict accuracy requirement associated with core-biopsy and FNA is due to the small samples obtained compared to surgical excision. Techniques to ensure biopsies are performed accurately are considered in the next section.

1.7 Biopsy Guidance Techniques

The simplest method to guide needle biopsy, or wire localization is done using palpation. With the lesion in one hand, and the needle in the other, the physician guides the procedure by feel. This procedure known as clinical guidance, works well if the lesion is palpable, but imaging techniques are required if it is not [65,66]. The use of mammography, ultrasound and MR to guide needle positioning is explained in the following sections.

1.7.1 X-ray Guidance

Needle biopsy and wire localization of mammographically visible lesions can be accomplished using grid coordinate systems or stereotactic guidance [62,67]. These techniques use two X-ray views of the lesion at different angles to determine the required needle position.

1.7.1.2 Grid Coordinate Systems

The grid coordinate system uses a standard mammography unit with an attached needle localization grid. This grid is a fenestrated plate with radiographically visible alpha-numeric indicators. The breast is initially compressed in the craniocaudal orientation. A film is taken and the needle position determined at the appropriate site guided by the alpha-numeric indicators. The radiologist positions the biopsy needle by hand using the feel of the needle in the tissue as a guide. Positioning the needle in this manner is inaccurate since it is done by estimation and positioned by hand. After the needle is inserted, a second film is taken to confirm its position. The film is placed in the orthogonal position and another film taken. This image determines if the depth of the needle is correct relative to the lesion. The position of the needle is modified and checked with subsequent films until the positioning is correct. The precision with which needles can be positioned using this technique is acceptable for wire localization procedures. The failure rate associated with this technique has been estimated to be between 1 to 8 percent [68]. However, the use of this technique for guided core biopsies is not acceptable. [62,67]

1.7.1.3 Stereotactic system

A different needle positioning technique is used to guide core biopsies of the breast. Stereotactic systems use the information from two images taken at slightly different angles to infer the position of the lesion in the breast, and use that information to position a biopsy needle accurately. Typically two views of the lesion in the compressed breast are acquired at 15-degree angles from a centre-line. The lesion will appear to shift in the image depending on the depth of the lesion in the breast. Two positions of the lesion can be determined by measuring the position of the lesion relative to a target, while the depth is determined by measuring the amount of shift, or parallax, between the two images . A computer program is used to calculate the required position of the needle once the operator indicates the lesion position in the images. The needle is positioned using a needle guidance system, which is affixed to the table at a known position relative to the reference marker that appears in the X-ray images. Images are then acquired to determine if the needle is in the correct position before the biopsy device is fired. In order to improve the

probability of sampling the correct lesion, or to sample various parts of the lesion, multiple cores are obtained. The same procedure is used, except that another part of the lesion is targeted and the calculation of needle position is done such that the same incision point for needle entry into the breast is used.[67]

There are generally two types of systems used for stereotactic biopsy, add-on systems and dedicated prone tables [62,67]. The spatial precision of these systems has been shown to be better than a millimeter under optimal conditions [68] and within 1-2 millimeters during a typical procedure [64]. The diagnostic accuracy of these techniques has been shown to be dependent on the number of core samples obtained. Increasing the number of core specimens improves accuracy for which a diagnosis of an invasive cancer can be made. One study indicated that the accuracy improves from 70% with one sample to 94% when 5 or more samples are obtained [69]. Although this technique is widely used, there are still problems including limited access to lesions near the chest wall, patient motion, lesion motion and needle deflection in the breast [68].

1.7.2 Ultrasound Guided Biopsy

The use of ultrasound to guide needle core biopsy and needle localization is a preferred method due to the ability of US to provide real-time guidance for the needle during the biopsy procedure. The procedure involves the use of a hand-held high frequency linear array (5.0MHz – 10.0MHz) in one hand, while positioning the needle with the other. Using the ultrasound images as a reference, the needle position is validated relative to the lesion using the strong echo created by the biopsy needle. The best images of the needle are obtained when it is parallel to the face of the transducer as shown in Figure 1.10. When performing a core biopsy procedure the pre-fire and post-fire positioning of the needle is validated to ensure it has totally passed through the lesion. This technique has been demonstrated to be a highly effective biopsy guidance technique with minimal cost, time and highly accurate results, with one group demonstrating 100% correlation of core biopsy results with surgical excision findings [70].

Figure 1.10: Ultrasound Needle Guidance: In these images a core biopsy needle, identified by the large arrows, is being guided into a suspicious lesion, identified by the arrowheads. a) The needle can be seen in the pre-fire position. The tip of the needle is evident as identified by the curved arrow. b) The needle position is verified in the post-fire position as passing through the lesion.

1.7.3 MR Guided Biopsy

Stereotactic mammography and ultrasound-guided biopsy techniques have been demonstrated to be successful only if the lesion can be adequately visualized in their respective imaging modalities. Lesions that are detected only by MRI however require a different biopsy guidance technique. Biopsies of lesions occult to all imaging modalities except MRI are currently done using two different classes of MR guided techniques: stereotactic and real-time biopsy systems.

1.7.3.1 MR Guided Stereotactic Biopsy Techniques

MRI stereotactic systems operate using the same fundamental concept as the mammography systems. Imaging the breast using two different views determines the lesion position in three dimensions. The use of a reference, or fiducial marker that is visible in the images allows the position of the lesion in images to be associated with a position relative to the biopsy apparatus. [2]

Various groups have independently developed biopsy and localization systems [71-78]. Although

2 The use of the term "stereotactic" to describe the MRI biopsy systems in current literature is inaccurate. An orthogonal pair of MR images is used as opposed to a stereo pair used in mammographic stereotactic. In order to avoid confusion, the term stereotactic is used throughout this thesis to describe the MRI technique.

the positioning of the patient and immobilization of the breast are different with each system, they operate fundamentally in the same manner. An example of one of the first systems developed by MD Schnall, is shown in Figure 1.11 [71]. Seen in this image is a woman lying on the apparatus in the prone position, with her breast compressed in a medial-lateral conformation. The lateral compression plate of the apparatus is perforated with a set of holes sized to enable needle access to the breast. On the plate is attached a fiducial marker used to reference the breast to physical positions in the MR images.

A system based upon the Schnall design was developed and used clinically in the breast screening study at SWCHSC. This system is used as an illustration of the general concept of MR-guided stereotactic needle localization in Figure 1.12.

Figure 1.11: MR biopsy apparatus developed by MD Schnall. Consists of a lateral compression plate with array of access holes. Fiducial marker and needle are shown in the plate [71].

A patient selected for an MR biopsy will have a lesion that has been detected in a previous contrast- enhanced MRI study and is occult to other modalities. Using the prior knowledge of lesion position, the breast of interest is compressed in the apparatus and a dynamic imaging sequence similar to the one described in Section 1.5.3.3 is performed. The first image, Figure 1.12 a, demonstrates an axial view of the breast compressed in this apparatus.

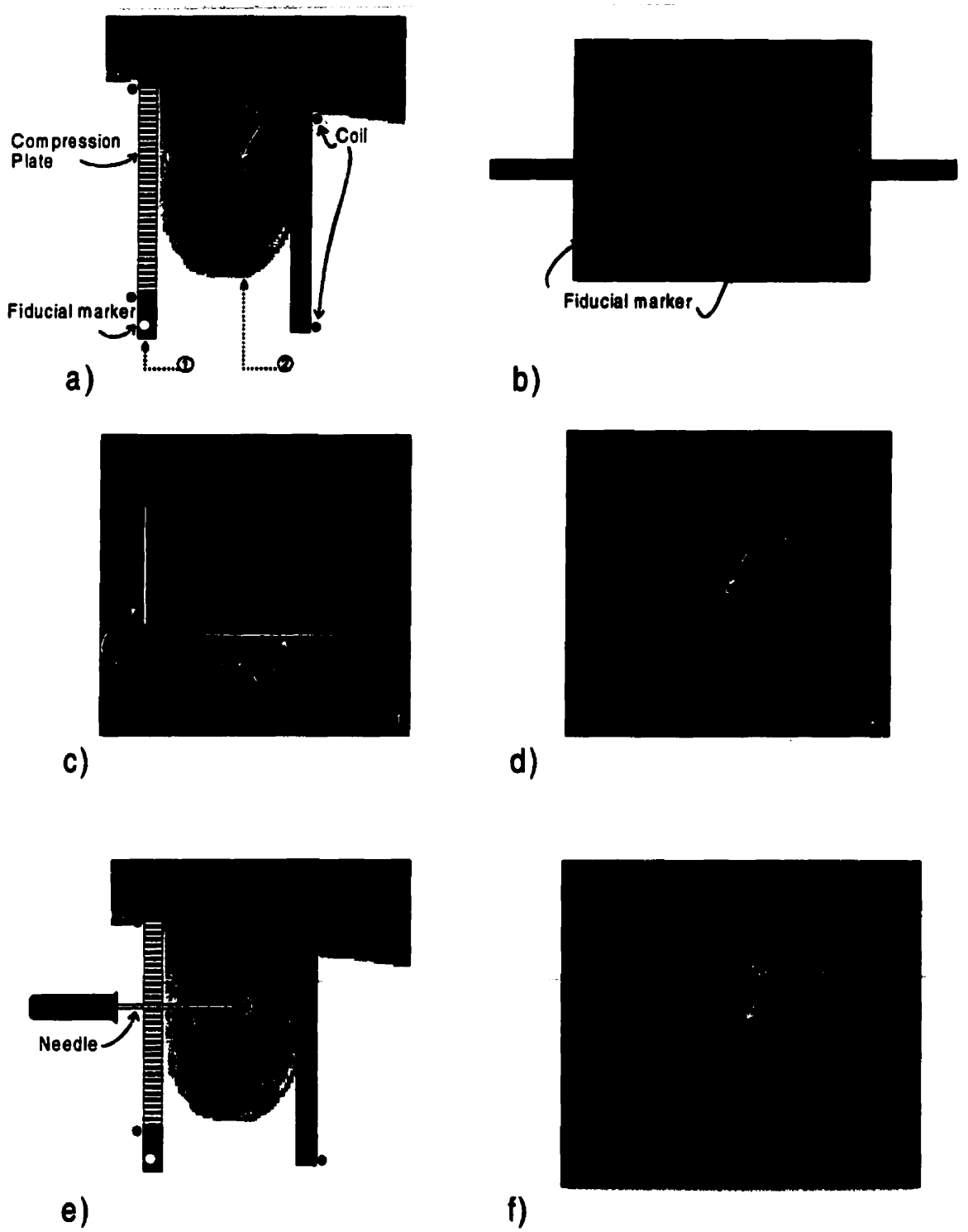

Figure 1.12: MR-guided stereotactic breast biopsy: a) Axial view of the breast in biopsy apparatus. b) Lateral view of the compression plate. c) Sagittal MR image of the fiducial markers. d) Sagittal Fat saturated MR image of breast with enhancing lesion. e) Axial view, with needle positioned based on fiducial and lesion position f) Sagittal verification image with needle artifact indicating needle position.

The lateral compression plate of the screening apparatus was removed, and replaced with a specially designed biopsy plate. The plate consists of a set of holes spaced at 2.5 mm intervals that allow passage, and guide a 20-gauge localization needle. On the outer surface of the plate attaches a coil, which is required for MR imaging. Embedded into the plate are fiducial markers that are visible in the MR images. This plate is illustrated in a lateral view of the plate as seen in Figure 1.12 b, showing the plate with the array of holes at a known distance from the fiducial markers. The plate itself acts as a stereotactic frame. The imaging sequence performed is a sagittal, fat saturated, T1-weighted 2D-SPGR sequence in concert with intravenous contrast agent injection. The imaging volume includes the entire breast and the fiducial markers, Figure 1.12 c. After imaging the breast for a period of time, the lesion should appear as a quickly enhancing bright region, Figure 1.12 d. After re-identification of the lesion in the MR images, the position of the lesion relative to the MR visible fiducial markers is determined. Using a conversion calculation, the position of the needle on the stereotactic frame is determined. The patient is then removed from the bore of the MR magnet and the needle positioned into the calculated access hole at the required depth in breast, Figure 1.12 e. The position of the needle is then verified using another MR imaging sequence by bringing the patient back into the bore of the magnet. The verification image is shown in Figure 1.12 f.

The biopsy systems used throughout the world differ in regard to the methods of breast compression, patient positioning and imaging sequences whereas the use of fiducial markers and grids is similar in all systems. The various apparatus and some of their features are listed in Table 1.2.

Biopsy needles and hook wires used for these MR guided procedures are designed to be compatible with the MR magnetic field. The needles are typically made from titanium and when imaged will create an artifact in the MR image. This artifact, due to the perturbation of the local magnetic field around the needle resulting in a signal void, is indicated in Figure 1.12f). It is this artifact that is used to indicate the position of the needle relative to the lesion. Typically two verification views are used to indicate that the needle is correctly positioned in the correct puncture hole, and at the correct depth. Modifications can be made according to these MR images

until the needle is in the correct position. Once the needle is in the proper position the wire is threaded through the needle, or the biopsy device is fired to obtain a biopsy sample depending on the biopsy technique.

Group	Patient Position	Compression	Description
Kuhl, et al [70]	Semi-prone.	Medial-Lateral.	Perforated compression plate. Bushing used to guide needle. Fiducial markers positioned outside of plate.
Schnall, Orel, et al [69]	Prone.	Medial-Lateral.	Perforated compression plate. Fiducial marker positioned on surface of plate.
Fischer, Doler, et al. [71,72,73]	Supine.	Angled against chest wall.	Two angled compression plates pressed against breast. Access to the breast through puncture channels.
Daniel, et al. [74]	Prone.	None. Molded plastic frame around breast.	Formed mesh around the breast allows access. Free-hand technique which the radiologist approximates needle position and verifies with an MR update scan.
Heywang-Kobrunner, et al. [75]	Prone.	Medial-Lateral.	Plastic ribs used for compression. Spacer is placed to separate ribs for access. Biopsy device held is fixture attached to patient couch.
Liney, Turnbell, et al. [76]	Prone.	Medial-Lateral, with option to adjust angle.	Perforated compression plate. Fiducial marker casing attached to plate.

Table 1.2: MR guided core biopsy systems currently developed by various groups.

The success rates of localization procedures vary from group to group, ranging from 90% to 100% success [71,72,74,76,77]. Published data with respect to the accuracy of core biopsy are limited. Techniques currently used for MR-guided wire localization are considered to be successful, but there remain many problems with performing MR-guided biopsies with the stereotactic technique [72].

The ability to access lesions near the chest wall with all of the current systems is a continuing problem. The use of a system where the breast is compressed against the chest wall allows needle

access, but the firing of the needle straight into the chest is not acceptable. Other systems that compress the breast in a medial-lateral conformation, with the needle approach parallel to the chest wall, demonstrate limited access to all regions of the breast. Lesions near the chest wall, or in the upper quadrant of the breast are inaccessible, while lesions that are medial in the breast are difficult to access without traversing a large amount of tissue. A system that provides adequate breast immobilization while still providing access to all areas of the breast is currently not available.

The visualization of the lesion is an issue with all techniques. Although the lesion may be apparent in the early dynamic images, contrast can wash-out during the biopsy procedure and make the lesion difficult to distinguish from the background tissue. The amount of time the lesion is apparent in the MR images depends on the uptake and clearance characteristics of the lesion and surrounding parenchyma. In bilateral screening studies performed at SWHSC, we found that in some cases the lesion was only distinguishable from the background for 10 minutes. This would pose a problem for current stereotactic techniques, which require approximately 5-10 minutes to remove the patient from the magnet, position the needle and image the breast again. This leaves little time to perform repositioning and verification of needle position imaging. Although this issue is not the most challenging issue associated with MRI biopsy, it deserves adequate consideration.

The accuracy of current stereotactic techniques remains the most significant problem. It has been advised that only lesions larger then 1cm should only be considered for core biopsy [11]. Since it is the goal of breast screening to detect and diagnose lesions at the earliest possible stage, this restriction is limiting the effectiveness of MR as a screening tool [11]. Small lesions detected by MR alone that are suspicious, but do not warrant an excisional biopsy, are often managed by a follow-up examination at a later date. This presents the risk of delaying a cancer diagnosis.

There is a series of factors affecting the accuracy of this technique. As the needle is pushed into the breast, it tends to deflect and bend due to the stiffness of the breast and the numerous heterogeneous interfaces throughout the breast [68]. When the needle intercepts an interface it will tend to deflect towards the softer tissue, traversing the path of least resistance. Another issue

is the mobility of the lesion within the breast. Often lesions are stiffer and more dense then the surrounding parenchyma tissue. When the needle advances towards the lesion it may tend to move out of the way of the needle path. These two phenomenon are illustrated in Figure 1.13. In an attempt to correct for these problems the needle position is validated intermittently with another imaging series as previously mentioned. The restriction of the closed-bore of the MR magnet requires the patient to be brought out into the magnet fringe field each time the needle position needs to be validated. A solution to this problem is the use of a different MR biopsy technique that is capable of real-time monitoring of the needle position while the user corrects the needle position. This technique is explained in the next section.

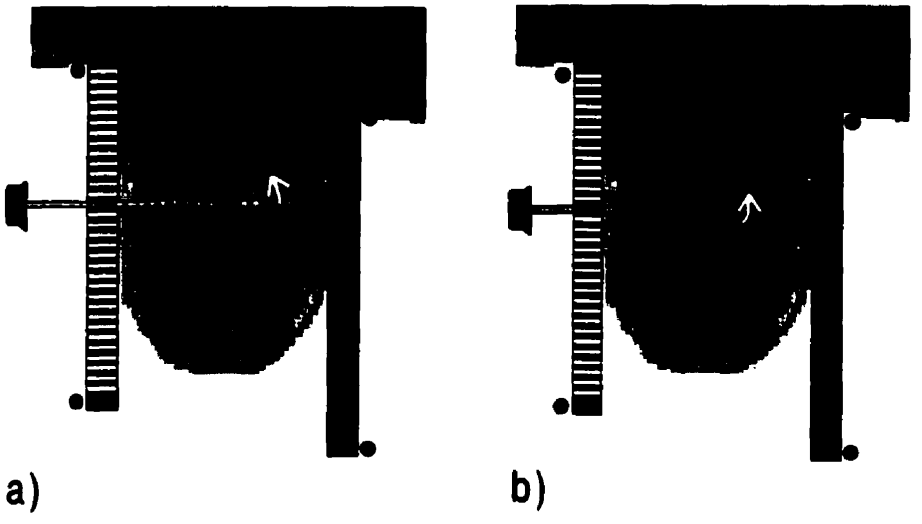

Figure 1.13: Needle and lesion movement in a breast. a) As the needle moves through the breast, it may deflect due to the stiffness of the breast and miss the desired trajectory (dashed line). b) Even if there is no needle deflection, a stiff lesion may move out of the way of the needle. Both of these affects lead to inaccurate biopsy results.

1.7.3.2 MR Guided Real Time Biopsy Techniques

Real-time biopsy techniques involve imaging the patient constantly while the needle is inserted into the breast. These techniques often involve a specialized magnet to enable access to the breast. These magnets are designed for open access to the patient and typically have lower magnetic field strengths. One such system employs a "double donut" magnet configuration (0.5T Signa-SP, GE Medical Systems, Milwaukee, Wis) and is depicted in Figure 1.14 a [76]. Another system

available for breast applications uses a "clam-shell" magnet configuration (0.2T Magnetom Open, Siemans, Erlangen, Germany) [80]. This system is shown in Figure 1.14 b. The magnet architecture for each of these systems enables access to the breast while the system is obtaining images.

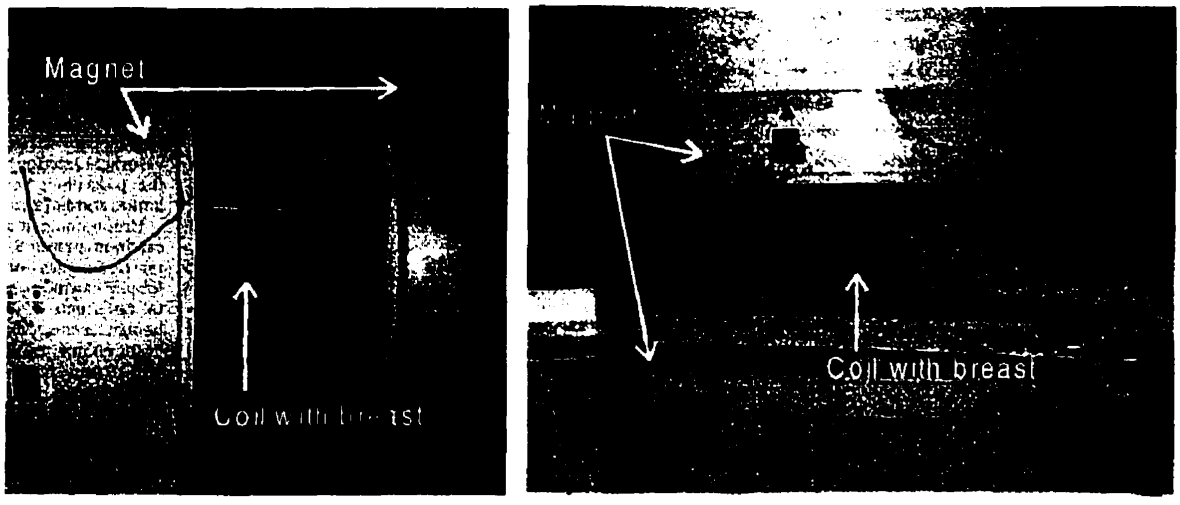

Figure 1.14: Intervention magnet designs. a) This "double donut" interventional magnet allows access to the breast while real-time images can be used to guide needle positioning. b) This "clam shell" magnet design is another popular interventional magnet design.

The biopsy technique is similar to the stereotactic strategies described in the previous section. The imaging sequence used is a fast T1-weighted sequence with intravenous injection of gadolinium. The needle is advanced by hand into the breast where the artifact created by the needle is used to infer needle position. The use of optical tracking devices can track the biopsy needle allowing improved visualization of the needle within the MR images. This open magnet design enables access for real-time manipulation of the needle within the breast while fast imaging facilitates the radiologist in guiding the needle based on real-time images.

There are some technical issues associated with these real-time techniques. The first problem is the limited time that the lesion is visible in the images. This is an issue in the stereotactic systems, which is not avoided here. The second problem is the dependence on the needle artifact to locate the needle position. If very small lesions, for example on the order of 4 mm, require biopsy, then

they would be totally obscured by the needle artifact. The third problem is the reduced image quality associated with the open architecture systems. These systems have magnetic field strengths on the order of 0.2 to 0.5 Telsa, which results in a reduced image SNR.

These specialized interventional magnets can be utilized for a variety of interventional procedures, ranging from liver and breast biopsy to head and neck interventions [81,82,83]. Although the magnets can be used for a variety of purposes, there are currently few of these specialized systems relative to the standard MR imaging systems. The limited number of such systems occludes their use for breast biopsy applications. The use of current 1.5T systems is more appropriate for breast biopsy procedures.

1.7.4 Retrospective Biopsy Techniques

The problem of obtaining a biopsy of a lesion that is only evident only on a MRI can be considered from a different standpoint when one considers clinical practice. Lesions may often be occult to a radiologist on a particular modality during screening when the entire breast is being simultaneously examined. These same lesions however, may be evident when the radiologist is given information on where, and what to look for, helping them focus their search. Often, if a lesion is detected in one modality, it may be detected using another modality retrospectively. Radiologists have successfully used this approach with mammography to detect lesions initially in a screening context, and then using this information, to guide positioning of an ultrasound probe. This retrospective technique is used to biopsy lesions using US when it is preferred for biopsy guidance over stereotactic mammography.

1.7.4.1 Directed Ultrasound Biopsy

The concept of retrospective lesion detection has been extended to biopsy occult lesions detected with MRI. The position and characteristic features of a lesion in the MR images can be used to locate the lesion in a retrospective ultrasound imaging procedure. This technique has been used successfully at SWHSC in many patients including the case shown in Figure 1.15. In this case, a

small rim-enhancing lesion appeared in an MRI follow-up examination. Using the MRI information, a small, 4 mm lesion was detected with US and successfully biopsied. The pathology report indicated an invasive carcinoma. Other groups have indicated similar success using MRI-guided ultrasound for guidance of FNA of occult breast carcinoma [84].

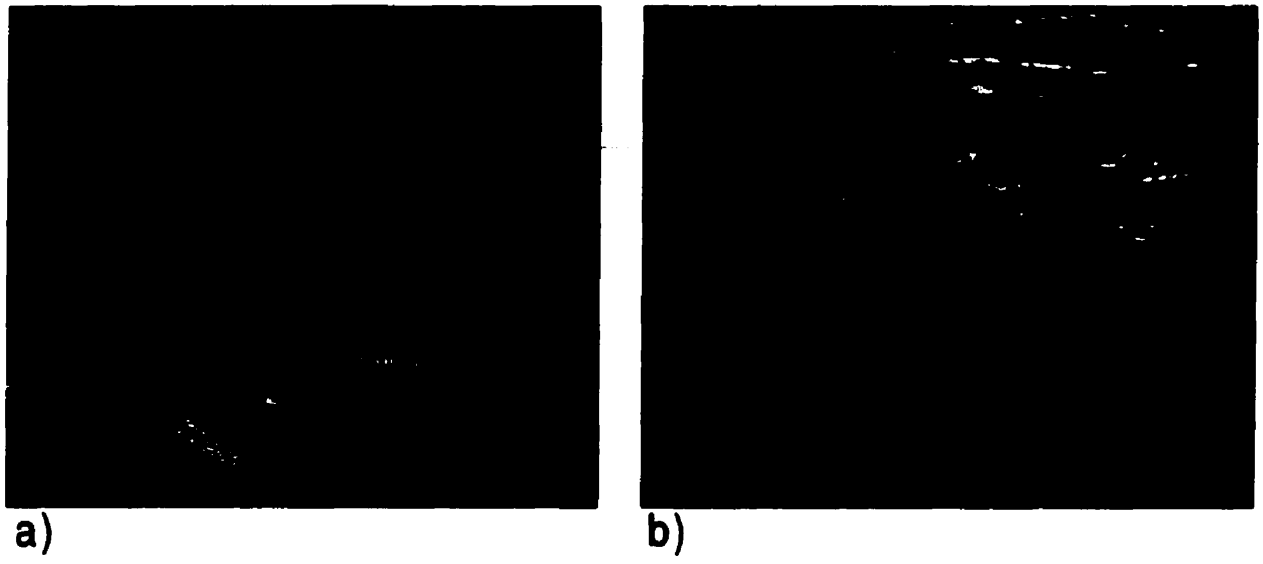

Figure 1.15: Carcinoma detected in MR and US. a) Small rim-enhancing lesion was detected in the fat-saturated MR image. b) Lesion was missed in screening US, but using the MR information, was subsequently dectected and biopsied under US guidance.

The transformation or registration between two imaging modalities required for retrospective lesion detection is essentially done in the mind of the radiologist. This can be a difficult task considering that the breast is imaged and compressed in completely different configurations during MRI, US or mammography. Another difficulty arises when a radiologist tries to find a lesion detected with MRI in an US image when normal tissue, or other lesions in the vicinity look similar. In US images, fat lobules or ducts can often appear similar to lesions as seen in Figure 1.15 b. When lesions are detected in US, little contrast difference from normal tissue makes them difficult to visualize, while matching the orientation of the lesion in US and MR can be problematic. Confidently matching what is seen in MR and US is difficult. A final problem is related to the time required to locate the lesion. It is highly dependent on operator skill. The case illustrated in Figure 1.15 took almost one hour with an experienced ultrasonographer.

Even with these problems, retrospective biopsy using directed US is standard practice. A method that could more accurately and reliably register the US imaging plane with the MR detected lesion would be tremendously beneficial and may provide a solution to the problem of MR-guided biopsy.

1.8 MRI/US Registration

There are many different techniques used to register data between imaging modalities. They can be considered in two categories as follows:

- computer-assistcd registration
- mechanical registration

The first category, computer-assisted registration, uses computer algorithms to assist in manipulation of the images so the features are accurately registered. This may require the user to define landmarks that are evident in each modality and then use this as input to a computer program, to warp one image to match the other [85]. Registration techniques that use finite-element modeling to simulate the deformations of tissue under certain loading conditions such as mammography have also been developed [86]. These techniques can be very computationally intensive and are yet developed suitably for widespread clinical use.

The second category, mechanical registration, is a simple solution to the registration problem. Keeping the breast in the same conformation to perform both imaging procedures, simplifies the problem of image registration tremendously. This has been demonstrated for ultrasound and mammography with clever compression devices [86]. As far as can be determined from the available literature, this has not yet been demonstrated for registration between MRI and ultrasound. The purpose of the work outlined in this thesis is to apply a similar technique to co-register MR and US for the purpose of real-time US breast biopsy.

1.9 Summary

The use of contrast-enhanced MRI of the breast has proven to be an advantageous imaging technique for early breast cancer detection. Although groups have demonstrated high sensitivity, the specificity remains poor, and is a topic of considerable research. Currently, the only way to determine if a tumour is in fact cancerous requires acquisition of a tissue sample through an invasive biopsy procedure. Systems and techniques are currently used to perform MRI-guided biopsy, but they have limitations. It is widely recognized that in order for breast MRI to become a universal clinical technique, the capability to perform MRI-guided breast biopsy accurately is essential.

1.10 Summary – Thesis Outline

A novel technique to perform MR-guided breast biopsy is investigated in this thesis. The biopsy strategy presented has been developed though integration of established technologies and clinical procedures. A biopsy apparatus and the related techniques and protocols are presented in Chapter 2. The operation of the system, biopsy strategies and novel techniques for image registration and needle positioning are presented, as well as detailed explanations of the various apparatus components.

A series of experiments investigating the accuracy of the biopsy apparatus and biopsy techniques are presented in Chapter 3. The first set of experiments examines the accuracy of the system in optimal conditions, while the second set examines the accuracy using a breast-mimicking phantom. In this chapter sources of inaccuracy are examined and explained.

In Chapter 4, the results of clinical application of the biopsy system and possible future applications of the system are presented. Actual clinical cases, including needle localization, core biopsy and MR/US image registration are presented. Directions for further improvement and potential applications of this work are discussed.

References

1. Murphy G. (ed), Lawerence W. (ed), Lenhard R. (ed), Textbook of Clinical Oncology, Second Edition, American Cancer Society, Atlanta GA, 1995.

2. Hoskins W.J. (ed.), Perez C.A. (ed.), Young R.C. (ed.), Principals and Practice of Gynecologic Oncology, Second Edition, Lippincott-Raven,1997.

3. Sickles E.A. Breast Imaging: From 1965 to Present. Radiology. 2000. 215:1-16.

4. Bird RE, Wallace TW, Tankaskas BC. Analysis of cancers missed at screening mammography. Radiology 1992; 184:613-617.

5. Harms SE, Flamig DP. MR Imaging of the Breast. Journal of Magnetic Resonance Imaging. 1993; 3:277-283.

6. Weinreb JC, Newstead G. MR Imaging of the Breast. Radiology. 1995; 196:593-610.

7. Heywang-Kobrunner SH, Viehweg P, Heinig A, Kuchler C. Contrast enhanced MRI of the breast: accuracy, value, controversies, solutions. European Journal of Radiology. 1997; Volume 24, Issue 2: 94-108.

8. Nunes LW, Schnall MD, Orel SG, et al. Breast MR Imaging: Interpretation Model. Radiology. 1997; 202: 833-841.

9. Gilles R, Guinebretiere JM, Lucidarme O, Cluzel P, et al. Nonpalpable Breast Tumours: Diagnosis with Contrast-enhanced subtraction Dynamic Imaging. Radiology. 1994; 191:625-631.

10. Kaiser WA, Zeitler E. MR Imaging of the breast: fast imaging sequences with and without Gd-DTPA. Radiology 1989; 170:681-686.

11. Kuhl KC, Leutner CC, et al. Breast MR Imaging Screening in 192 Women Proved or Suspected to be Carriers of a Breast Cancer Susceptibility Gene: Preliminary Results. Radiology. 2000; 215:267-279.

12. National Cancer Institute. SEER cancer statistics review, 1973-1995: Section 4-breast. Female breast cancer trends in SEER incidence and U.S. mortality. Available at: http://seer.cancer.gov/Publications/CSR1973_1996/overview/overview24.pdf. Accessed February 26,2001.

13. National Cancer Institute of Canada. Canadian Cancer Statistics, 2000, Current incidence and mortality, Estimated new cancer cases and deaths for 2000. Available at: http://www.cancer.ca/stats2000/pdf/stats00e.pdf. Accessed February 26, 2001.

14. Claus EB, Schildkraut JM, Thompson WD, Risch NJ. The genetic attributable risk of breast and

ovarian cancer. Cancer 1996; 77:2318-2324.

15. National Cancer Institute. SEER cancer statistics review, 1973-1995: Section 4-breast. Female breast cancer trends in SEER incidence and U.S. mortality. Available at: http://www-seer.ims.nci.nih.gov/Publications/CSR7395/breast.pdf. Accessed February 26,2001.

16. Weber BL. Susceptability genes for breast cancer. N Eng J Med 331:1523-1524, 1994.

17. Easton DF, Bishop DT, Ford D, Crockford GP, and the Breast Cancer Linkage Consortium. Genetic Linkage analysis in familial breast and ovarian cancer: results from 214 families. Am J Hum Genet 1993; 52:678-701.

18. Weinreb JC, Newstead G. MR Imaging of the Breast. Radiology. 1995; 196:593-610.

19. Murphy, Lawrence, Lenhard. Clinical Oncology 2nd Ed., American Cancer Society, 1995, pp 198-219.

20. Des E. Recent Advances in systemic therapy for breast cancer, Curr Opin Oncol, 1998; 10(6):517-522.

21. Sewell CW. Pathology of benign and malignant breast disorders. Radiol Clin North Am. 1995; 33:1067-1080.

22. Rosen PP. Anatomy. in "Breast Pathology". (Rosen PP Ed.), Philadelphia, Pa: Lippincott-Raven, 1997;pp1-15.

23. Carter D. Interpretation of Breast Biopsies. New York: Lippincott-Raven; 1996.

24. Trott P.A. Breast Cytopathology. New York: Chapman & Hall Medical; 1996.

25. Folkman J, Klagsbrun M. Angiogenic Factors. Science 1987; 235:442-447

26. Gasparini G, Harris AL. Clinical Importance of the determination of tumour angiogenesis in breast carcinoma: much more than a new prognostic tool. J Clin Oncol 1995; 13:765-782

27. Passe TJ, Bluemke DA, Siegelman SS. Tumor angiogenesis: Tutorial on Implications for Imaging. Radiology 1997; 203:593-600.

28. Buadu LD, Murakami J, Murayama S, et al. Breast Lesions: Correlation of Contrast Medium Enhancement Patterns on MR Images with Histopathologic Findings and Tumor Angiogenesis. Radiology 1996; 200:639-649.

29. Shapiro S, Venet W, Strax P, et al. Ten to Fourteen-year effect of screening on breast cancer mortality. J Natl Cancer Inst 1982; 69:349.

30. Johns PC, Yaffe MJ. X-Ray characterization of normal and neoplastic breast tissues. Phys. Med. Biol. Vol. 32, No 6, 675-695.

31. Fletcher SW, Black W, Harris R, Ritmer BK, Shapiro S. Report of the International Workshop on Screening for breast cancer. J Natl Cancer Inst 1993; 85:1644-1656.

32. Poplack SP, Tosteson AN, Grove MR, Wells WA, Carney PA. Mammography in 53,803 Women from the New Hampshire Mammography Network. Radiology 2000; 217:832-840.

33. Rosenburg RD, Hunt WC, Williamson RM, et al. Effects of age, density, ethnicity, and estrogen replacement therapy on screening mammographic sensitivity and cancer stage at diagnosis: review of 183,134 screening mammograms in Albuquerque New Mexico. Radiology 1998; 209:511-518.

34. Pisano ED. Current Status of Full-Field Digital Mammography. Radiology 2000; 214: 26-28

35. Jackson VP. The Role of US in Breast Imaging. Radiology 1990; 177:305-311.

36. Foster SF, D'Astous FT. Frequency Dependence of Ultrasound Attenuation and Backscatter in Breast Tissue. Ultrasound in Med & Biol. Vol 12, No.10, pp. 795-808, 1986.

37. Lockwood GF, Foster FS, Hunt JW. A Ray Tracing Method For Calculating The Speed of Sound in a Nonparallel Layered Model Using Pulse Echo Ultrasound. *Ultrasonic Imaging*. Vol 11, pp 106-118, 1989.

38. Kishell EK, Foster FS, Connor T, Khodai M, Harasciewicz, Hunt JW. Clinical Performance of a Cone/Annular Array Ultrasound Breast Scanner. *Ultrasound in Med & Biol.* Vol 16, No.4, pp. 361-374, 1990.

39. Wolbarst AB. Physics for Radiologists. Prentice Hall, Toronto, 1993.

40. Foster SF. Medical Imaging with Ultrasound. Physics in Canada. July-September, 1995. pp.182:189.

41. Rumack CM, Wilson SR, Charboneau JW. Diagnostic Ultrasound. Volume 1, Second edition, 1998, Mosbey-Year book, St. Louis Missouri.

42. Rizzatto G, R Chersevani. Breast Ultrasound and New Technologies. European Journal of Radiology. 27 (1998) p 242-249.

43. Jackson VP. Breast Sonography. Breast Disease. 10(3,4) (1998) pp. 55-66

44. Mendelson EB. Current Status of Breast US. Categorical Course in Diagnostic Radiology for Physics: Physical Aspects of Breast Imaging – Current and Future Considerations. 1999 Syllabus, pp. 295-309

45. Rahbar G, Sie AC, Hansen GC, Prince JS, Melany ML, Reynolds HE, Jackson VP, Sayre JW, Bassett

LW. Benign verses Malignant Solid Breast Masses: US Differentiation. Radiology 1999; 213:889-894

46. Stravos TA, Thickman D, Rapp CL, Dennis MA, Parker SH, Sisney GA. Solid Breast Nodules: Radiology 1995; 196:123-134

47. El Yousef SJ, Duchesneau RH, Alfidi RJ. Magnetic resonance of the breast. Radiology 1984; 150:761-766.

48. Stelling CB, Wang PC, Lieber A, et al. Prototype coil for magnetic resonance of the breast. Radiology 1985; 154:457-462.

49. Dash N, Lupetin AR, Daffner RH, et al. Magnetic resonance imaging in the diagnosis of breast disease. AJR 1986; 146:119-125.

50. Heywang SH, Wolf A, Pruss E, et al. MR imaging of the breast with Gd-DTPA: use and limitations. Radiology 1989;171:95-103.

51. Orel SG. Differentiating Benign from Malignant enhancing lesions identified at MR imaging of the breast: Are time signal intensity curves an accurate predictor? (ed). Radiology 1999; 211:5-7.

52. Kuhl CK, Mielcareck P, Klaschik S, et al. Dynamic Breast MR Imaging: Are signal intensity time course date useful for differential diagnosis of enhancing lesions? Radiology 1999; 211:101-110.

53. Tofts PS, Berkowitz B, Schnall MD. Quantitative analysis of dynamic Gd-DTPA enhancement in breast tumors using a permeability model. MRM 33:564-568 (1995).

54. Nunes LW, Schnall MD, et al. Diagnostic performance characteristics of architectural features revealed by high spatial-resolution MR imaging of the breast. Am J Roentgenol (1997) 169: 409-415.

55. Nunes, LW, Schnall, MD, Orel, SG. Update of Breast MR Imaging Architectural Interpretation Model. Radiology 2001; 219: 484-494.

56. Weinstein D, Strano S. Cohen P, Fields S, Gomori JM. Degani H. Breast Fibroadenoma: Mapping of Pathophysiologic Features with Three-Time-Point, Contrast-enhanced MR Imaging—Pilot Study. Radiology 1999; 210: 233-240.

57. D.G Nishimura, "Introduction to Magnetic Resonance Imaging", Dept Electrical Engineering, Standford University, 1996.

58. D.D Stark (ed), W.G Bradley (ed). "Magnetic Resonance Imaging", Second Edition, 1992, Mosbey-Year Book, Inc, St. Louis Missouri.

59. Kuhl CK. MRI of Breast Tumors (review article). European Radiology 2000; 10:46-58.

60. Greenman RL, Lenkinski RE, MD Schnall. Bilateral Imaging using separate interleaved 3D volumes

and dynamically switched multiple receive coil arrays. MRM 39:108-115 (1998).

61. Teh W, Wilson ARM. The Role of Ultrasound in Breast Cancer Screening. A Consensus Statement by the European Group for Breast Cancer Screening. European Journal of Cancer 1998; Vol 34. No 4. pp 449-450.

62. Deshaw D, Techniques for Imaging-Guided Needle Core Biopsy, in "Breast Pathology – Diagnosis by Needle Core Biopsy". (Rosen PP Ed). Lippincott Williams and Wilkins, Philidelphia, 1999.

63. Teixidor HS, Wojtasek DA, Minik CR. Fine-needle aspiration of breast biopsy specimens: correlation of histologic and cytologic findings. Radiology 1992; 184, 55-58.

64. Fornage BD, Percutaneous needle biopsy of the breast. in "Mastology - Breast Diseases". (Figueria ASS Ed.). Elsevier, New York, 1994.

65. Liberman L. Percutaneous Imaging-Guided Core Breast Biopsy. AJR 2000; 174:1191-1199.

66. Liberman L, Ernberg LA, et al. Palpable Breast Masses: Is there a role for percutaneous imaging-guided core biopsy? AJR 2000; 175:779-787.

67. Willison KM, Fundamentals of Stereotactic Breast biopsy. in "A Comprehensive Approach to Stereotactic Breast Biopsy".(Fajardo LL Ed, Willison KM Ed.). Blackwell Science, Boston, 1996.

68. Fisher PR, Problems and Pitfalls in Core Biopsy. in "A Comprehensive Approach to Stereotactic Breast Biopsy".(Fajardo LL Ed, Willison KM Ed.). Blackwell Science, Boston, 1996.

69. Liberman L, Dershaw DD, Rosen PP, et al. Stereotactic 14-gauge Breast Biopsy: How many core specimens are needed? Radiology 1994; 192:793-795.

70. Parker SH, Jobe We, Dennis MA, Stavros AT, et al. US-guided automated large-core breast biopsy. Radiology 1993; 187, 507-511.

71. Orel SG, Schnall MD, Newman RW, Powell CM, Torosian MH, Rosato EF. MR Imaging-guided Localization and Biopsy of Breast Lesions: Initial Experience. Radiology 1994: 193:97-102

72. Kuhl CK, Elevelt A, Leutner CC, Gieseke J, Pakos E, Schild HH. Interventional breast MR imaging: clinical use of a stereotactic localization and biopsy device. Radiology 1997: 204:667-675

73. Fischer U, Vosshenrich R, Keating D, Bruhn H, Doler W, Oestmann JW, Grabbe E. MR-guided Biopsy of Suspect Breast Lesions with a Simple Stereotaxic Add-on Device for Surface Coils. Radiology 1994: 192:272-272

74. Doler W, Fischer U, Metzger I, Harder D, Grabbe E. Stereotaxic Add-on Device for MR-guided Biopsy of Breast Lesions. Radiology 1996: 200:863-864

75. Fischer U, Vosshenrich R, Doler W, Hamadeh A, Oestmann JW, Grabbe E. MR Imaging-guided Breast Intervention: Experience with two systems. Radiology 1995: 195:533-538

76. Daniel BL, Birdwell RL, Ikeda DM, Jeffery SS, Black JW, Block WF, Sawyer-Glover AM, Glover GH, Herfkens RJ. Breast Lesion Localization: A Freehand, Interactive MR Imaging-guided Technique. Radiology 1998: 207:455-46.

77. Heywang-Kobrunner SH, Heinig A, R.-P. Spielmann, et al. MR-Guided percutaneous excisional and incisional biopsy. European Radiology 1999. 9:1656-1665.

78. Liney G.P, Tozer DJ, Turnbull LW et al. Bilateral Open Breast Coil and Compatible Intervention Device. Journal of Magnetic Resonance Imaging 2000. 12:984-990.

79. Andolina V, Lille S, Willison K. Mammographic Imaging, New York: Lippincott J.B.;1992.

80. H. Sittek, C.Perlet, K. Herrmann, E. Linsmeier, H.Koleum, M.Untch, M.Kessler, M.Reiser. MR Imaging of the breast. Localization of focal breast lesions with the magnetom open at 0.2 T. Volume 37, Issue 9, pp 685-691, Der Radiologe.

81. Jolesz RB. Interventional and Intraoperative MRI: A general overview of the field, Journal of Magnetic Resonance Imaging 8, 3-6 (1997).

82. Lufkin RB. Interventional MR Imaging, Radiology 1995; 197, 16-18 (1995).

83. Silverman SG, Collick BD, Figueria MR, Jolesz FA, et al. Interactive MR-Guided biopsy in an open configuration MR Imaging system. Radiology 1995; 197:175-181.

84. IMA Obdeijn, Brouwers-Kuyper EMJ, Tilanus-Linthorst MMA, Wiggers T, Oudkerk M. MR Imaging-Guided Sonography Followed by Fine Needle Aspiration Cytology in Occult Carcinoma of the Breast. AJR 2000; 174:1079-1084.

85. Corneau RM, Sadikot AF, Fenster A, Peters T. Intraoperative ultrasound for guidance and tissue shift correction in image-guided neurosurgery. Med Phys 2000; 27(4):787-799.

86. Richter K, Prihoda H, Heywang-Kobrunner SH, Hamm B. Description and first clinical use of a new system for combined mammography and automated clinical amplitude/velocity reconstructive breast sonography. Invest Radiol 1997; 32(1):19-28.

Chapter 2

Apparatus and Techniques

2.1 Introduction

As explored in Chapter 1, a biopsy system that could incorporate the sensitivity of contrast-enhanced MRI and the real-time imaging of ultrasound may provide a solution to the problem of obtaining biopsy samples of occult lesions. This chapter details a system and a set of accompanying techniques that brings this idea to fruition. Section 2.2 explains the general concept of the hybrid biopsy technique, while Section 2.3 defines the requirements such a system must fulfill. The apparatus is presented in Section 2.5, while the associated techniques are explained in Section 2.6.

2.2 General Concept: Hybrid Biopsy Solution

The hybrid biopsy system proposed in this thesis detects breast lesions using contrast-enhanced MRI as outlined in Section 1.5.3.3, and targets these lesions using a stereotactic technique as outlined in Section 1.7.3.1.This system is based upon adaptation of the MR imaging techniques and apparatus used in the Sunnybrook and Women's College Health Sciences Centre (SWHSC) screening study. A schematic of the system is given in Figure 2.1 a. Here, the breast of interest is shown in an axial view compressed in a medial/lateral conformation. The compression plates are

specially designed for interventional purposes. The lateral plate has an array of square apertures, which allow access to the breast with a biopsy needle, while the medial plate allows ultrasound imaging through an acoustically transparent membrane. A biopsy needle is depicted approaching the lesion through an opening in the lateral plate at an angled approach. An ultrasound transducer is positioned in line with the lesion and the biopsy needle. With the transducer in this orientation, the needle and lesion can be visualized in the real-time US images as the needle approaches the target.

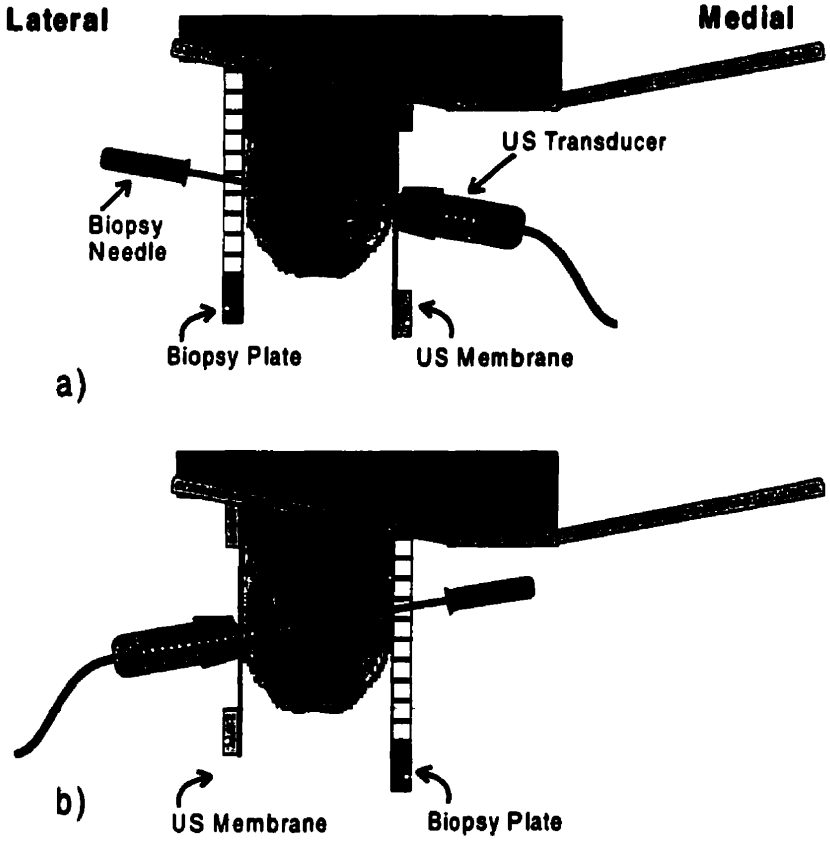

Figure 2.1: Axial schematic of MR biopsy apparatus: a) Compression plates that allow access to the breast for intervention with biopsy needles, and allow US imaging form the basis for the hybrid biopsy system. Alignment of the US imaging scan plane (dashed line) and the biopsy needle trajectory is demonstrated. b) The plates are interchangable, to allow medial or lateral interventional access.

Compression of the breast in this manner offers a number of advantages. The medial/lateral compression reduces the amount of breast motion during imaging and intervention while

minimizing the depth of tissue that the biopsy needle or US beam must traverse. Another feature of this system is the ability to switch positions of the two plates (Figure 2.1b), thereby allowing access to the breast for intervention either medially or laterally. This system enables the radiologist to select either a medial or lateral biopsy approach. This feature is a very important consideration from a clinical standpoint, it is desirable to take the shortest path to the lesion in order to minimize tissue damage in the breast, as well as reduce the likelihood of needle wander.

The entire MR/US hybrid biopsy concept is better demonstrated in Figure 2.2, illustrating interactions of the three components: the biopsy apparatus, the US and MR imaging systems. A candidate for this procedure would be a patient who presented a suspicious lesion on a screening MRI that was occult to other imaging modalities. The breast and the approximate position of the lesion in the breast are determined from the previous screening examination. The patient is positioned in the apparatus so that the breast containing the lesion is compressed between two compression frames while a flexible plastic member compresses the contralateral breast against the chest allowing access to the breast of interest from the medial direction. A pair of MR imaging coils are affixed the apparatus compression frames and the patient is advanced into the MR magnet. The breast is then imaged with two different types of MR pulse sequence sets. The first determines the position of the fiducial origin on the apparatus relative to the breast, while the second is done in conjunction with the injection of gadolinium for lesion visualization. The breast is imaged using the second MR sequence in a dynamic fashion over the entire volume of the breast until the lesion appears. The lesion and fiducial marker coordinates are identified in the resulting MR images and recorded. A calculation is performed using these values to determine the parameters that define the biopsy needle trajectory. The patient is then removed from the magnet, the patient bed detached from the imager, and removed from the MR magnetic field into an adjoining room to prepare for the biopsy. The patient is still in the apparatus with her breast firmly compressed, and should be transported so as not to move her position relative to the apparatus frame. Any movement of the breast would negatively impact the accuracy of the procedure. An US transducer is positioned on the apparatus at the calculated position and angle so as to be co-linear with the calculated biopsy needle trajectory and the lesion.

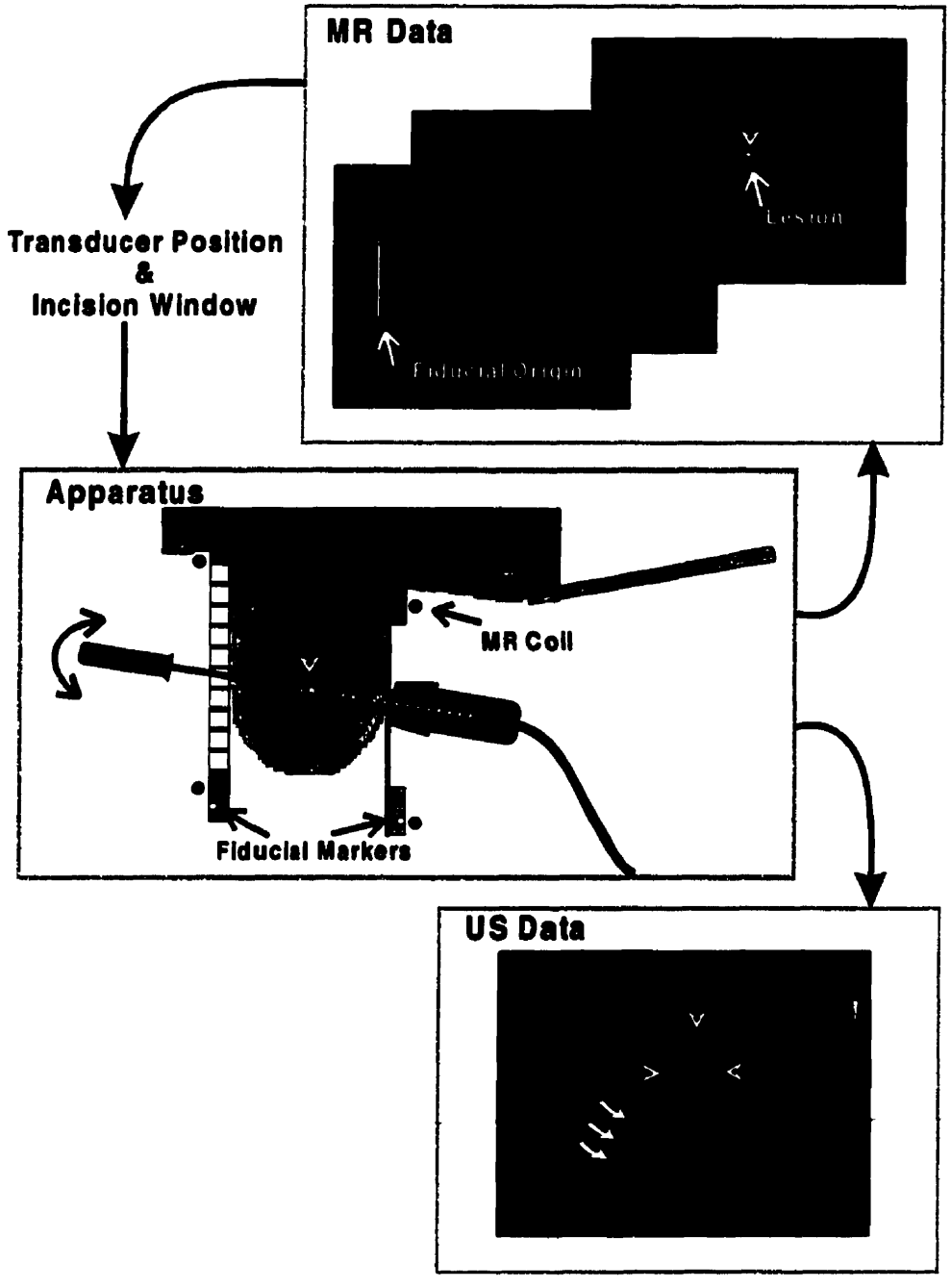

7

Figure 2.2: Hybrid biopsy procedure: The three main components of the biopsy system are demonstrated; apparatus, MR and US imaging systems. The lesion is identified by the arrow head in the breast and in the MR and US images. The breast of interest is compressed in the apparatus, and imaged using contrast-enhanced MRI. In the sagittal images of the MR data, the fiducial origin and lesion will appear. Entering the MR coordinates into a software program determines the needle trajectory and US transducer positions required for the lesion, and needle trajectory to be co-planer. The needle is pushed into the breast while being monitored using the US images. The needle appears as a bright line in the US images (curved arrows indicate a superimposed illustration of a needle). The needle is shown here only as a illustration, in reality it will not be as apparent. The needle position can be validated in pre and post-fire positions with the user modifying the needle position as required.

An incision is then made in the breast, and the biopsy needle is advanced through the tissue towards the lesion. Real-time US can then be used to show the lesion and needle in the middle of the imaging plane during needle insertion. Modifications can be made to the needle trajectory as it advances towards the lesion to correct for lesion movement and needle wander. The biopsy device is fired when the needle is in the proper pre-fire position relative to the lesion. US imaging is again used to determine if the needle did indeed pass through the lesion. The needle is then withdrawn from the breast, and the core sample removed. Using the same incision point, other samples can be obtained at various positions relative to the lesion centre. This improves the probability of accurately sampling the lesion, as well as allows examination of the lesion periphery as is often done in stereotactic mammography procedures.

2.3 System Requirements

In order for this system to operate successfully, five requirements must be met. Each of these described in detail below:

1) Improved access to the breast in a closed MRI system

The traditional design of the bore of an MR magnet is a closed design as described in Section 1.5.3.3. This design makes it very difficult to perform intervention within the bore itself, despite efforts by some groups to perform biopsy inside the bore [10]. Improved access to the breast must be obtained by modification of the patient bed and compression technique.

2) Visualization of the lesion in MR

In this biopsy protocol, the lesion of interest has been detected in a previous screening protocol but this does not guarantee that the lesion will appear during the biopsy procedure. More aggressive compression must be applied to ensure the breast is immobilized for biopsy. Previous investigators have shown that aggressive compression on the breast with a biopsy system such as

this can cause changes in the amount, or kinetics of breast cancer enhancement. However these changes are shown to be relatively small, and do not result in changing the total number of lesions that enhance with and without compression.

Some lesions may appear at the beginning of the procedure, but may vanish as time passes as described in Section 1.7.3.1. Care must be taken to ensure that persistent lesions will appear throughout the biopsy procedure. The MR pulse sequence and imaging apparatus must be designed to take these factors into consideration.

*3) **Accurate delivery of a needle to a point in space guided by a set of MR images***

In order to biopsy the lesion, the needle must be positioned accurately in physical space, based upon the MR data. Although US information will allow for adjustments to the needle trajectory, the initial estimate is based solely upon the MR information. If the lesion is not evident in the US image, then the needle trajectory based upon the MR information must be considered the best estimate.

*4) **Accurate registration of an ultrasound plane and MR visualized lesion***

Image registration between MR visualized lesion and the US imaging plane is required for needle position verification. The registration must ensure that the US transducer acoustic field is prescribed at the same angle as the needle trajectory, and centred on the lesion. Accurate registration of the MR data and US imaging plane will facilitate visualization of the lesion and the needle in the US images. Accurate registration also enables biopsy strategies where viable core samples may still be obtained despite inadequately visualized lesions in the US images.

*5) **Visualization of the needle and the lesion in the ultrasound imaging plane***

In order to monitor the progression of the needle as it approaches the lesion, the needle and lesion

must be visualized in the US images. The real-time US images are used as feedback to correct the needle trajectory if the needle wanders or the lesion moves during needle advance. The method of needle delivery must accommodate the ability to make changes in the position of the needle as it advances. The more accurately the needle and lesion can be visualized, the more certain the operator can be about the results of the biopsy.

2.4 Conceptual Overview

If the requirements in the previous section can be satisfied with a hybrid biopsy system, it follows that the same system could accommodate various biopsy strategies. As outlined in Section 1.6, wire localization and needle core biopsy are functions that are required in conjunction with MRI breast cancer detection. A system that can provide both functions would be advantageous. In fact, the system described in the remainder of this chapter can accommodate the following breast lesion biopsy strategies:

1) MR and US, hybrid guided biopsy
2) MR guided biopsy
3) MR guided wire localization

The first strategy, MR and US guided biopsy, was described in Section 2.2. The second strategy involves guidance of the core biopsy needle using only MR images, and the third strategy involves guidance of a localization needle using the MR images. These methods are outlined in Section 2.6.

2.5 Apparatus Components

The components of the biopsy apparatus can be categorized into four different functional groups: patient support, breast compression, targeting and imaging. These components are examined in

the proceeding sections.

2.5.1 Patient Support

This first grouping of components forms the framework of the apparatus. They are primarily involved with patient support and transport as well as improving access to the breast.

2.5.1.1 Biopsy Bed Frame and Tabletop

To improve access to the breast, a modification had to be made to the patient couch of the standard MR imaging system (GE Medical Systems, Milwaukee, Wis). This patient couch is shown in Figure 2.3.

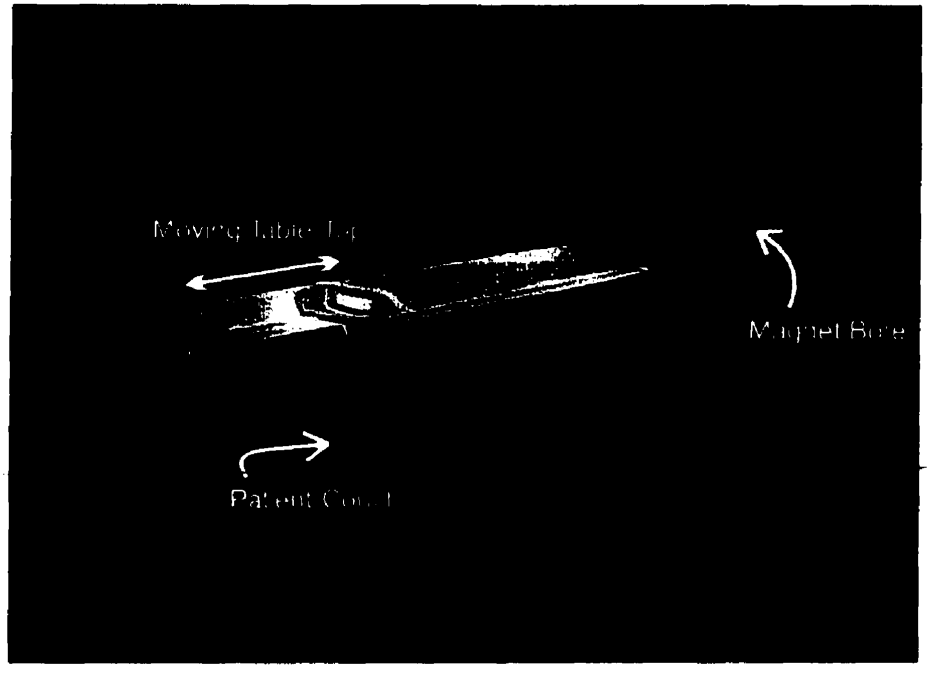

Figure 2.3: MR Magnet and patient couch. Shown here is the front end, and bore of the MR imager. The patient couch has a moveable tabletop that transports the patient into the bore for imaging.

A novel solution was developed by taking advantage of two features of the couch 1) ability to be undocked from the imager 2) ability to lower and raise couch. Lowering the patient couch allows

the addition of a frame for the biopsy system. This frame performs a similar function as that of the standard GE patient couch in guiding the moving tabletop. The frame consists of two sections, which are both attached rigidly to the lowered patient couch. On top of the biopsy frame, a modified tabletop is placed as shown in Figure 2.4. The wheels of the tabletop are designed so that they align with alignment rails of the MR magnet. By raising the bed to the correct height and docking the patient bed, the imager accepts the tabletop as if it was the original. This tabletop is designed in two parts that are held together by the main support frame as described in the next section.

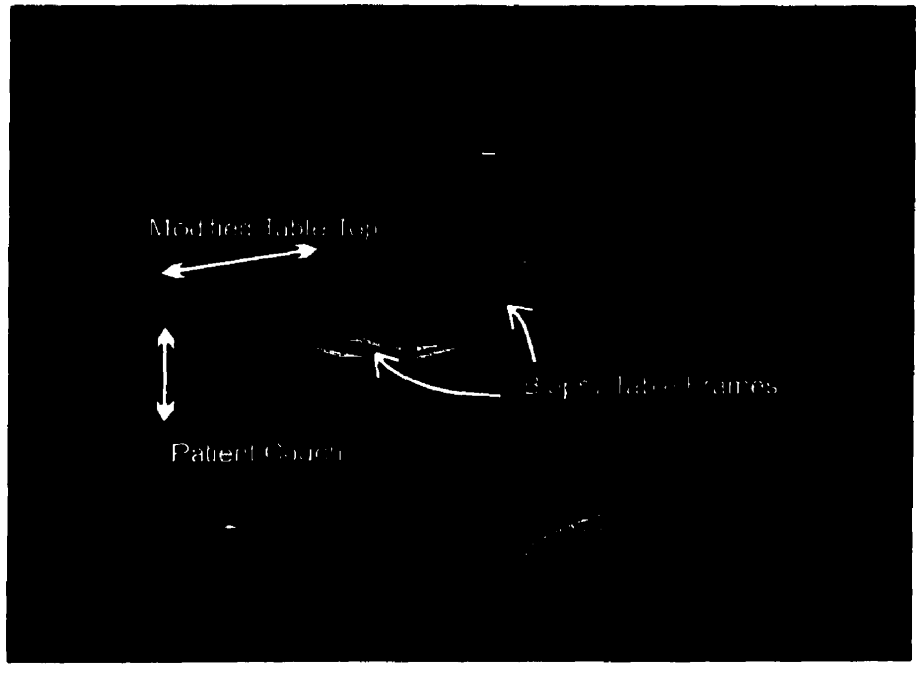

Figure 2.4: Modified tabletop for biopsy purposes: The original patient couch has been lowered and two frame components have been attached. On top of the frame sits a modified tabletop. The tabletop is designed to match the geometry of the magnet bore allowing it to move easily in and out of the bore.

2.5.1.2 Main Support Frame

On top of the modified table top and biopsy bed frame rests the backbone of the biopsy system, the main support frame. This is the framework on which the patient rests her upper torso during the procedure, as well as the structure to which the compression frames attach. The main support

frame of the apparatus consists of two sections that attach to the tabletop. A Delrin bridge member connects these sections so the tabletop and main support frame can move as one continuous piece in and out of the magnet. The bridge member is held in place by two bolts that can be loosened and removed while the patient is on the apparatus. These components are shown in multiple views attached to the modified tabletop in Figure 2.5.

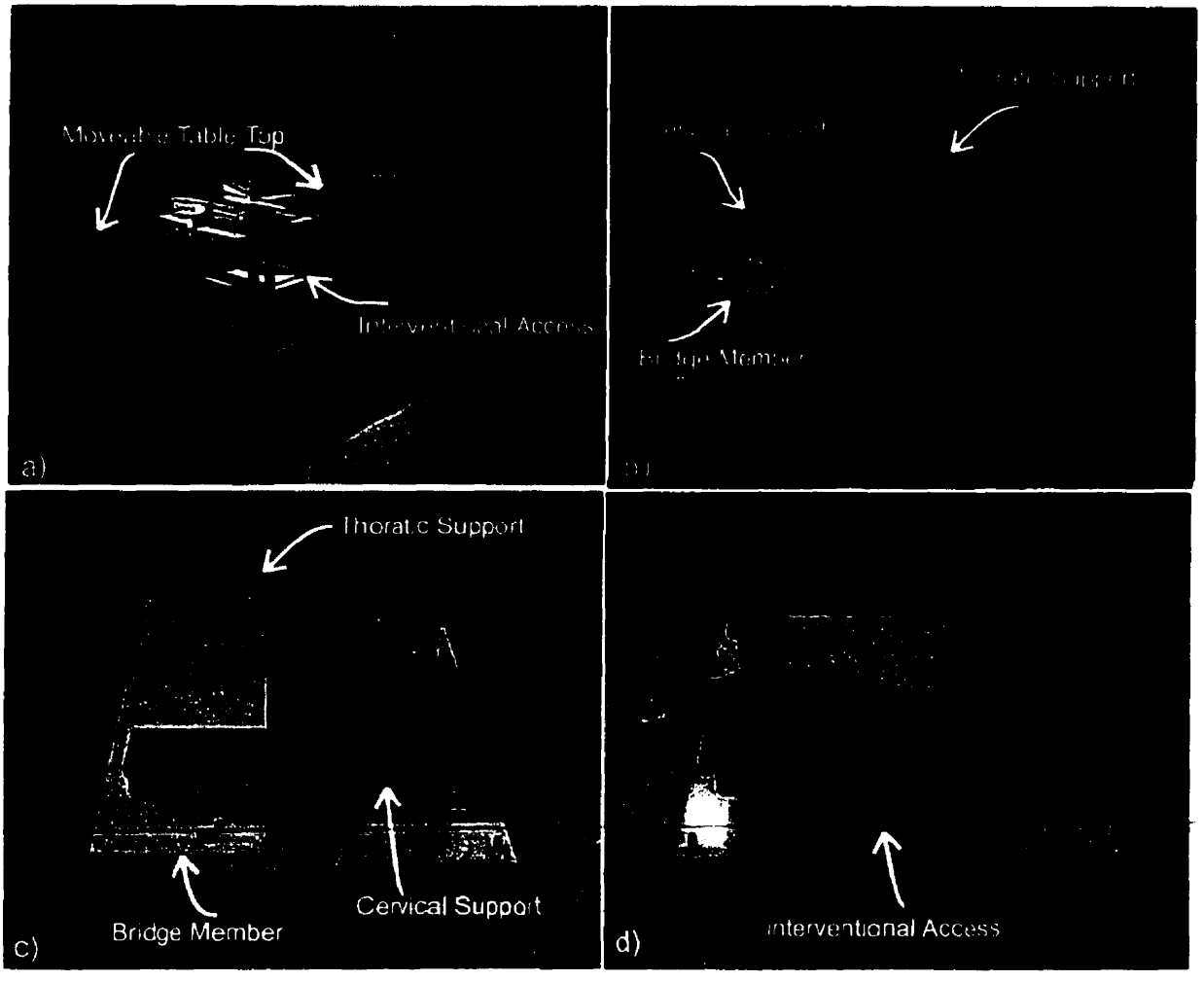

Figure 2.5: Main support frame: a) On top of the modified biopsy bed frame attaches two main support sections. These support sections act as the backbone of the biopsy system, providing support for the patient and attachment points for the compression plates. b) Close up view of main support frame. The upper torso of the patient rests on the cervical support while the upper torso rests on the thoratic support. These two sections are attached to the tabletop linked by the Delrin bridge member. c) Top view. Here we can see the bridge member acting as a linkage keeping the two support frames rigidly attached. This member allows the system to move as a continuous unit in and out of the magnet d) Side view. The amount of interventional access space provided by this system is evident in this image.

The biopsy apparatus is shown completely assembled in Figure 2.6 a. The compression plates, upper bridge member, coils and padding are shown. The patient lies on the apparatus in the prone position with her feet pointing into the bore of the apparatus. The weight of the patient is distributed through all of the components of the support frame with added padding and transition ramp provided for patient comfort. This is better illustrated in the Figures 2.6 b, c and d. The padding and coils have been removed to demonstrate the main support frame components clearly. The addition of the compression frames and the upper support member, Figure 2.6 b, complete the main support frame. The breast of interest is compressed in the medial-lateral conformation, while the other breast is pushed up, out of the way to allow medial access. Only enough compression is used to ensure immobilization of the breast. The system is designed to ensure the patient is comfortable while limiting any motion of the breast. The apparatus is shown in the lateral view, showing the lateral compression frame along with the access allowed by the use of the biopsy bed frame, Figure 2.6 c. The medial view, Figure 2.6 d, shows the medial compression frame and the medial access available when the bridge member is removed.

The tabletop can move in and out of the magnet bore using the standard controls on the magnet console. When the tabletop is completely removed from the magnet, a device locks the tabletop in place. When locked in position, the Delrin bridge member can be removed, providing full access to the breast medially and laterally as demonstrated in Figure 2.6 c and d. The entire patient bed can be removed from the magnet room in the interventional position by undocking it from the magnet, and wheeling it into the adjoining room.

2.5.2 Breast Compression

The second group of components is associated with immobilization of the breast and access for intervention and imaging. Compression is achieved with a pair of frames (Section 2.5.2.1) and interchangeable inserts (Sections 2.5.2.2, 2.5.2.3).

2.5.2.1 Compression Plate Frames

The compression frames support the patient's weight and compress the breast in a medial-lateral conformation. The frames can be locked in place along the tracks of the thoracic and cervical sections of the main support frame with a pair of locking mechanisms and a set of alignment grooves. These grooves ensure the compression frames are geometrically symmetrical for subsequent stereotactic guidance and localization.

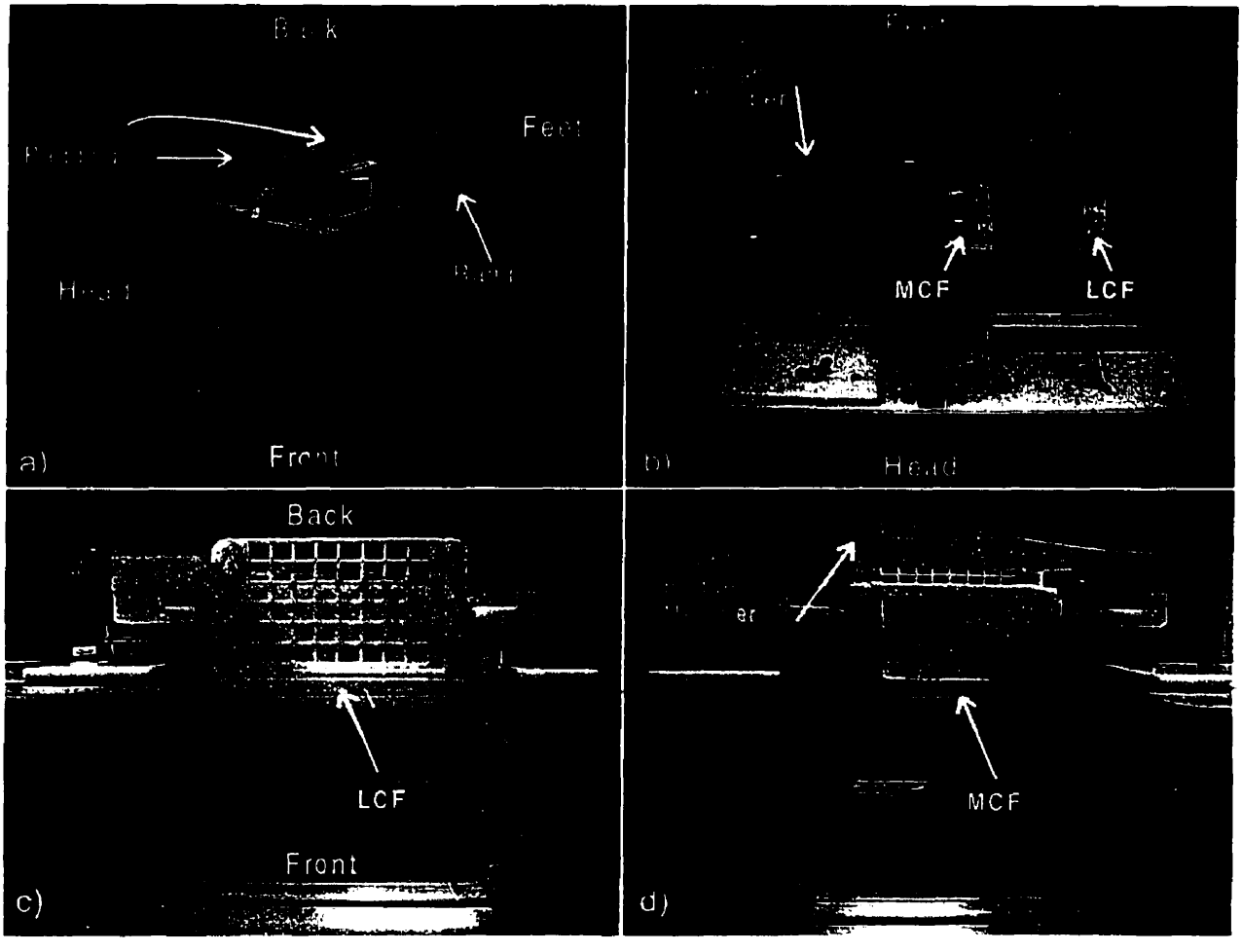

Figure 2.6: Complete biopsy apparatus: These images show different views of the complete biopsy apparatus. a) The lateral and medial compression plates (LCF, MCF), secondary supports and padding on the apparatus, ready for a patient. b) Top view with padding and coils removed. c) Lateral view of apparatus showing biopsy insert. d) Medial view of apparatus showing ultrasound insert. Note the delrin bridge member has been removed for improved access. The upper bridge member acts to hold the contralateral breast out of the way during a procedure.

In order to accommodate biopsy and US inserts, the frames have vertical slots designed to support these structures as shown in Figure 2.7a and b. The frames are shown with the two types of insert in Figure 2.7a and 2.7b. Having the inserts independent of the compression frames offers two advantages; 1) the inserts can be easily sterilized 2) interchanging the ultrasound and biopsy frames allows either a medial or lateral approach for an MR/US guided biopsy. Another important feature of the frame design the vertical and horizontal axis formed by two slots milled into the frame. These slots contain the fiducial markers. These markers are 3.5 mm diameter tubes filled with a solution of distilled water and gadolinium. The centres of the slots are milled at specific positions relative to the edge of the slot for the inserts. Two key slots are also milled into the frame at specific heights relative to the fiducial marker slots as indicated on Figure 2.7 a. These slots accommodate pins of matching geometries allowing a quick and an accurate way to attach an ultrasound transducer positioning system and coil frames.

2.5.2.2 Biopsy Insert

The biopsy insert is used to compress the breast, while still allowing interventional access through a grid of 5/8-inch square openings as shown in Figure 2.7b. The insert is placed in the compression frame corresponding to the desired biopsy approach (medial or lateral). This design allows access to make an incision in the skin to facilitate biopsy needle insertion. The dimensions of the slots fit localization and biopsy plugs (2.3.1, 2.3.2) required for needle positioning.

2.5.2.3 Ultrasound Insert

The ultrasound insert is used to compress the breast, while allowing ultrasound imaging through the acoustical membrane (Figure 2.7a). The insert consists of a frame and a layer of 0.45 mm thick polystyrene. The composition of the polystyrene is a close match to the acoustical properties of human breast tissue. The membrane offers very little attenuation of the acoustic beam in the frequency range of 4-7 MHz as well as little reflection artifact.

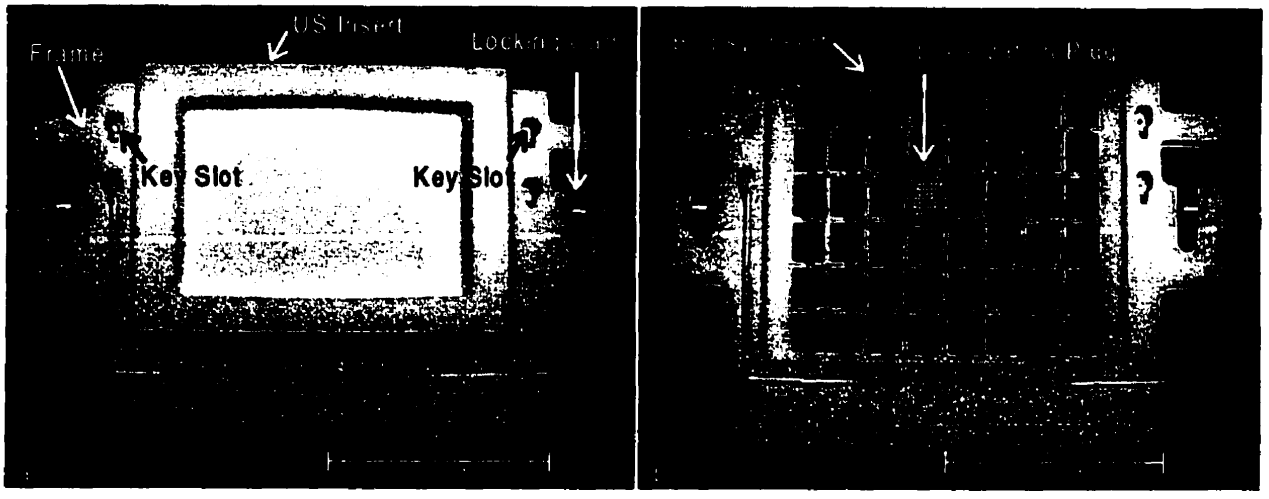

Figure 2.7: Compression plate with interchangeable inserts. a) The medial compression plate is shown here with the US, acoustical membrane insert. b) The inserts are designed to be interchangeable The biopsy insert demonstrated in this image. A localization plug is positioned in one of the access holes.

2.5.3 Targeting and Positioning

A third group of components facilitates the targeting and positioning functions of the system. A square plug that is inserted into the square apertures of the biopsy insert is used to support the orientation and location of a biopsy or localization needle (Sections 2.5.3.1, 2.5.3.2). Similarly a positioning device for the US transducer can be rigidly attached to the compression frame by a set of key slots indicated in Figure 2.7 (Section 2.5.3.3). A device known as a goniometer is used to prescribe trajectory of the biopsy plug mentioned previously (Section 2.5.3.4).

2.5.3.1 Localization plug

In order to accurately guide a localization needle, a plug containing a set of guidance holes is required. This plug fits into the openings of the biopsy insert as shown in Figure 2.7 a). The plug developed for this purpose is shown in Figure 2.8 and is known as a localization plug. It consists of a 7 by 7 array of boreholes (2.5 mm spacing) to fit a 20-gauge needle.

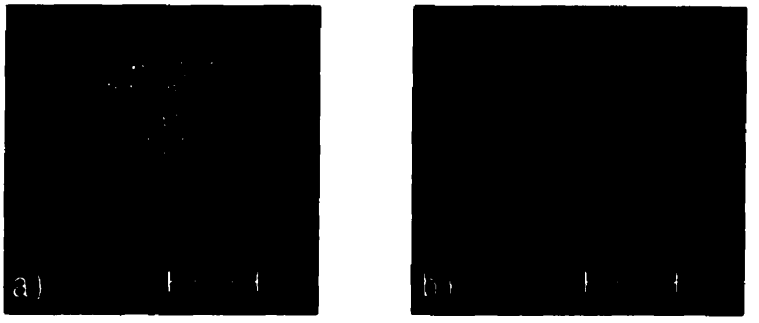

Figure 2.8: Localization plug. a) Front view. b) Side View. It is designed to fit the openings of the biopsy plate.

2.5.3.2 Biopsy plug

A method to guide a biopsy needle at a set trajectory is accomplished with a plug shown in Figure 2.9. This plug functions as an angled needle guide for a 14-gauge biopsy needle. The plug fits snug into the biopsy insert apertures in a specific orientation defined by a small locator pin in the plug, and an offset slot in the insert. The plug consists of three components, a ball and shaft, a base and a collar. The ball fits in a pocket in the base, and the collar screws into the base, forming a simple ball joint. When the collar is loose, the shaft can pivot freely. When the collar is tightened, the shaft is locked in a specific orientation. The position of the shaft is defined uniquely by two angles as shown in Figure 2.9 b and c. These angles are respectively known as the arch angle, and the disc angle. The device that precisely defines these angles is explained in Section 2.5.3.3. A pin on the base of the biopsy plug uniquely defines the orientation of the plug. This locator pin fits into a set of alignment slots located on the biopsy insert. The locator pin and alignment slot ensure that the biopsy plug can only be positioned into the biopsy insert in one orientation.

2.5.3.3 Goniometer

A device used to prescribe the trajectory of the biopsy plug accurately is demonstrated in Figure 2.10. This device, known as a goniometer, allows the two angles of the biopsy plug to be set independently. The frame of the goniometer consists of a square base with a central circular opening and a semicircular arch. A circular insert, or base disc insert fits into the centre opening

and rotates relative to the base, while a collar slides along the circumference of the arch. The movement of these two components allows the biopsy plug angles to be set independently on linear scales. The biopsy plug fits into a slot at the centre of the base disc insert such that the centre of the ball joint corresponds to the centre of the arch. The biopsy plug can only fit into the slot in one orientation so that the locator pin in the biopsy plug base matches the corresponding locator slot.

An extender arm fits over the shaft of the biopsy plug linking it to the arch collar. When the biopsy plug collar is loose, the ball joint is free to move with two degrees of rotation. The biopsy plug arch angle can be set by moving the arch collar, while the plug disc angle can be set by rotating the base disc insert. When both angles are defined, the biopsy plug collar is tightened locking the shaft in the trajectory defined by the goniometer.

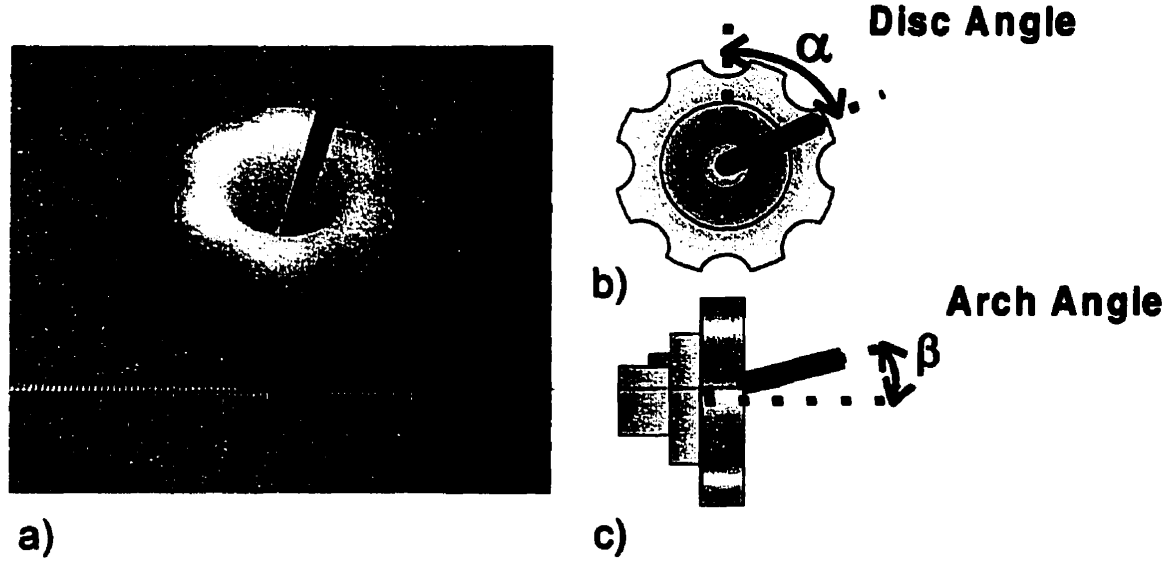

Figure 2.9: Biopsy plug. a) The plug consists of a base, collar, ball and shaft shown in this image. The shaft holds a 14-gauge biopsy needle. b) Biopsy plug shown assembled: The shaft is capable of freely pivoting when the collar is loose. Tightening the collar fixes the shaft orientation. c) Top view of the plug: The angle that the shaft makes relative to the base defines one trajectory coordinate. d) Side view of plug: The other coordinate is defined by the maximum angle the shaft makes with the centreline of the plug.

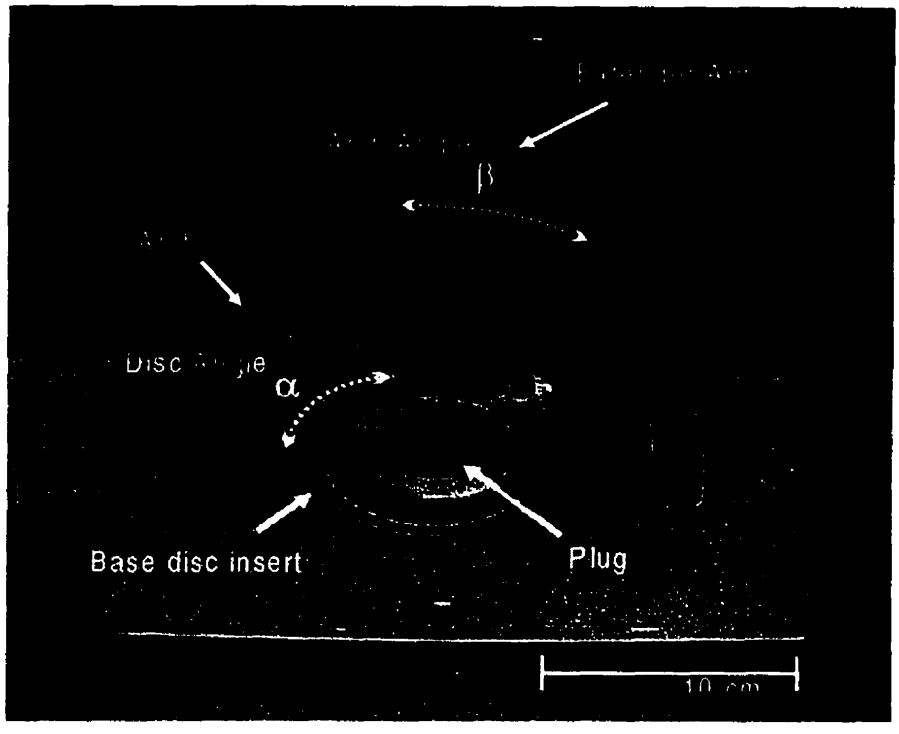

Figure 2.10: Goniometer with biopsy plug. The goniometer was designed to set the angles of the biopsy plug. The arch collar and base disc insert move and lock into position independently. The dashed arrows indicate direction of movement. Two scales on the arch and the base define 1-degree gradations.

2.5.3.4 Ultrasound Transducer Positioning System

The ultrasound transducer positioning system (UTPS) shown in Figure 2.11a attached to the lateral compression frame holds the US transducer at a known position relative to the fiducial axis. The UTPS consists of a frame, main platform and turret. The frame of the UTPS attaches to the lateral and medial compression frames by two pins, which fit into two corresponding key slots. The US transducer is held in the UTPS by a padded casing that slides into the turret.

The system allows 5 degrees of freedom for transducer positioning. The coordinate system associated with the UTPS is shown in Figure 2.11b. The linear 1mm-gradation scales affixed to the UTPS define the position of the transducer accurately in the x and y directions. The angular 1-degree gradation scales affixed to the UTPS define the angle of the transducer in the x-z and y-z planes. By rigidly linking the UTPS and the compression plates, the x and y axis are parallel to the

axis of the fiducial axis and the UTPS x and y position scales are at known positions relative to the fiducial origin. This greatly simplifies the mapping of positions relative to the fiducial axis and the UTPS as will been seen in later sections.

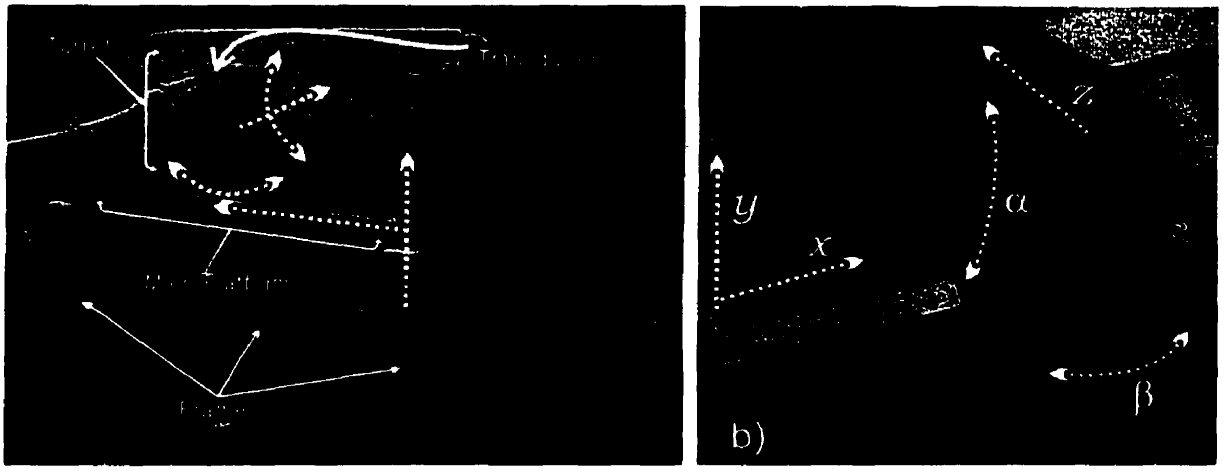

Figure 2.11: Ultrasound transducer positioning system (UTPS). a) The device attaches to the lateral, or medial compression plates in place of the MR rf coils. The US transducer is held in a padded casing with its imaging plane corresponding to a coronal orientation. It is capable of movement in 5 dimensions as defined by dashed lines. b) Scales are associated with each degree of freedom allow accurate positioning of the transducer.

2.5.4 Imaging Components

2.5.4.1 MR Coils

The MR coils are used to detect the free induction decay signal from a single breast. The imaging coil configuration for this apparatus consists of a pair of coils operating as a phased array. This configuration has been successfully used in the imaging procedure described in Section 1.5.3.3. The coils are attached to the lateral and medial compression plates by two pins, which fit into two corresponding key slots. The ability to remove the coils quickly and easily after MR imaging improves access for intervention.

2.6 Techniques

Techniques were developed to satisfy the requirements outlined in Section 2.3. These techniques are required to detect the lesion using MRI, reference the lesion to the apparatus, position the needle relative to the apparatus to intercept the lesion and verify the position of the needle relative to the lesion using MR or US imaging. These techniques are explained in the following sections:

1) Stereotactic Reference
2) MR Lesion Visualization
3) Coordinate System Mapping and Positioning
4) Needle Position Verification and Modification

2.6.1 Stereotactic Reference

An accurate method to reference the position of an MR visualized lesion to a position on the apparatus is necessary for needle positioning. Many different stereotactic referencing strategies have been used in current biopsy systems, as discussed in Chapter 1. These strategies involve imaging a fiducial marker, which is located at a known position relative to a set of needle access holes. In the process of imaging the fiducial marker, its position may be inaccurate due to susceptibility effects and non-linear magnetic fields. The technique described in this section takes these phenomena into consideration in an attempt to improve the positional accuracy of the system.

The definition of the fiducial marker position is critical to the success of accurate needle positioning and image registration. The fiducial marker provides a reference point between MR space, apparatus space and US space. The MR space refers to positions within the MR images, the apparatus space refers to positions on the apparatus and within the breast, while the US space refers to positions within the US images. These spaces each are defined by unique coordinate systems.

2.6.1.2 Coordinate systems

Coordinates relative to the body in the prone position define the MR space, which is depicted on Figure 2.12. These coordinates are used to define positions in the MR images and can be read off the user console by moving a cursor to a position within the image. The three Cartesian axes are defined by right/left, anterior/posterior and superior/inferior orientations. Every point in MR space is defined with the letter (L/R, A/P and S/I) to define the axis and a number to define the distance from origin in millimeters (i.e. R123.4, A89.4, S99.4). The origin of this coordinate system is defined when the imaging session is initiated. A function called *landmarking*, references a physical position on the patient bed with the origin of the MR coordinates. The positions of the MR scan planes are defined by this coordinate system, and a function called image prescription allows scan planes to be defined relative to one another while maintaining the same relative MR positioning system.

The pair of fiducial axis located on the medial and lateral compression frames define the apparatus space. The coordinates (X_M, Y_M, Z_M) define the medial and (X_L, Y_L, Z_L) define the lateral origin as depicted on Figure 2.12. The horizontal and vertical fiducial slots define the Cartesian axis and where they cross is the origin. Every position in apparatus space can be defined relative to the medial or lateral fiducial axis. When the frames are aligned with the apparatus and the patient bed, then the axes of the apparatus space correspond to the axes of the MR space.

Coordinates relative to the centre of the US transducer acoustic field define the US space. These coordinates are used to define a position in the ultrasound image. These axes are defined by the axial and lateral directions relative to the orientation of the transducer. The positions are defined as transducer (X_{OFFSET}, Z_{DEPTH}) on Figure 2.12. The origin of this coordinate system is defined by the front and centre position in the acoustic field.

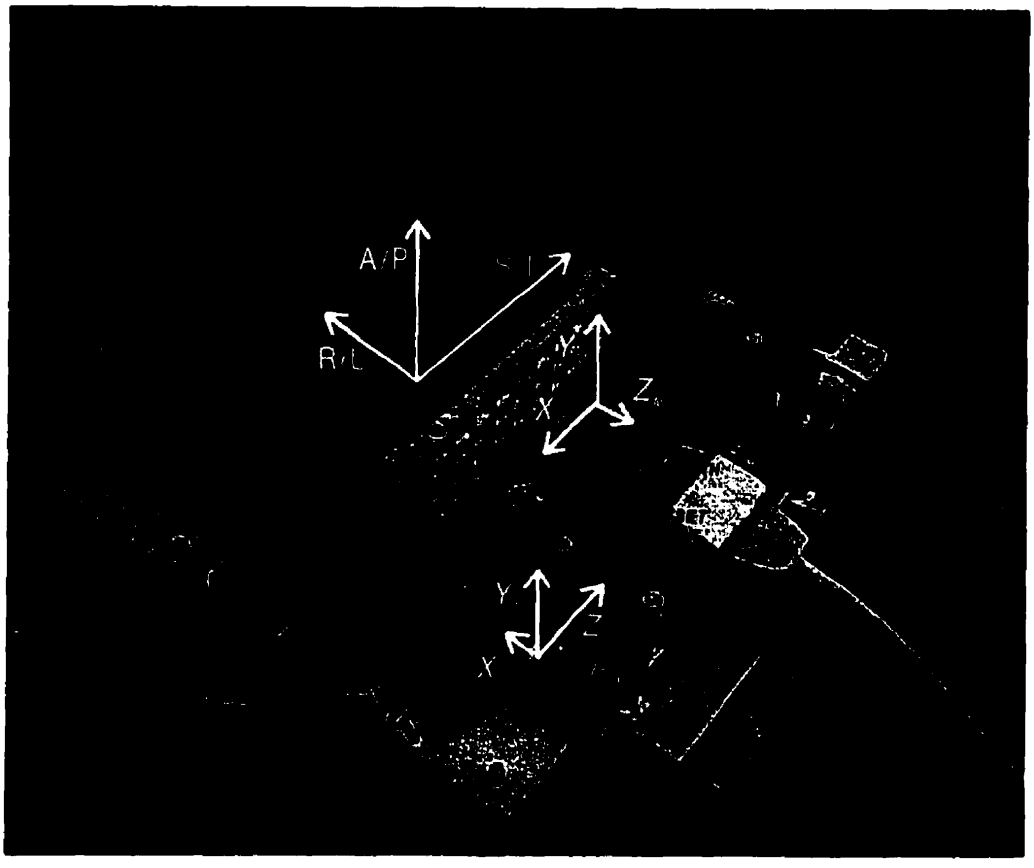

Figure 2.12: Coordinate Systems associated with biopsy apparatus. Three different Cartesian coordinate frames define three different spaces as shown here: 1) the MR space coordinates (R/L, A/P, S/I). 2) Apparatus space coordinate frames are located at the fiducial marker origin on the medial and lateral frames (X_M, Y_M, Z_M), (X_L, Y_L, Z_L). 3) US space is defined at the front, and middle of the transducer face on a plane defined by the body of the transducer (X_{OFFSET}, Z_{DEPTH}).

2.6.1.3 Fiducial origin determination

Fiducial axes are defined by a pair of fiducial markers on the compression frames. The imaging pulse sequence that is used to define these fiducial axes must take into consideration the physical phenomena that will effect its position in the MR images. Positions within an MR image are assigned to signals through the use of three independent gradients, which manipulate the frequency and the phase of MR signals as explained in Chapter 1. These gradients, known as the slice-select, phase-encode and frequency encode gradients (G_Z, G_Y, G_X), are superimposed upon the main magnetic field B_0 to change the magnetic field strength at a point within the imaging

space as follows:

$$B(x,y,z) = B_0 + G_x(t)x + G_y(t)y + G_z(t)z$$

Anything that changes this magnetization value $B(x,y,z)$ from its desired value, results in a spatial distortion in the resulting image. This may occur from many sources, including magnetic susceptibility of an object in the magnetic field, non-linearities associated with the gradients or inhomogenities of the main magnetic field. Any object with a non-zero magnetic susceptibility will change the magnitude of the local magnetic field that it is placed into. This can be modeled in the above equation as an added perturbation to the local field at a point:

$$B(x,y,z) = B_0 + G_x(t)x + G_y(t)y + G_z(t)z + \Delta B(x,y,z)$$

This field perturbation is a function of the geometry and susceptibilities of objects in the local imaging region. This magnetic susceptibility is known to have a substantial affect on the apparent position of objects within an MR image. This is explained in detail in the papers referenced at the end of this chapter [1-7]. These susceptibility differences play a role in apparent displacement of objects in the frequency encode direction (G_X) of MR images and displacement of objects between slices due to inaccurate slice selection (G_Z). However, the positions in the phase-encoding direction (G_Y) are not affected [6]. Further spatial distortions occur due to magnetic field inhomogeneties in the main magnetic field created by the scanner and the non-linearities associated with the gradients. The main magnetic field of the MR scanner is not perfectly uniform. It changes slightly across the field of view, which results in different precession frequencies within an object. This was a major problem with MR systems of the past, but methods to correct for this through magnet shimming and distortion correction schemes have made it less of a concern [3]. On the other hand, the non-linearity of the gradients poses more of a problem. The reconstruction of the MR image from the detected signals done is under the assumption that the gradients used to encode the phase, frequency and slice selection are linear. In practical use, the gradients are non-linear as explained in a paper by Sumanaweera [3]. He explains that there are essentially three

types of gradient non-linearity distortion in 2D MR imaging which he refers to as; the "*barrel aberration*", the "*potato chip*" and "*bow tie*" effect.3 In a given slice, the phase-encode and frequency encode gradients produce a warped image as depicted in Figure 2.13b. The *potato chip* effect results in an MR slice being warped into a saddle-shaped surface, while the *bowtie* effect results in a the MR slice not being a constant slice thickness, but rather it increases towards the edges. All these warping effects become worse as you move away from the isocentre of the gradient coils.

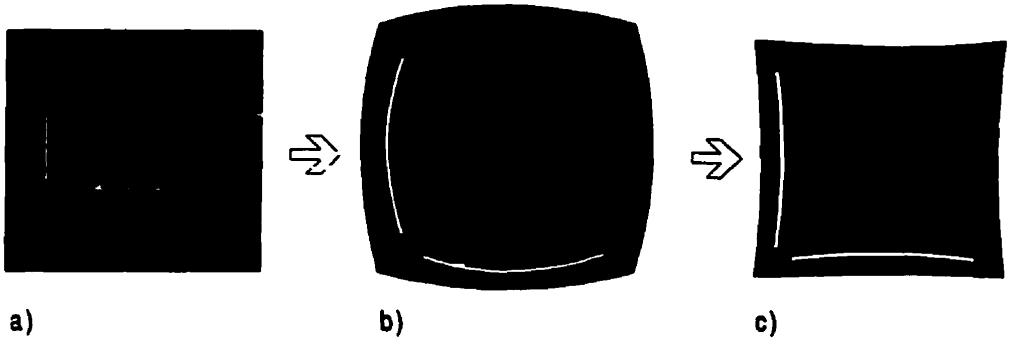

Figure 2.13: "Barrel aberration" and effects of non-linear gradients. a) An ideal 2D spin echo MR image of fiducial markers with no grad warp effects. b) Image of the fiducials non-linear gradients and no correction. c) Correction provided by MRI manufacturers. The resulting spatial correction for the pixels in the image is actually an over correction around the edges of the image.

Magnet manufactures have implemented a form of 2-D correction in the image reconstruction software for the *barrel aberration* as depicted in Figure 2.13c. This has been reported to correct for distortions that are as large as 4mm in a 200 by 200 mm view, and reduce them to 1 mm [3]. Other techniques have been suggested to improve this correction, as well as correct for the more complicated *potato chip* and *bow tie* effect [3,5,7].

The ability to use MR to guide interventions precisely has become a major issue for neurosurgical applications. Many different groups have independently attempted to improve the spatial accuracy of MR images [2-7]. It was found that the use of 3D imaging sequences where phase encoding is used in two directions with full volume excitation and weak slice selection provided substantial

3 These terms are used throughout published literature and as a result will be used in this thesis.

improvements in spatial accuracy. This imaging technique provided a substantial improvement where an error greater than 2 mm was identified in 0.8% of the imaged volume, compared with 12% in the comparable 2D imaging sequence [5]. This improvement was determined to be associated with the reduction of some of the gradient non-linearity effects, such as the *potato chip* and *bowtie* effect, as well as reducing the errors in the frequency-encoded directions.

These problems were considered in the context of the imaging sequence developed for the breast biopsy procedure. In order to ensure all three coordinates associated with the fiducial origin are determined properly, three separate imaging sequences were used, each one determining only one coordinate for each medial and lateral fiducial marker. It was decided that the sequence could take advantage of the fact that breast screening protocol explained in section 1.5.3.3 required an axial and coronal spin-echo sequence to determine the position of the breast in the imaging field before contrast agent is administered. The three imaging series are listed in Table 2.1 and shown in Figure 2.14. Using the MR user console, the positions of the fiducial markers can be measured from the screen. The use of these three scans is such that the measurement direction is always associated with the phase-encode direction.

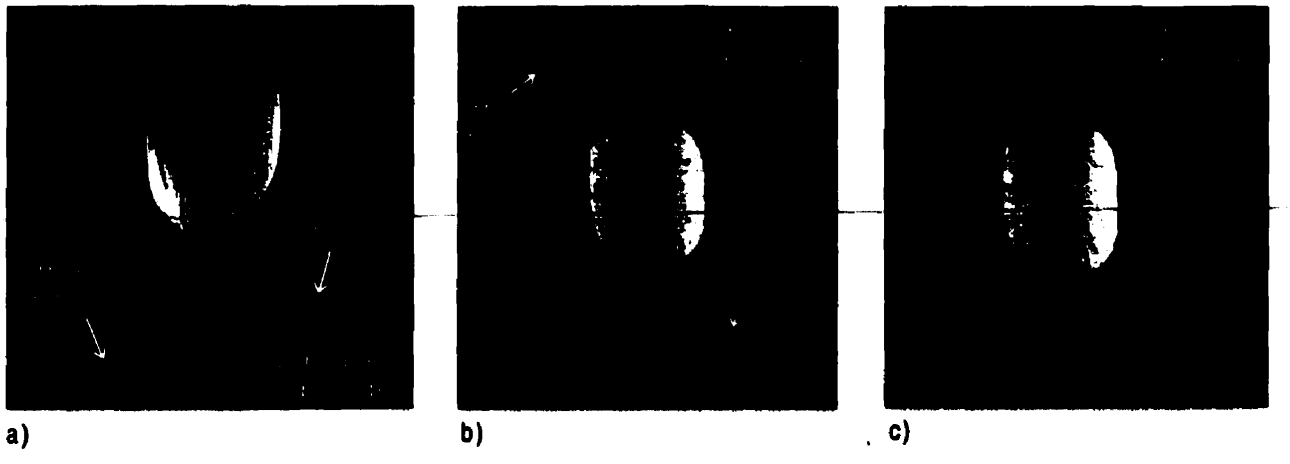

Figure 2.14: Imaging sequence to determine fiducial positions. a) Axial spin echo image of a breast in the compression apparatus. Fiducial markers appear as indicated. The fiducial positions in the phase encode direction determine the A/P position of the fiducials. b) Coronal spin echo image of the same breast and fiducials. The fiducial positions are accurate in the L/R direction corresponding to the phase encoding. c) Identical coronal spin-echo image as b), except the phase encode has been switched. The fiducial positions in the S/I direction are determined in this image.

This technique only requires one extra coronal scan compared to the clinical screening procedure. Imaging the fiducials in this manner eliminates the shifts associated with the suspectibility change from air to the gadolinium-doped water contained in the fiducials, and reduces the dependence on accurate slice selection. This imaging method does suffer from the fact that the fiducial markers are located on the outside edges of the MR images far from the isocentre of the gradient coils, where gradient warp is the worst. The imaging sequences invoke the "*gradwarp*" correction algorithm supplied with the GE Signa system, but this is believed to have some associated inaccuracies as is demonstrated in Figure 2.13. [4]

Slice Orientation	Axial	Coronal	Coronal
Frequency Encode	L/R	S/I	L/R
Coordinate Determined	A/P	L/R	S/I
Pulse Sequence	T1-weighted 2D Spin Echo	T1-weighted 2D Spin Echo	T1-weighted 2D Spin Echo
Acquisition Matrix	256 x 128	256 x 128	256 x 128
Field of View	24 cm x 24 cm	26 cm x 26 cm	26 cm x 26 cm
Pixel Size (freq,phase)	0.9x1.8 mm	1.0x2.0 mm	1.0x2.0 mm
Slice Thickness	7.0 mm	7.0 mm	7.0 mm
Time per Acquisition	70 seconds	70 seconds	70 seconds

Table 2.1: Imaging sequence used to determine fiducial marker location. To accurately determine the medial and lateral fiducial marker origins, three separate imaging series are used.

2.6.2 MR Lesion Visualization

In order to visualize the lesion an MR contrast enhanced imaging procedure is required. The procedure explained here is based upon the fat-suppression sequence described in Chapter 1. As discussed in requirement 2, it is presumed that the lesion has already been detected in an MR

4 The term *gradwarp*, is a term coined by General Electric to describe the algorithm to correct for the image warping associated with non-linear gradients. This term will be used throughout this thesis.

screening procedure, therefore the breast, and the quadrant that the lesion appears in are already known. The breast of interest is moderately compressed in the biopsy apparatus. Compression of the breast should be enough to ensure that the breast is immobilized, but not so much as to affect visualization of the lesion [8].

The imaging sequence used to detect the lesion is listed in Table 2.2. The sequence is a T1-weighted fat-saturated 2D-spoiled gradient sequence, with an intravenous injection of *0.1mL/kg* concentration of gadolinium. The sequence is fast, allowing good temporal resolution to identify the lesion at the earliest possible instance. The fat-saturation ability of the sequence provides a mechanism for visualization of the lesion without image subtraction, which simplifies the procedure. A scan prior to the injection of the gadolinium is typically done to ensure the image quality and fat suppression is satisfactory.

Lesion Visualization and Needle Verification Imaging Sequences		
Imaging Parameter	Pulse Sequence for Needle Verification	
Slice Orientation	Sagittal	Axial
Frequency Encode	A/P	A/P
Pulse Sequence	2D T1-weighted SPGR	2D T1-weighted Spin Echo
Acquisition Matrix	256 x 128	256 x 128
Field of View	18 cm x 18 cm	24 cm x 24 cm
Pixel Size (freq,phase)	0.7x1.4 mm	0.9x1.8 mm
Fat Suppression	Fat Saturation	Fat Saturation
Slice Thickness	5.0 mm	3.0 mm
Time per Acquisition	20 sec	1:20 min

Table 2.2: Imaging sequence used to detect the lesion as well as verify needle positioning. The same imaging sequence is used before contrast agent is injected, and many times after injection. The breast is imaged until the lesion becomes evident and its position can be determined using the user console. After the needle is positioned this same sequence is used to validate proper positioning in the sagittal plane. A final verification sequence listed in the second column is used to determine if the needle has been placed at the appropriate depth.

2.6.3 Coordinate System Mapping and Positioning

2.6.3.1 Mapping MR Space to Apparatus Space

Mapping between positions in the MR and apparatus space requires knowledge of the precise position of the fiducial origin and lesion in a set of MR images. The mapping between these two spaces is simply a shift of the origin when the compression frames are aligned with the MR imaging axis. This mapping is demonstrated in Figure 2.15. A target in MR space can be mapped to a position relative to the medial and lateral compression frame. Once mapped to apparatus space a calculation can be made to position a localization or biopsy needle to intercept this point. In order to facilitate these calculations, a computer program was developed that gives localization and biopsy needle positions when the fiducial origin and lesion coordinates from the MR image set are provided as input.

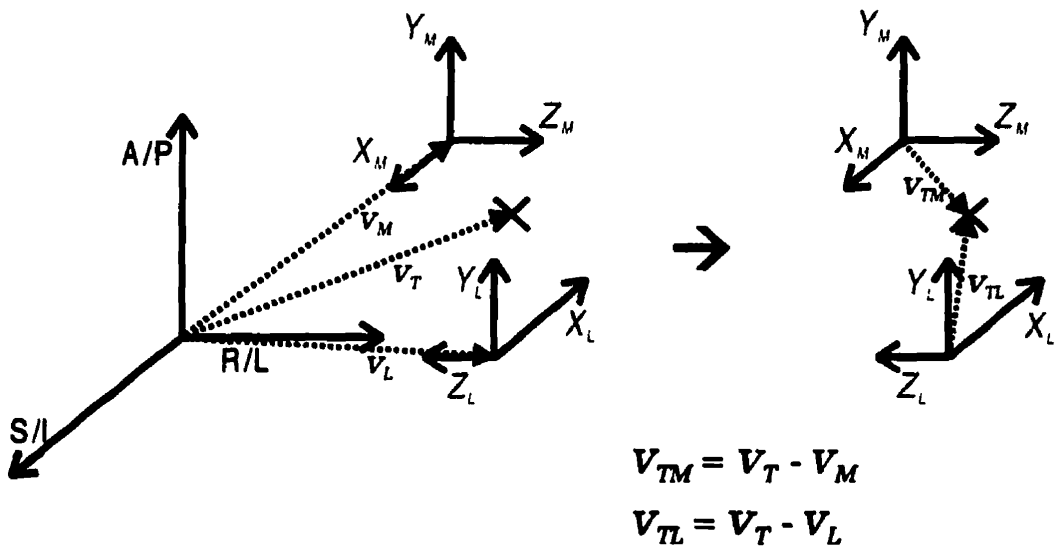

Figure 2.15: Vector representation of MR to Apparatus mapping. Shown on the left are the axes associated with MR coordinate space, and the medial and lateral apparatus space, respectively labeled with M, L subscripts. The vector V_T indicates the position of the target relative to the MR space while vectors V_M and V_L indicate the position of the medial and lateral fiducial origins. Simple vector subtraction allows the position of the target to be referenced relative to the apparatus as indicated by vectors V_{TM} and V_{ML}.

2.6.3.1.1 Localization Needle Positioning

Once the lesion position is mapped to a position relative to the apparatus, a set of needle

positioning parameters may be calculated. These parameters are calculated as demonstrated in Figure 2.16. The fiducial origin is located at a fixed position relative to the windows of the biopsy insert. This allows calculation of the window index that is closest to the lesion in the apparatus space x/y plane by minimizing the distance from the window centre to the lesion centre. Once the appropriate window is determined, the localization plug borehole index is determined by minimizing the distance from the hole to the lesion centre again defined as a vector. The needle depth required is calculated by determining the distance from the lesion centre to the back edge of the localization plug. In most cases there will be a compromise associated with the positioning of the needle in the x/y plane due to a finite number of bore holes in the localization plug, and window positions in the biopsy insert.

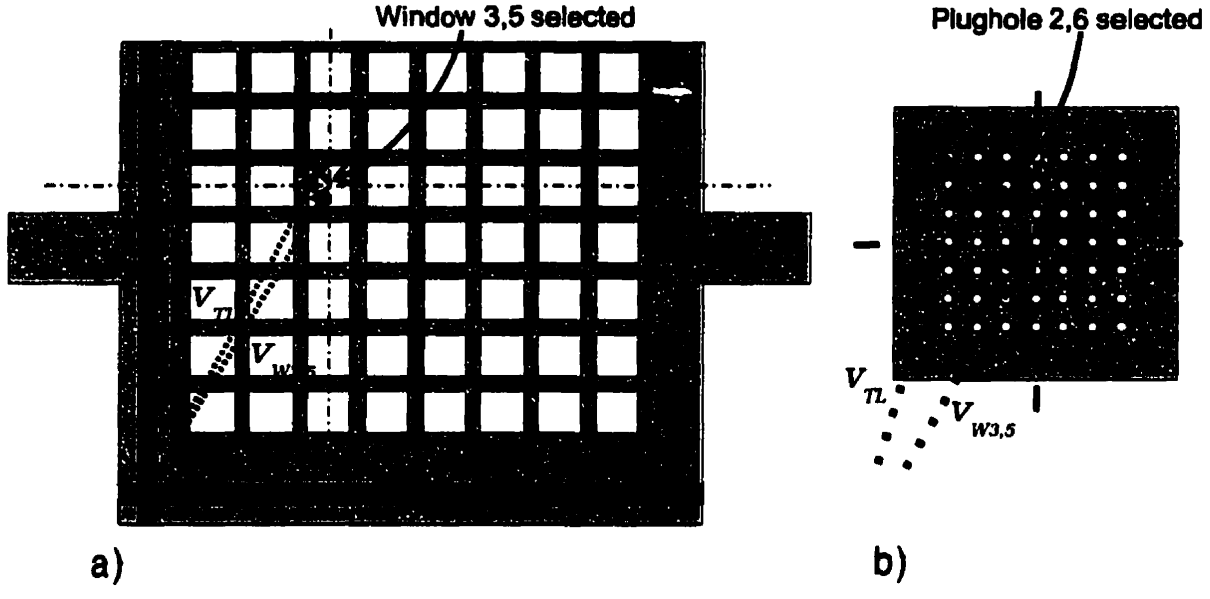

Figure 2.16: Illustration of needle localization calculation. a) Shown here is a lateral view of a compression plate with a target superimposed. The coordinates of the target are known relative to the apparatus fiducial marker origin. A simple calculation determines the closest access window to the target, $V_{W5,5}$. b) Shown here is the front view of the localization plug positioned into window 3,5. A simple calculation determines the closest plughole to the target centre. The required depth of the localization needle is determined in a similar manner.

2.6.3.1.2 Core Biopsy Needle Positioning

The calculation of the core biopsy needle parameters is done slightly differently than the localization needle. The parameters defining the core biopsy needle position are the index of the

biopsy insert window, the two angles defining the biopsy plug trajectory and the depth of the needle. The biopsy window index is calculated in the same manner, but the biopsy plug trajectory involves a mapping from a Cartesian coordinate system to a polar coordinate system corresponding to the goniometer. This mapping is demonstrated in Figure 2.17.

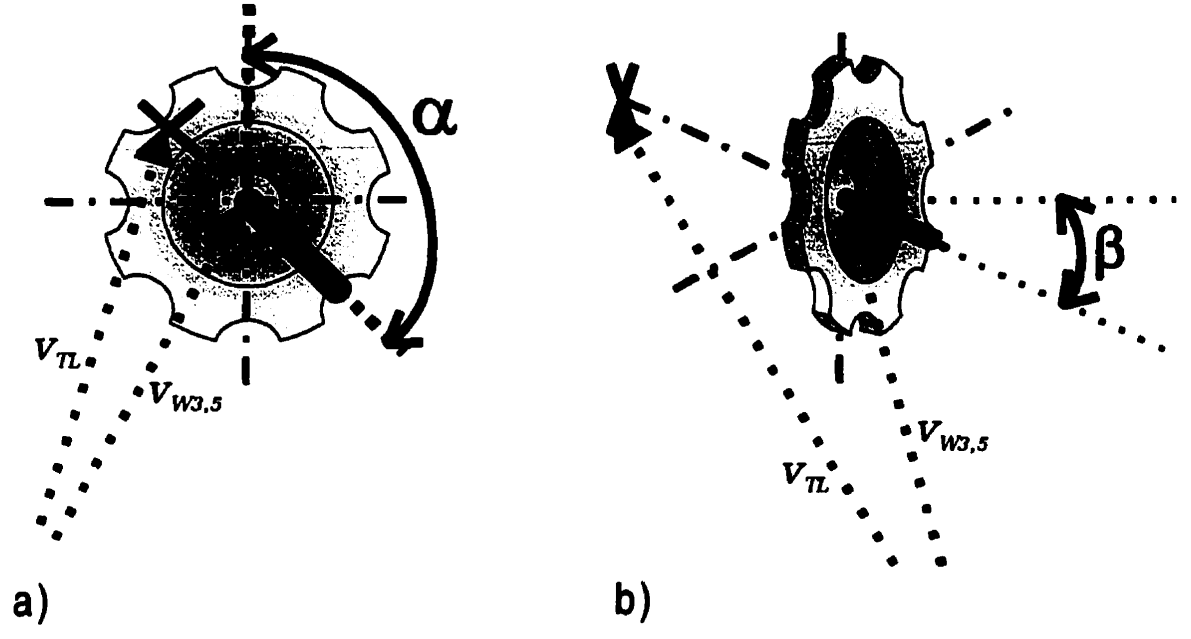

Figure 2.17: Illustration of the biopsy plug angles associated with the position of the target vector v_{TL} and access window centre $v_{W3,5}$. Using these two vectors the required needle trajectory angles can be calculated using simple trigonometric relations. a) The disc angle is determined by determining the angle of the vector that links the centre of the plug, to the centre of the lesion in the x-y plane. b) The arch angle is calculated by determining the angle of the vector linking the target and the centre of the plug relative to a vector perpendicular to the x-y plane in 3 space.

The computer program will calculate the positioning parameters based on the minimum distance from the biopsy plug centre to the lesion centre, but a feature in the program allows the user to override this. By entering the desired biopsy window into the program, it will determine the required plug trajectory from that window centre. This is an important feature if multiple samples of the lesion are required. In order to limit the number of incisions made in the breast, it is important to use the same incision point, and therefore the same biopsy window. The positioning of the biopsy needle using the angulated biopsy plug does not suffer from the problems associated with the finite positioning of the localization plug, but limited access is a limitation as examined in Chapter 3.

2.6.3.2 Mapping MR space to US space

Mapping positions from MR space to US space involves positioning the US transducer relative to the apparatus, then mapping the position of the lesion relative to the transducer. Positioning of the US transducer is done using the UTPS (Section 2.3.4), which can be affixed to the apparatus compression frame. The UTPS enables accurate positioning of the transducer given a set of positioning parameters. The positioning parameters are the x and y transducer position and the transducer angle. These parameters are calculated as demonstrated Figure 2.17. The same computer program used to determine needle trajectory is used to determine the transducer positioning parameters.

The transducer angle is defined to match the angle of the biopsy needle trajectory. The transducer y coordinate is calculated so the plane of the transducer intercepts the lesion centre, and the x coordinate is calculated so the lesion appears in the centre of the transducer acoustic field in the x-z plane. The lesion position in US space is determined by calculating the lesion position relative to the front and middle of the US transducer. The two parameters that define lesion position in US space are the lesion z depth and the x offset. The z depth is determined by calculating the distance from the lesion centre to the front of the transducer. The x-offset component is 0 when the transducer is centred on the lesion in the x direction.

2.6.3.3 Registration of US to MR data

Positioning the transducer to intercept the lesion and biopsy needle trajectory effectively registers the ultrasound plane to the centre of the MR visualized lesion at a defined angle. The computer program allows the user flexibility to change the angle of the US transducer and recalculate the positioning of the transducer so that it will still intercept the lesion centre. Targeting of the US transducer in this manner results in registration of the US scan plane and the MR images to a single point at an arbitrary angle. Another variation of US/MR registration involves registration of an entire imaging plane of interest rather then just a point. This would enable visualization of the

same plane in MR and US. This type of registration would help in identifying an inconspicuous lesion in the US image by using the corresponding MR data as a reference.

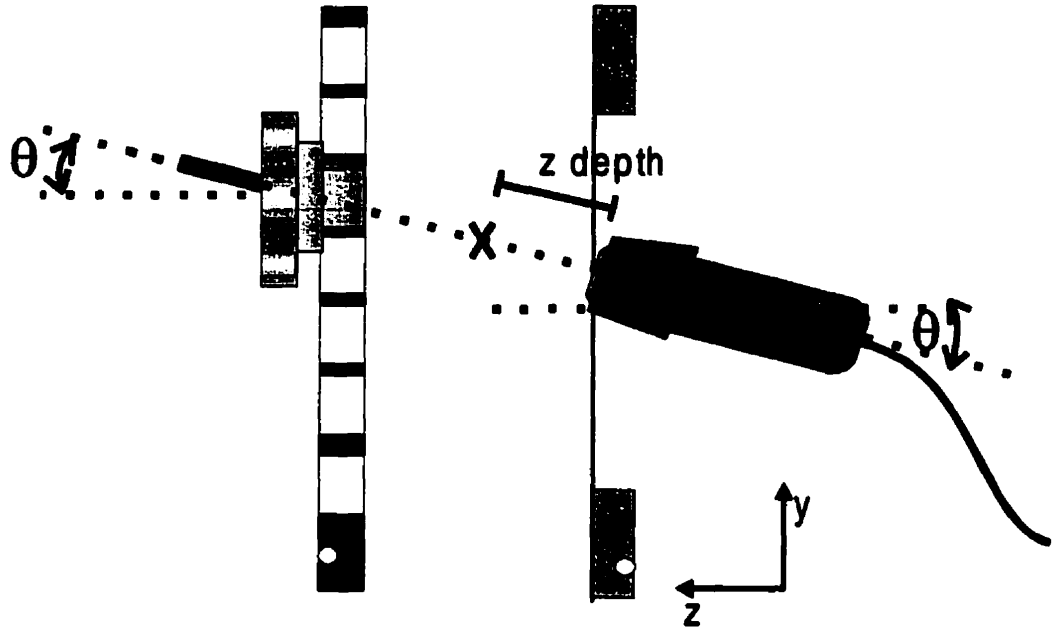

Figure 2.18: US corregistration and positioning of the UTPS. Here we see the position of the biopsy plug such that it makes an angle, θ, with the z-y plane of the apparatus. This angle is determined by projecting the vector defining shaft position onto the y-z plane. The ultrasound transducer is positioned at this same angle θ and positioned at a height y, such that the US scan plane will intercept the lesion and the trajectoy of the biopsy needle. In the x-z plane, the transducer is positioned so that the centre of the transducer corresponds with the centre of the lesion. If this can not be done due to positioning restrictions an offset value will define the position of the target in the US image. The depth of the target in the US image, is calculated as demonstrated above.

In some cases, visualization of the lesion in the US plane can be difficult. Referencing the lesion to native landmarks in the breast, such as fat and fibroglandular tissue can help in its location. If the lesion can be referenced to these landmarks in an MR image, then these same landmarks found in a registered US image can be used to indicate the lesion position. Obtaining an MR image that corresponds to the US image targeted on the lesion centre can be done either by reformatting a 3D set of MR data or acquiring a set of images at an oblique angle corresponding to the angle of the US transducer. These two concepts are discussed in Chapter 4.

2.6.4 Needle Position Verification and Modification

Depending on the biopsy strategy used, either MRI or US can be used to validate correct placement of the needle. The needle position verification using MRI as explained in Section 1.3.2, involves inferring the needle position relative to the lesion by way of the needle artifact [9]. A similar technique is explained in Section 2.6.4.1 for the verification of the localization and core biopsy needles with our biopsy system. The validation of needle position using US is explained in Section 2.6.4.2.

2.6.4.1 MRI needle position verification

After the breast has been scanned, and the required needle trajectory calculated (Sections 2.3.1.1, 2.3.1.2), the patient is withdrawn from the magnet bore and the needle is inserted into the breast. The patient is then moved back into the magnet for a set of verification images. The position of the needle is inferred from the signal void created from an artifact in the MR images. The same imaging sequence used to detect the lesion (sagittal T1-weighted fat saturated sequence), is used for verification imaging as shown in Table 2.2. The sagittal verification images determine if the needle is positioned correctly relative to the lesion in the S/I and L/R imaging plane. A second verification scan is required in the axial plane to determine if the needle depth is correct. If the positioning of the needle is determined to be correct in the sagittal and axial images, then the hook wire is threaded through the localization needle, or the core biopsy device is fired and a core sample is obtained. If the needle position is incorrect, the position is corrected using the MR verification images as a guide. There are problems associated with using MRI to validate needle position relative to the lesion as discussed in Section 1.3.

2.6.4.2 Ultrasound needle guidance

The use of US imaging to guide and verify needle placement for breast biopsies is advantageous due to its real-time imaging ability. A similar technique has been developed for our biopsy

apparatus as described in Section 2.1.4. The first step as explained in Section 2.3.3 is to position the US transducer to visualize the lesion and map its position to US coordinates. When the transducer is correctly positioned, the lesion must be identified in the US image *(The US imaging system used for the initial development of this technique was an ATL HDI-5000 ultrasound system (ATL Inc., Bothell, WA, USA) with a L4-7 linear array transducer also from ATL. The specific imaging settings used are explained in Chapter 3).* The needle is then inserted into the breast using the biopsy plug set at the appropriate trajectory. The needle will appear as a hyperechoic line in the US images as depicted in Figure 2.19. The progression of the needle through the breast can be monitored relative to the lesion using the real-time US information. If registration is perfect, and there is no lesion motion or needle wander, then the needle will move towards the lesion at the position indicated by the US lesion coordinates.

In the real breast, the needle and lesion can move, requiring modification of the needle trajectory. Loosening the collar of the biopsy plug allows correction of the needle position while using the real-time US information as a guide.

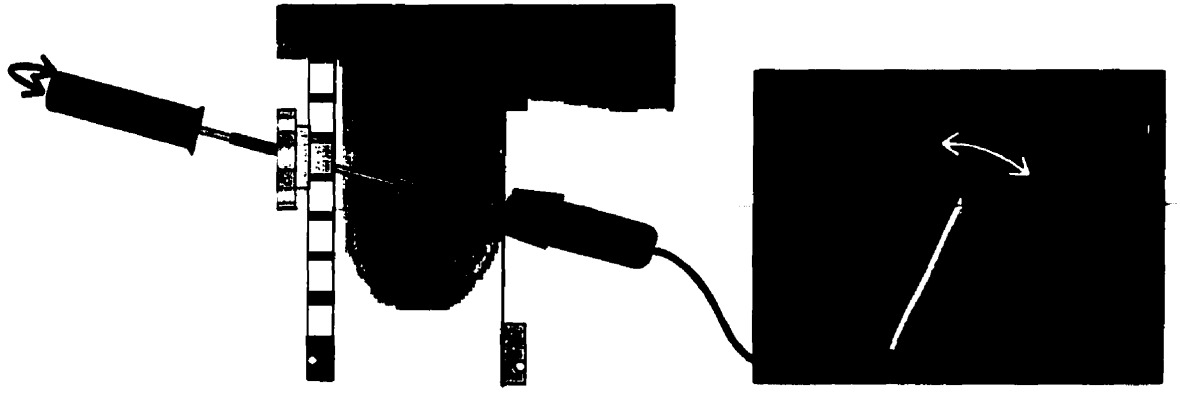

Figure 2.19: Needle position validation using US. Here we see the needle approaching the lesion based upon the trajectory determined by the MR information. With the US transducer in position, the needle can be monitored using the US images. By loosening the biopsy plug, the needle position can be modified as required based on the US images.

The lesion should appear in the US images at the position defined by the US coordinates,

although it may not initially appear due to many different factors including inaccurate registration, poor lesion contrast or US image mis-registration associated varying velocity of the US beam in the breast. If the registration is inaccurate, or if the patient has moved, then moving the transducer in the x and y directions, or slightly changing the angle of the transducer may identify the lesion. If the lesion is poorly visualized due to poor contrast of the lesion with the surrounding dense parenchyma other techniques that will be discussed in Chapter 4 can be employed.

2.7 Summary

In this chapter, an MR/US guided breast biopsy system was described. The modular design of this hybrid system enables many different, yet complementary biopsy strategies, including MR guided wire localization, MR guided core biopsy and MR/US guided core biopsy. The fundamental needle targeting concepts of these biopsy strategies differ only in their needle verification strategies.

A series of technical developments, and the merger of imaging technologies, results in a novel biopsy concept. The redesign of the patient bed, and compression apparatus improves access to the breast in both the lateral and medial approaches. The use of fiducial markers to guide needles at angled approaches provides access to previously inaccessible regions of the breast, and affords the opportunity to acquire many core samples using the same incision point. The ability to position an ultrasound transducer in the same manner as biopsy needles provides an accurate registration technique between MR and US images allowing real-time monitoring of needle progression.

In order to determine the suitability of such a system for clinical applications, the apparatus and techniques presented in this chapter must be tested. The experiments in Chapter 3 attempt to classify the accuracy of the biopsy strategies through a set of targeting and phantom experiments.

References

1. Schenck JF. The role of magnetic susceptibility in magnetic resonance imaging: MRI magnetic compatibility of the first and second kinds. Med. Phys:1996; 23(6):815-850.

2. Sumanaweera T, Glover G, Song S, Adler J, Napel S. Quantifying MRI Geometric Distortion in Tissue. MRM 1994; 31:40-47.

3. Sumanaweera T, Glover G, Song S, Adler J, Napel S. Characterization of Spatial Distortion in Magnetic Resonance Imaging and its implication for stereotactic surgery. Neurosurgery 1994; 35: 696-704.

4. Walton Lee, Hampshire A, Forster D, Kemeny A. A Phatom Study to Assess the Accuracy of Stereotactic Localization, Using T1-weighted Magnetic Resonance Imaging with the Leksell Stereotactic System. Neurosurgery 1996; 38:170-178.

5. Walton Lee, Hampshire A, Forster D, Kemeny A. Stereotactic Localization with Magnetic Resonance Imaging: A Phantom Study to Compare the Accuracy Obtained using Two-dimensional and Three-dimensional Data Acquisitions. Neurosurgery 1997; 41:131-139.

6. Wies J, Ericsson A, Silander S, Hemmingson A. Magnetic Resonance Spectroscopic Imaging for Visualization and Correction of Distortions in MRI: High precision applications for Neurosurgery. Magnetic Resonance Imaging 1998; 16:1265-1272.

7. Langlois S, Desvignes M, Constans JM, Revenu M. MRI Geometric Distortion: A Simple Approach to Correcting the Effects of Non-Linear Gradient Fields. JMRI 1999; 9:821-831.

8. Kuhl CK. MRI of Breast Tumors (review article). European Radiology 2000; 10 (46-58).

9. Butts K, Pauly JM, Daniel BL, Kee S, Norbash AM. Management of Biopsy Needle Artifacts: Techniques for RF-Refocuses MRI. JMRI 1999; 9:586-595.

10. Kaiser WA, Fischer H, Vagner J, Selig M. Robotic system for Biopsy and Therapy in a high-field whole-body Magnetic Resonance Tomograph. Proc. Intl. Soc. Mag. Reson. Med. 2000, pg 411.

Chapter 3

Accuracy Measurements

3.1 Introduction

This chapter presents a set of experiments developed to test the accuracy of the biopsy system and associated techniques presented in chapter 2 as well as attempt to compare the efficacy of the biopsy strategies in a tissue equivalent phantom. The first set of experiments (Section 3.2) tests the system under ideal conditions, i.e. a non-deflecting phantom, with an immovable target. The second set of experiments (Section 3.3) uses a breast-tissue-equivalent phantom, in an attempt to model the actual clinical application.

3.2 Targeting Experiments

3.2.1 Introduction

A simple experiment was developed to test the accuracy of using MR images to position a needle tip. An MR visible target was used to define a position precisely in both the MR space and the apparatus space. A mapping was made between MR and apparatus space to calculate the needle

trajectory that intercepts the target. The discrepancy between the physical position of the needle tip, and the position of the target was measured. This targeting experiment was used for both the wire localization technique, and the angular core needle biopsy techniques previous presented in Sections 2.5.3.1 and 2.5.3.2.

Testing the ability to perform hybrid MR/US guided core biopsy further requires accurate positioning of the ultrasound scan plane. A phantom was developed that contained a set of targets that could be visualized using MR and US imaging modalities. The phantom was imaged using MRI to locate the target positions relative to the apparatus. The position of these targets relative to the visible fiducial markers determined the position of the targets in the apparatus space. An ultrasound transducer was then positioned using the technique outlined in Section 2.5.3.4. The accuracy of this targeting experiment was defined by a set of distances in 3 dimensions.

3.2.2 MR Guided Needle Localization

The purpose of the first experiment was to measure the ability to place a localization needle in space to intersect an MR visible target using a localization needle plug. This experiment quantified the accuracy of MR guided wire localization while in a later experiment the accuracy using a biopsy needle plug was examined.

3.2.2.1 Procedure and Apparatus

The apparatus presented in chapter 2 was used in this experiment. In an attempt to model the clinical situation, equipment and techniques were used in the experimental procedures similar to those that would be used in the clinical applications. The apparatus used for this experiment is demonstrated in Figure 3.1 b, illustrating the biopsy fenestrated insert in the lateral compression frame, and the targeting apparatus in the medial frame.

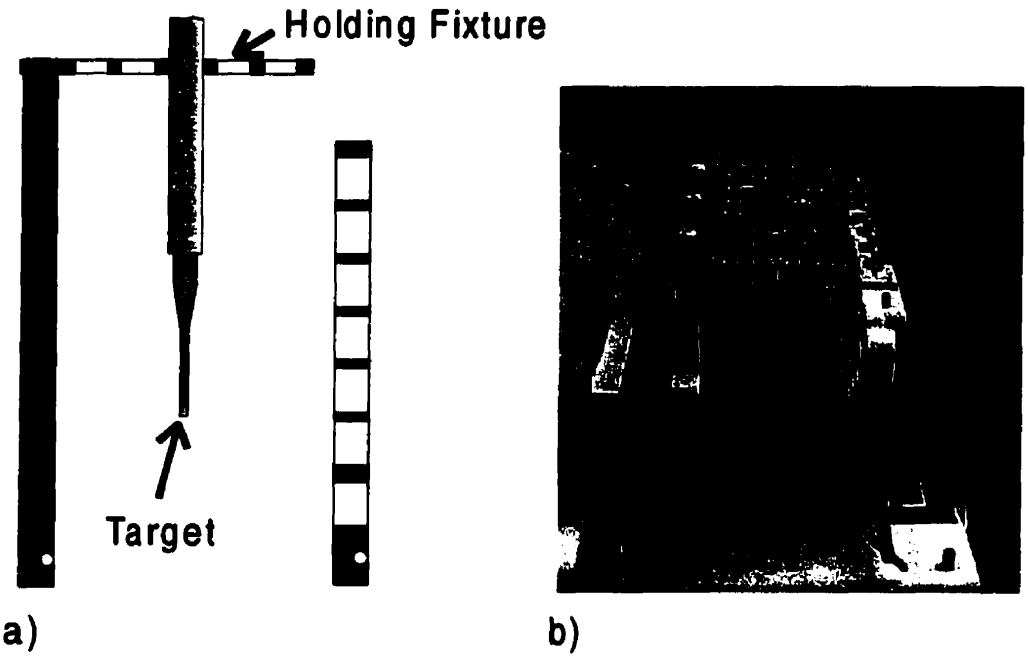

Figure 3.1: Diagram of the targeting fixture. a) Diagram of the target fixture and target used in the targeting experiments in an axial view. b) Picture of the targeting fixture positioned in the apparatus at an oblique axial view.

The target and holding fixture are shown in Figure 3.1 a. The target used was a plastic pointer used in neurological biopsy procedures (Image Guided Neurologics Inc. Melbourne, Florida, USA). The target was filled with a gadolinium and water mixture. The target holding fixture enabled positioning of the target tip at various positions within a volume of 20 cm by 15 cm by 15 cm in the S/I, A/P and L/R directions respectively.

A single trial in this experiment involved positioning the needle tip to intersect the tip of the target. The error associated with this technique was measured as the distance from the needle tip to the target tip. This trial was repeated many times for various target positions in the biopsy volume. Each trial involved fixing the target at an arbitrary position within the biopsy field, determining the target and fiducial marker positions with a series of 3 MR imaging sequences and positioning the needle based on this information. All MR imaging in this chapter was performed using a 1.5T clinical whole-body MRI system (Signa, GE Medical Systems, Milwaukee, WI). The technique used to determine the fiducial origin and the target position was described in

Sections 2.6.1 and 2.6.3 and the pulse sequence used is summarized in Table 3.1. Three separate spin-echo imaging series were used to define the target and fiducial marker locations accurately. The phased encode direction was selected to correspond with the coordinate of interest in each sequence. The fiducial markers and target are evident in Figure 3.2. The positions of the fiducial markers and target were recorded from the MR user console. The position of the fiducial origins, target in MR space (L/R, A/P, S/I) and the approach were then entered into the computer program to calculate the needle trajectory parameters as discussed in Section 2.6.1. The output from the program was the biopsy insert window index, localization bore hole index, and the needle depth.

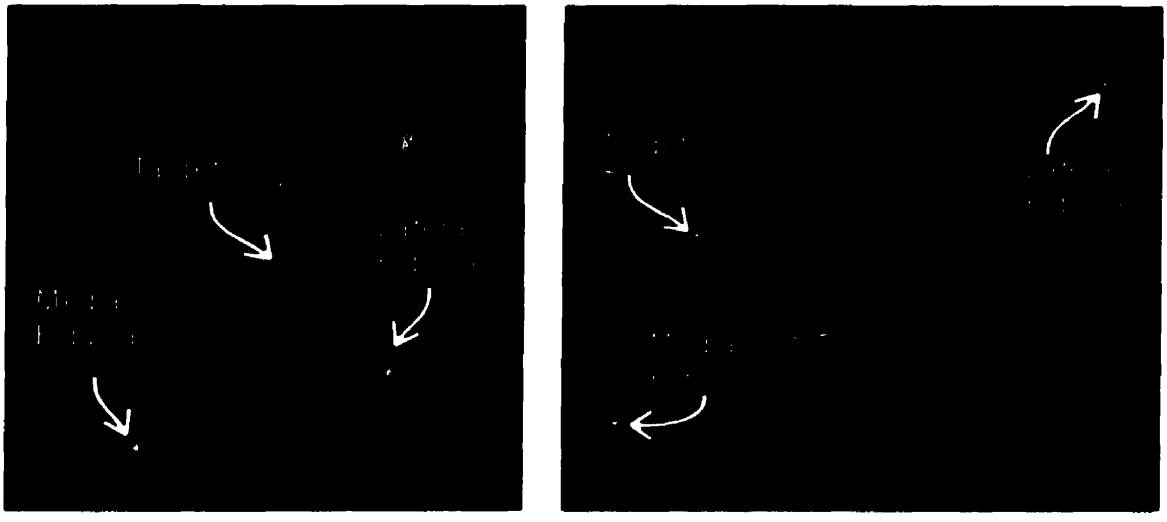

Figure 3.2: MR images of target and fiducial markers. a) Axial spin-echo image of the target and fiducial markers., (TR/TE, $N_{PHASE}/N_{FREQUENCY}$, FOV; 350/14 ms, 256/128, 24cm). b) Coronal spin-echo image of the target and fiducial markers, (TR/TE, $N_{PHASE}/N_{FREQUENCY}$, FOV; 350/14 ms, 256/128, 26cm). The large object at the centre of the image is a water bottle used to load the imaging coils properly.

With the apparatus removed from the bore of the magnet, the localization plug was positioned and the needle advanced to the appropriate depth. The total distance from the tip of the needle to the tip of the target was measured and recorded. This measurement was the magnitude of the distance between the localization needle and the target tip using MR guidance for one trial. This measure is referred to as the needle positioning error and is recorded in units of millimeters (mm).

Slice Orientation	Axial	Coronal	Coronal
Frequency Encode	L/R	S/I	L/R
Coordinate Determined	A/P	L/R	S/I
Pulse Sequence	T1-weighted 2D Spin Echo	T1-weighted 2D Spin Echo	T1-weighted 2D Spin Echo
Acquisition Matrix	256 x 128	256 x 128	256 x 128
Field of View	24 cm x 24 cm	26 cm x 26 cm	26 cm x 26 cm
Pixel Size (freq,phase)	0.9x1.8 mm	0.9x1.8 mm	1.0x2.0 mm
Slice Thickness	5.0 mm	5.0 mm	5.0 mm

Table 3.1: Imaging sequence used for targeting experiments. Three separate scans are used to determine the positions of the target and the fiducial markers.

3.2.2.2 Results

The test was preformed 26 times, with the target distributed throughout the biopsy volume on the left (13 trials) and right (13) side of the apparatus, using both lateral (13) and medial (13) approaches. The resulting magnitude of the average needle positioning error over all trials was 2.9 mm, with a standard deviation of 1.0. The maximum error was 6.0 mm, while the minimum error was 2.0 mm. The large variation between the minimum and maximum error values was due to the finite needle positioning limitations. This will be discussed in the following section.

3.2.2.3 Conclusion

The needle positioning error was due to errors from many different sources. These sources include errors due to MR imaging of the target and fiducials, imprecision associated with measurements of the MR images, mechanical errors and the finite positioning resolution associated with the biopsy insert and localization plug.

3.2.2.3.1 MR imaging errors

There are many phenomena that affect the ability of MRI to determine precisely the position of an MR visible target relative to a physical position in space. As discussed in Section 2.6.1.3, these errors can produce positional errors of several millimeters in the MR images. The use of the imaging protocol outlined in Table 3.1 attempted to minimize many of these errors. The most prominent source of positional error was believed to be from the non-linearity of the gradients. The imaging protocols used in this experiment enabled the *gradient warp* correction option on the user console but it seemed to overestimate the amount of warp as demonstrated in Figure 2.13. This was evident in the results obtained in this experiment. There was a constant error associated with the positioning of the localization needle that resulted in the needle position tending to be anterior to the target and either slightly superior or inferior to the target depending on the biopsy approach. This consistent error can be explained by an improper *gradient warp* correction. The fiducial markers were positioned on the outer region of the image, where the gradients are not linear. This resulted in their position in the MR image to appear offset from their actual physical position. This effect also distorted the position of the target within the MR image, but the effect was not as severe as the target was typically positioned near the centre of the image. This resulted in a constant error imparted by the shift in the fiducial origin in the MR images, and a smaller error associated with a shift in the position of the target that varied as a function of its position in the imaging volume. These errors and the potential to correct for them are explained in more detail in Chapter 4.

3.2.2.3.2 Measurement Uncertainties

The imprecision associated with the various measurements made in this experiment also contributed to the needle positioning error. The ability to define a position accurately depends on how well the fiducial centres and the target tip can be distinguished and the pixel size at which the images are acquired. For these imaging sequences, the images were acquired with a pixel size of 0.9x1.8 mm. Therefore the tip could only be determined with certainty related to that dimension. The depth of the biopsy needle and the measurement of the discrepancy of needle tip to target tip

also subject to error.

3.2.2.3.3 Mechanical Errors

Further errors were associated with mechanical inaccuracies of the apparatus. Imperfect machining and misalignments of the apparatus resulted in small needle positioning errors. The finite needle positions defined by the localization plug and biopsy insert resulted incomplete access to all positions within the biopsy volume. There will be an error associated with discrete positions of the needle. This error will be a maximum of 6 mm when the target falls directly behind two frames of the biopsy insert, and a maximum of 3.5 mm when the lesion falls on the diagonal between two localization plugholes, as indicated in Figure 3.3.

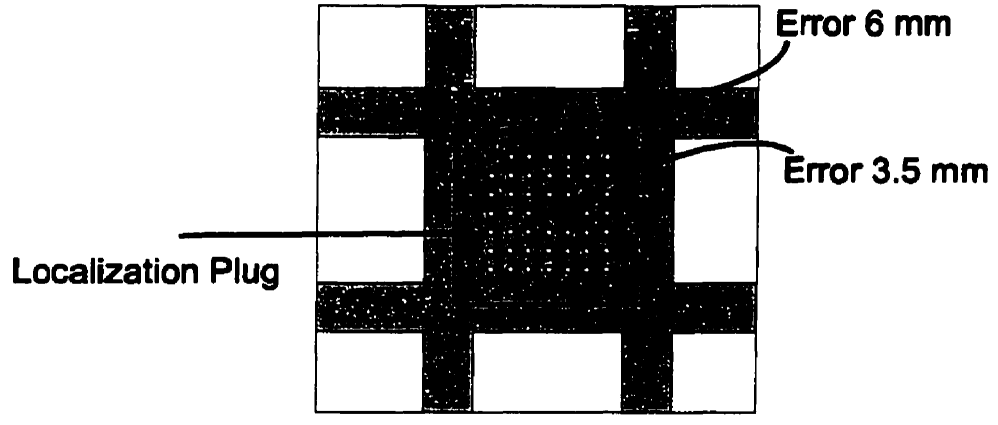

Figure 3.3: Illustration of errors introduced due to the geometry of the localization plug and biopsy insert. If a target was positioned directly behind the crossbars of the biopsy insert, the error associated with positioning the localization needle in the closest plughole is 6 mm. For a target positioned along a diagonal between two plugholes on the localization plug, the needle positioning error for the closest plughole would be 3.5 mm.

The results discussed in this chapter were obtained without doing any correction for the *gradient warp* over correction effect. This effect produced a consistent error in the S/I and A/P positioning of the needle due to incorrect visualization of the fiducial markers. This error was large enough that the computer program calculated an incorrect localization bore hole for the needle trajectory. This error was consistent throughout the experiment. Correcting for this error by adding a constant offset value to correct for the apparent shift in the fiducial origin position would have

reduced the final average error measurement substantially.

In terms of clinical acceptability for needle localization, the average error of 2.9 mm is an acceptable value considering the 2.5 mm resolution associated with the localization plug. The smallest lesions detected using MRI are currently around 4 mm in diameter [2]. The amount of tissue obtained from surgical excision in a wire localization procedure ensures margins of 1 cm on either side of the lesion [3]. Even considering the maximum error measured in this experiment (6 mm), if the appropriate margins were obtained, the lesion would be sampled, although clear margins would not be obtained. The ability to reposition the needle by re-imaging the needle and lesion after the needle was inserted was not considered in this experiment, but would be implemented in the clinical application. These results are acceptable for needle localization, but not for core biopsy. In the next section the intrinsic accuracy for positioning of a biopsy needle using MR guidance is examined.

3.2.3 MR Guided Needle Biopsy

The purpose of this experiment was to measure the ability to place a biopsy needle in space to intersect an MR visible target. This experiment attempts to quantify the accuracy of the angled core biopsy technique with the system described.

3.2.3.1 Procedure and Apparatus

The apparatus and technique used for MR-guided core biopsy was similar to that used for MR-guided wire localization. The delivery of the core biopsy needle in this experiment involved an angled trajectory, requiring a specially designed biopsy plug and goniometer as discussed in Section 2.6.3.1.2. The MR data was used to calculate the needle trajectory parameters; biopsy window index, the disc and arch angles of the biopsy plug, and the needle depth. The two angles were set using the goniometer. With the apparatus removed from the magnet, the biopsy plug was placed into the fenestrated plate and the biopsy needle was then advanced through the needle

guide to the calculated depth. The discrepancy between the tip of the needle to the tip of the target was measured.

3.2.3.2 Results

The test was preformed 26 times, distributed throughout the biopsy volume on the left (13 trials) and right (13) side of the apparatus, using both lateral (13) and medial (13) approaches. The resulting average of the magnitude of the error for all trials was 1.9 mm, with a standard deviation of 0.7. The maximum needle positioning error was 2.5 mm, while the minimum error was 0.7 mm.

3.2.3.3 Conclusion

The needle positioning error measured in this experiment was again due to errors from many sources, similar to those encountered in the needle localization experiment. The main difference in the source of error between this experiment, and the localization experiment was the apparatus associated with positioning the needle. The ability to angulate the needle reduced the amount of inaccessible space within the biopsy volume. This is demonstrated in Figure 3.4, where the inaccessible regions for the biopsy techniques are illustrated. It is believed that the major source of error in this experiment is again due to *gradient warp* for the same reasons indicated in the previous experiment.

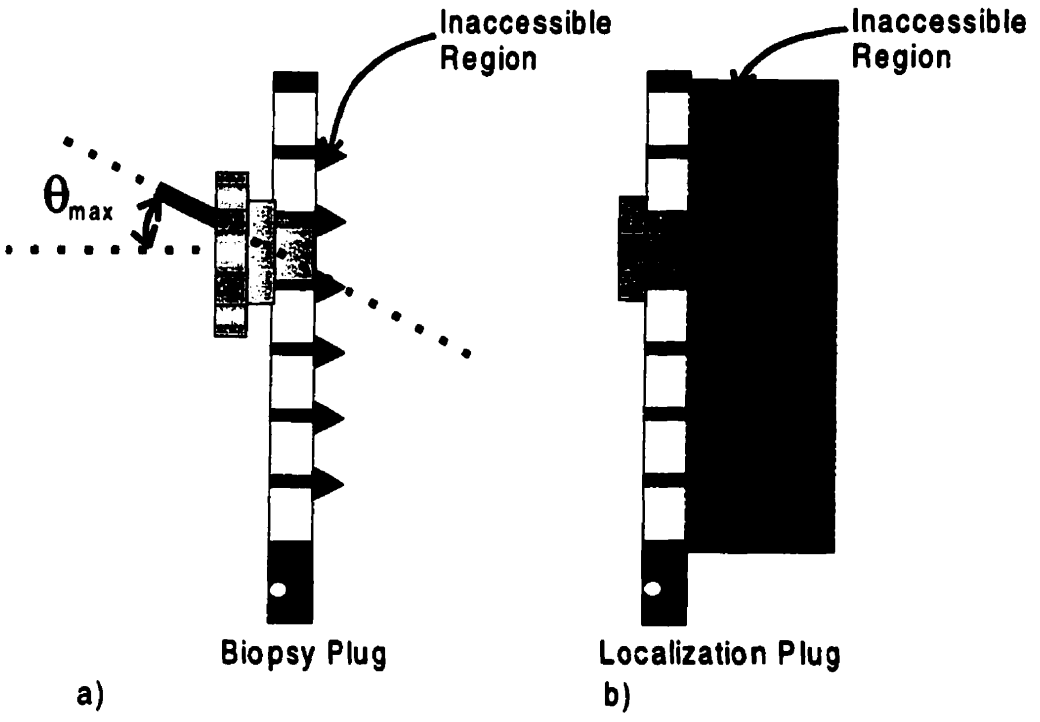

Figure 3.4: Comparison of the inaccessible interventional regions. a) Certain regions of the breast are inaccessible with the design of the biopsy insert and the biopsy plug. With the plug at its maximum angulation there are regions that are inaccessible for the biopsy needle behind the frames of the insert. b) The regions of inaccessibility are substantially greater when the localization plug is used.

These results were obtained without correcting for the error associated with *gradient warp*. An improvement in the accuracy would be expected if this were corrected. A substantial improvement in accuracy was demonstrated with the angled needle approach compared to the localization needle positioning as summarized in Table 3.2. This can be attributed to the ability to access more areas within the biopsy volume due to an angled approach. Although the accuracy of the core biopsy technique was improved compared to the localization technique, the accuracy requirement for core biopsy is more stringent as explained in Section 1.6.

With respect to clinical acceptability, the average error of 1.9 mm is a reasonable value. The maximum error value of 2.5 mm could be translated into the ability to obtain a biopsy of approximately a 5.0 mm diameter lesion. This lesion size would be considered small in terms of the lesions currently detected with MRI [2].

The precision with which this system could position a core biopsy needle is comparable with state-of-the-art MR breast biopsy systems. In the most recent publication, one group indicated they were able to position an MR compatible needle in a phantom within 5 mm of a target 87.5 % of the time [4]. State of the art stereotactic systems for the purpose of neurological biopsy have demonstrated mean absolute errors in positioning a biopsy needle to intersect a target in three dimensions (X= 0.4 mm, Y = 0.7 mm, Z = 1.3 mm) resulting in a total magnitude distance of 1.5 mm. This result is similar to the mean error in needle positioning of 1.9 mm presented in this Section for angled core biopsy [5].

Biopsy Technique	Number of Trials	Mean Tip Positioning Error (mm)	Standard Deviation	Minimum Needle Tip Positioning Error (mm)	Maximum Needle Tip Positioning Error (mm)
Needle Localization	26	2.9	1.0	2.0	6.0
Angled Core Biopsy	26	1.9	0.7	0.7	2.5

Table 3.2: Results from localization and angled core biopsy targeting experiments.

3.2.4 MR and Ultrasound Registration

The purpose of the third targeting experiment was to measure the ability to register an ultrasound scan plane with an MR visible target. This experiment quantified the ideal accuracy of MR/US image registration with the system described.

3.2.4.1 Procedure and Apparatus

The goal of this experiment was to detect a target in MR, and use the MR data to position an ultrasound transducer so the target appears in the centre of the ultrasound images. A novel multi-

modality phantom was developed for this experiment. The apparatus presented in chapter 2, including the UTPS described in Section 2.5.3.4 and techniques presented in Sections 2.6.3.2 and 2.6.3.3 were used in this experiment.

The unique components to this experiment are the water tank phantom as shown in Figure 3.5 and the UTPS. The phantom consisted of a set of MR and US visible targets distributed throughout the biopsy volume. The targets were plastic beads of various diameters (4 mm, 6 mm, 8 mm) and are suspended in a tank of gadolinium-doped water. The tank was rigidly held to the apparatus, fitting into the compression frame slots. The front surface of the tank was cut away and replaced by a polystyrene membrane. The beads were fixed into place on scaffolding of monofilament fishing line. Figure 3.6 demonstrates the tank in lateral frame with the UTPS attached.

The experiment involved locating the positions of the targets in MR images. These positions were used to calculate the US transducer position that would register the target with the centre of the ultrasound plane. A single trial consisted of registering a target detected using MR with the US plane. Any errors in registration were recorded in three dimensions x, y, and z corresponding to the superior/inferior, anterior/posterior, and medial/lateral directions respectively.

Imaging Parameters	Bead Frame Coronal	Bead Frame Sagittal	Bead Frame Sagittal
Slice Orientation	Coronal	Sagittal	Sagittal
Frequency Encode	S/I	S/I	A/P
Coordinate Determined	L/R	A/P	S/I
Pulse Sequence	T1 weighted 2D Spin Echo	T1 weighted 2D Spin Echo	T1 weighted 2D Spin Echo
Acquisition Matrix	256 x 256	256 x 256	256 x 256
Field of View	22 cm x 22 cm	25 cm x 25 cm	25 cm x 25 cm
Pixel Size (freq,phase)	0.9x1.8 mm	1.0x2.0 mm	1.0x2.0 mm
Slice Thickness	2.0 mm	2.0 mm	2.0 mm

Table 3.3: Imaging series used to locate bead and fiducial markers

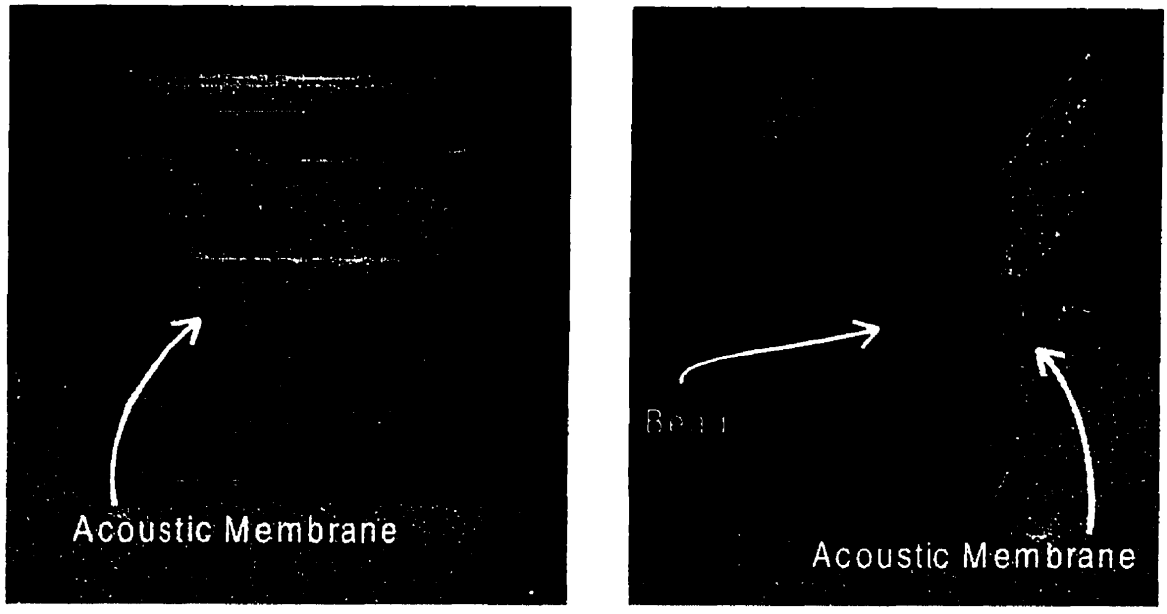

Figure 3.5: Ultrasound Phantom: a) Front view of the ultrasound water tank phantom b) Side view of US phantom. The plastic beads (black) are suspended in place by monofilament fishing line.

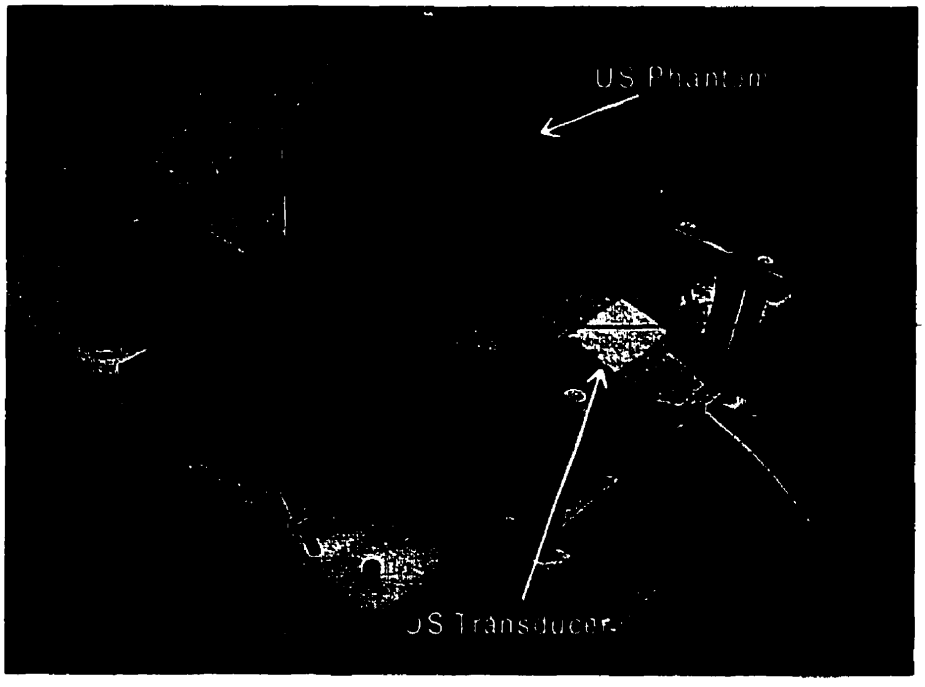

Figure 3.6: Ultrasound phantom and transducer held in position for experiment.

The US phantom was positioned in the apparatus and imaged using 3 separate MR imaging series as demonstrated in Table 3.3. Two of the resulting MR images are shown in Figure 3.7. In these T1-weighted spin-echo images, the beads appear as signal voids, while the gadolinium-doped water appears as a bright background signal. In each image, the coordinate corresponding to the phase-encode direction in that plane defined the accurate fiducial marker and bead position. This was done to reduce any shift in the position of the bead targets and the fiducial markers in the MR image due to the magnetic susceptibility difference between gadolinium-doped water, air and plastic.

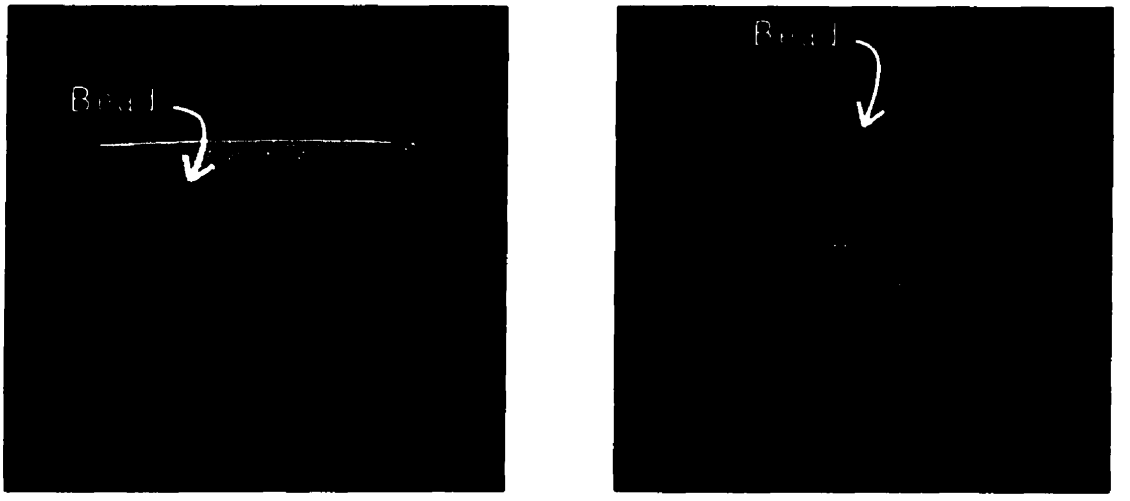

Figure 3.7: MR images of US phantom. The signal is from the gadolinium-doped water in the tank, while the signal voids arise from the plastic beads. a) Coronal image of phantom with phase encode in the L/R direction. b) Sagittal image of the phantom with phase encode in the S/I direction.

After the phantom was imaged, the apparatus was removed from the magnet room and the US transducer positioning system was attached as shown in Figure 3.6, 3.8. The targets detected using MR were investigated in order by first calculating the position of the transducer, positioning the transducer and then recording any errors in registration. The MR-measured coordinates of the target were entered into the computer program to calculate the transducer position as discussed in Section 2.6.3.3. The transducer was oriented perpendicular to the acoustic window by overriding the angle calculated by the computer program. The resulting output indicated the position of the

transducer in the x and y positions of the UTPS at 0 degree angle, as well as the US space target position (x-offset and z-depth).

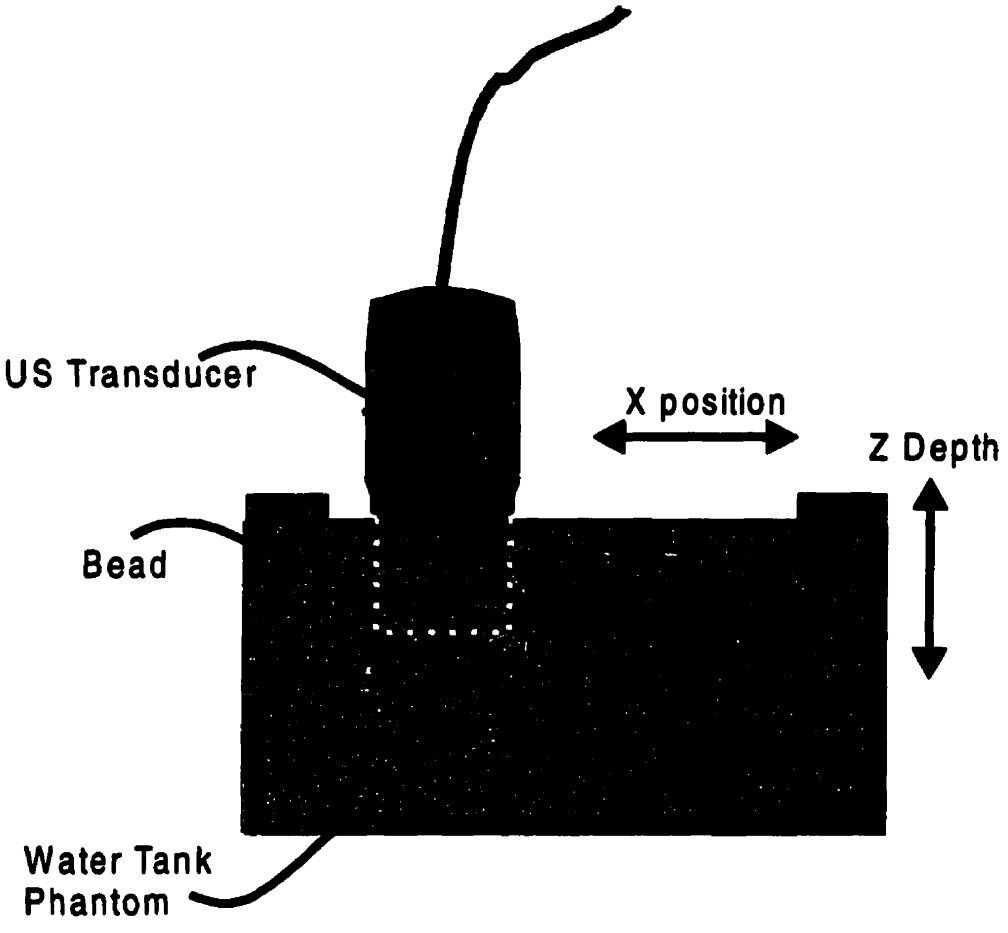

Figure 3.8: Top view of US phantom with transducer in position. The acoustic field of the transducer is outlined in a dashed white line.

The transducer was then positioned at the coordinates based upon the MR information. In Figure 3.9 the bead appears as a bright, highly echoic contour and the fishing line holding the bead as a bright line. Identifying the centre of the bead and measuring the discrepancy of the bead position relative to the US image provided a means to quantify the accuracy of image registration between MR and US in this experiment. The error was quantified in the x, y and z directions as indicated in Figure 3.9. These x, y, and z axes correspond to the superior/inferior, anterior/posterior, and medial/lateral directions in MR space respectively. The error in each axis was defined as the total

distance in millimeters the transducer would be required to move in order to achieve perfect registration.

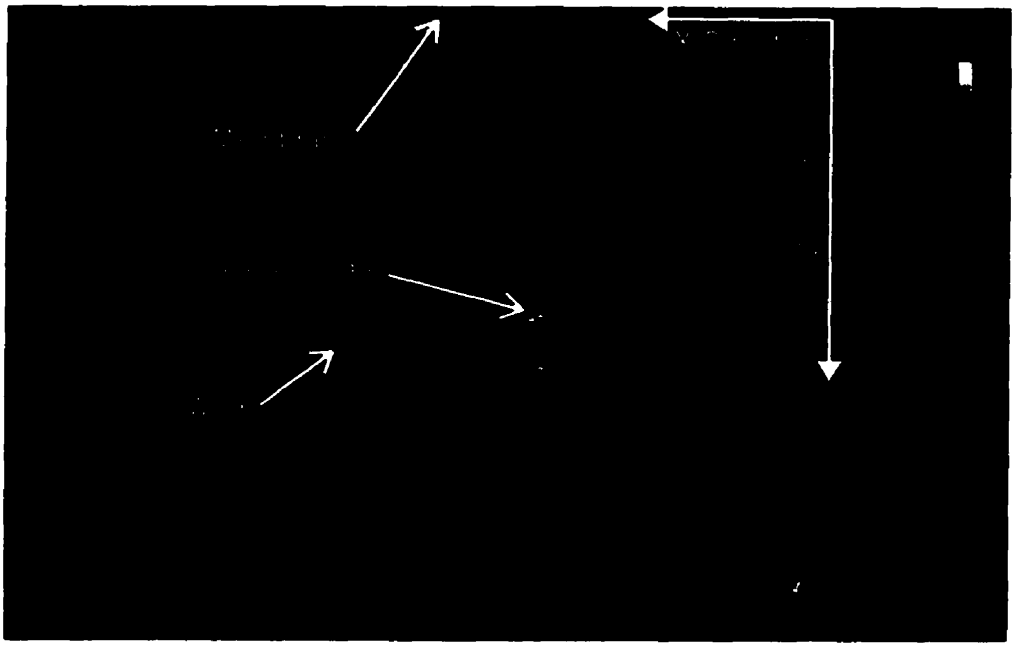

Figure 3.9: US image acquired when probe was positioned at MR based calculated coordinates. The large bead indicated in the image is the target selected. At the top of the image the membrane appears as a bright band. The x and z axis are shown at the right side of the image. The y-axis points out of the image.

Mis-Registration Error Measurement in Y direction

In order to determine the actual position of the bead relative to the US transducer positioning system, the transducer was scanned up and down in the y direction and locked in position when the echo from the bead was the brightest. The actual y value was recorded from the scale on the UTPS. For example, in Figure 3.10, the transducer has been repositioned in the y direction so that the bead appears brighter relative to the appearance of the bead in Figure 3.9. It is important to note that it is the appearance of the front edge of the bead, not the brightness of the fishing line that is important to consider. The bead center does not necessarily correspond to the position of the fishing line.

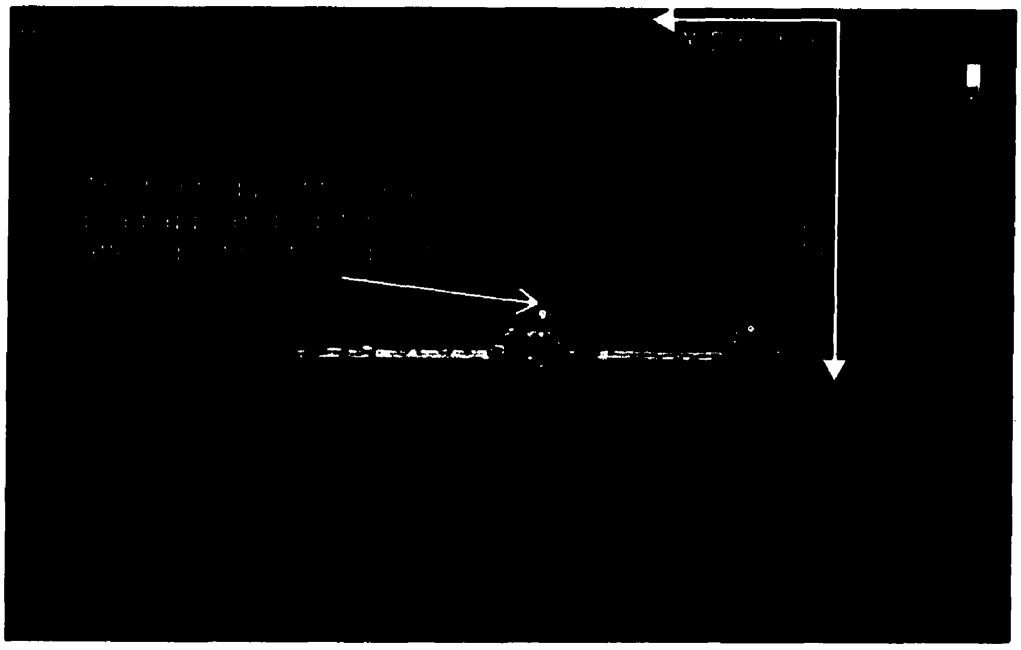

Figure 3.10: US image when the y position of the transducer has been positioned so that the bead signal is maximized. The transducer has been adjusted in the y direction (direction though image plane) such that the bead generates a brighter US signal relative to Figure 3.9. When the bead produces the brightest signal, or in other words strongest echo, the transducer is accurately registered to the bead in the y position.

Mis-Registration Error Measurement in X direction:

The transducer was positioned such that the bead should appear in the middle of the US image. The actual position of the bead relative to the centreline of the US image was determined by using the distance caliper function on the US system. This function enables measurements of distances on the screen by placing two cursors with a trackball. With the cursor positioned at the centreline of the acoustic field and the other positioned at the midpoint of the front edge of the bead, a error measurement was obtained as demonstrated in Figure 3.11. The total distance measured defined the error in the x direction. The centre of the bead could be defined with a precision of approximately 0.2 millimeters as determined by repeated measurements of bead positions.

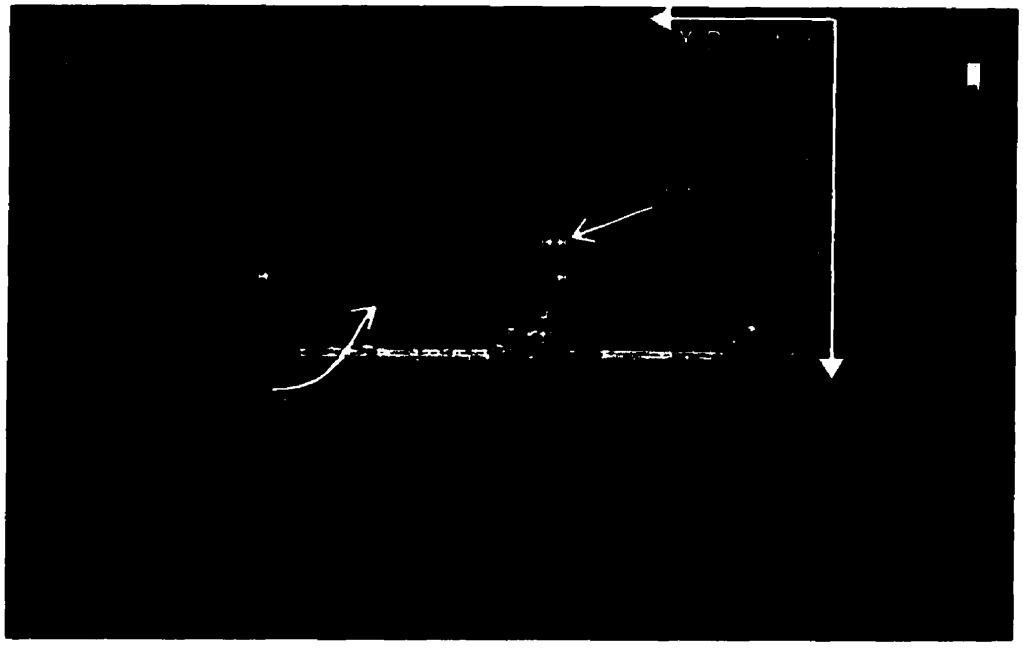

Figure 3.11: Measurement of the x-position of the bead centre. The distance from the edge of the acoustic field to the centre of the bead was measured with the caliper function on the US system as indicated. The error was measured by subtracting the amount, which it deviated from the centreline of the transducer. The long solid arrow indicates the position of the midline at 18 mm. The dashed arrow is the distance from the edge of the acoustic field to the centre of the bead as indicated by the calipers. The small solid arrow indicates the total error associated with the x coordinate of MR/US image registration. In this image the bead diameter is 6mm and the x positioning error is 0.7mm.

Mis-Registration Error Measurement in Z direction:

The error in the registration along the z direction was determined using the distance caliper function in a similar fashion to the x direction error. The bead centre was determined by locating the front edge of the bead and measuring back a distance equal to 1 bead radius, as indicated in Figure 3.12. One end of the cursor was positioned at the bead centre; the other was positioned on the echo representing the polystyrene membrane. The total distance measured represented the z distance as indicated on the US image. This was subtracted from the calculated distance.

3.2.4.2 Results

The test was repeated for 48 targets distributed at various depths throughout the phantom (19

targets at 23 mm depth, 20 at 43 mm, 9 at 64 mm). The mean of the absolute value of the error was calculated for the x, y and z directions for all trials. The mean of the magnitude of the absolute value of the error for all trials was also calculated and is shown in Table 3.4.

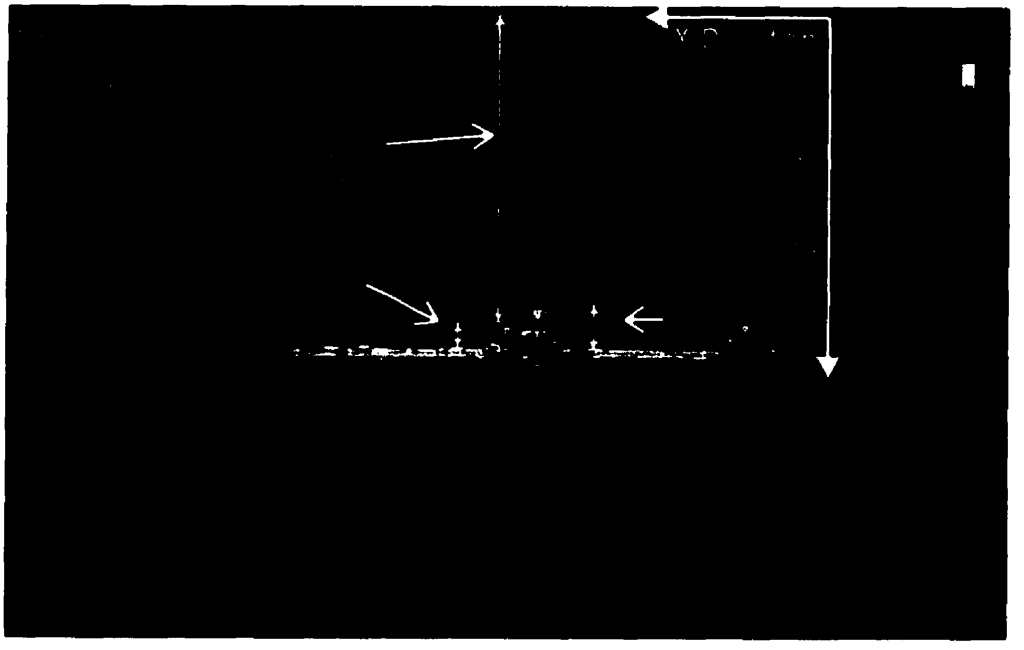

Figure 3.12: Measurement of the z position of the bead. The front edge of the bead is located, and the caliper is moved 1 radius back from this point to locate the centre of the bead. The caliper is then extended to the front edge of the membrane and the distance recorded. The error was measured by subtracting the amount, which it deviated from the z depth calculated by the computer script. The long solid arrow indicates the calculate position of the bead centre. The dashed arrow is the distance from the membrane to the centre of the bead as indicated by the calipers. The small solid arrow indicates the total error associated with the x coordinate of MR/US image registration. In this image the error was 0.6 mm.

	X Mis-registration Error (mm)	Y Mis-registration Error (mm)	Z Mis-registration Error (mm)	Magnitude Mis-registration Error (mm)
Mean	0.6	0.7	1.0	1.5
Standard Deviation	0.42	0.56	0.52	0.58
Maximum	2.0	2.5	2.5	3.3

Table 3.4: Results from MR/US registration experiment

3.2.4.3 Conclusions

The average error values in x, y and z directions demonstrate the inaccuracy associated with image registration between MR images and ultrasound images using the apparatus and techniques described. The registration error measured in this experiment was due to many sources including errors in MR imaging of the phantom and fiducial markers, precision associated with measurements, mechanical errors associated transducer positioning system and possible errors in US imaging of the targets.

The errors associated with the imaging of the phantom and the fiducial markers result from the phenomena outlined in the experiment of Section 3.2.1.3.1. Of these, *gradient warp* may have the largest effect on the error measures in the x and y directions. The constant offset error associated with a shift in the apparent position of the fiducial origin due to the non-linearity of the MR imaging gradients at the periphery of the images, as discussed in previous experiments, was reduced by shifting the position of the origin used in the calculations 1 mm in the x and y directions. However, no correction was made for any *gradient warp* errors in the position of the bead targets in the MR image. This would require a more sophisticated correction scheme as discussed in Chapter 4.

This shift in the position of targets in the MR images due to non-linear gradients resulted in an error that was a function of position. For instance, it was observed that the error associated with the x direction depended on the x position, (superior/inferior position) of the target. Targeting the beads located close to the sides of the phantom resulted in the largest x error values. While at a point somewhere near the centre of the phantom, the x registration error tended to be small.

The uncertainties associated with determining the position of the target and fiducial markers in MR images, the bead in US images, and positioning the US transducer contribute to errors in this experiment. The error in determination of target centres in the MR image is due to finite resolution of the MR images. These same effects limit the precision with which the targets can be

located in the US images. A further source of error that may not have been evident in this experiment, but may in fact be the largest source of error in clinical application of MR/US registration is apparent shifting of structures in US images due to the varying velocity of sound in the various tissues of the breast. This phenomenon occurs due the difference in the velocity of sound in fat and fibroglandular tissue as discussed in Chapter 1. The use of a tank filled with water ensured that the velocity of the US wave in this experiment corresponded well with the calculations used in the US system. This issue is examined in more detail in Section 4.2.4. The measurement of the ultrasound transducer position from the positioning apparatus using the millimeter scales also resulted in further measurement uncertainties.

The most substantial mechanical related errors in this experiment lie in the limitations of the UTPS. The transducer was positioned with an accuracy of only 1 millimeter graded scales as explained in Section 2.5.3.4. This allows accuracy of approximately 0.5 mm in positioning in the x and y axes relying on the eye of the operator. Another source of error in the z dimension is associated with the thickness of the ultrasound membrane, which was not accounted for in this experiment.

This registration method demonstrated in this experiment is very accurate compared to the smallest lesions we might encounter. This magnitude of the registration error determined in this experiment (1.5 mm) is less than half of the size of the smallest lesions (4 mm), that can be detected using contrast-enhanced MRI. Based on this result it appears that this technique is sufficiently accurate for clinical application.

3.3 Breast Equivalent Phantom Experiments

3.3.1 Introduction

A second set of experiments involved testing the accuracy of the biopsy strategies in a phantom model. A series of phantoms that modeled various degrees of target mobility and needle deflection were used.

3.3.1.1 Phantom Composition

The phantoms used in these experiments consisted of blocks of agar (Sigma-Aldrich Canada Ltd, Oakville Ontario) with embedded olives. The agar body of the phantom represented the tissue of the breast, while the pimento filled olives were composite targets modeling the breast lesions. Olives have been used for years in the field of radiology as targets in order test biopsy techniques [1]. The choice of olives as targets in this phantom was based on convenience; other types of targets could have been used in place. The agar was formed into a block of dimensions 65 by 150 by 110 mm. The olives are approximately 15 by 15 by 18 mm, while the cores of the olives are 7 by 7 by 10 mm. A diagram of the phantom is shown in Figure 3.13. The concentration of agar defined the stiffness of the phantom body. By changing the concentration of agar, the phenomena of concern in a real breast, needle wander and lesion motion, could be controlled.

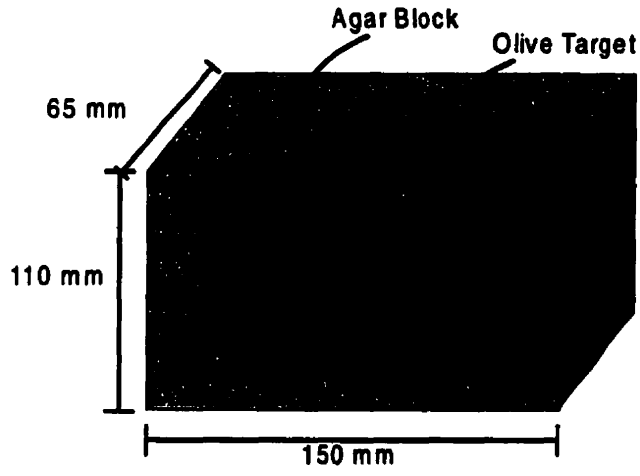

Figure 3.13: Diagram of biopsy phantom. Agar block was formed with embedded olives. The olives were positioned such that their long axis was parallel to the long axes of the phantom.

The higher the concentration of agar, the stiffer the resulting gel. By varying the stiffness of the gel, the amount of needle deflection could be controlled as demonstrated in Figure 3.14. The relative stiffness between the olive and the agar gel, on the other hand, determined the mobility of the olive. An olive stiffer then the surrounding gel has a greater tendency to move when poked by a needle. Therefore, at the lower concentrations of agar, the olive had greater tendency to move out of the path of the needle.

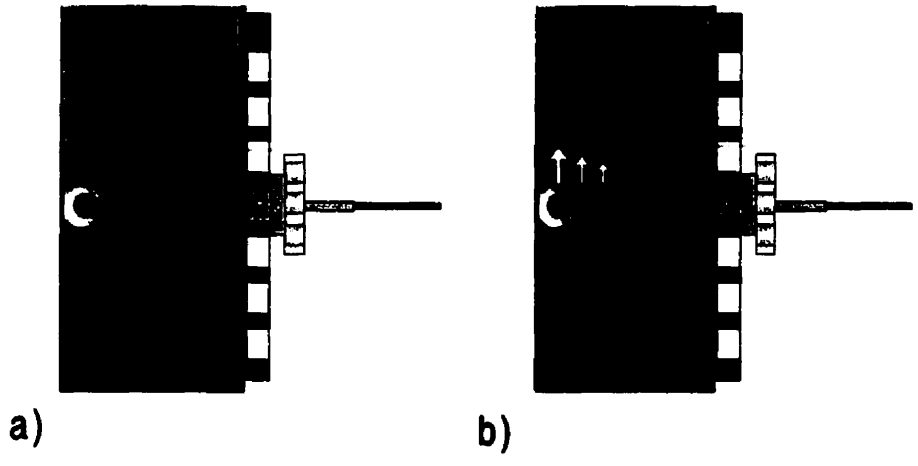

Figure 3.14: Comparison of needle deflection in phantoms of varying stiffness. a) In a phantom constructed from a low concentration of agar, the needle will tend to deflect slightly. b) By comparison, a stiffer phantom will tend to cause larger needle deflections.

3.3.1.2 Phantom Visualization

Aside from the mechanical properties of the phantom, adequate visualization of the phantom body and targets using MRI and US was essential. The phantom and its components were easily distinguished using an MR spin-echo imaging sequence and US B-scan imaging as demonstrated in Figure 3.15. The agar provided adequate scatter for visualization, as well as moderate attenuation. The strong attenuation caused by the pimento cores provided a realistic portrayal of the acoustical shadowing that occurs in some breast lesions [7]. This is an important phenomenon, because the shadowing affects the visualization of the needle as it approaches the lesion from the side opposite to the transducer face. The imaging and mechanical properties of the phantom described in this section provided a realistic simulation for the biopsy techniques.

Figure 3.15: Phantom imaging. a) US image of the phantom. b) Corresponding MR, T1 weighted spin-echo image of the phantom (TR/TE, $N_{PHASE}/N_{FREQUENCY}$, NEX; 350/12 ms, 512/512, 2). Note difference in depiction of the olive and pimento core. The shadowing generated by the pimento olive core is reminisent to the shadowing associated with carcinomas as depicted in Figure 1.4 of chapter 1.

3.3.2 MR Guided Needle Localization

This first phantom experiment was designed to determine the accuracy of the wire localization technique using a breast-tissue-equivalent phantom.

3.3.2.1 Procedure/Apparatus

This apparatus and techniques used in this experiment for needle delivery were equivalent to those of the experiment in Section 3.3.2. The target in this experiment was the core of an olive embedded within a block of agar (2.5% by weight) gel. This phantom was compressed between the lateral and medial frames as shown in Figure 3.16.

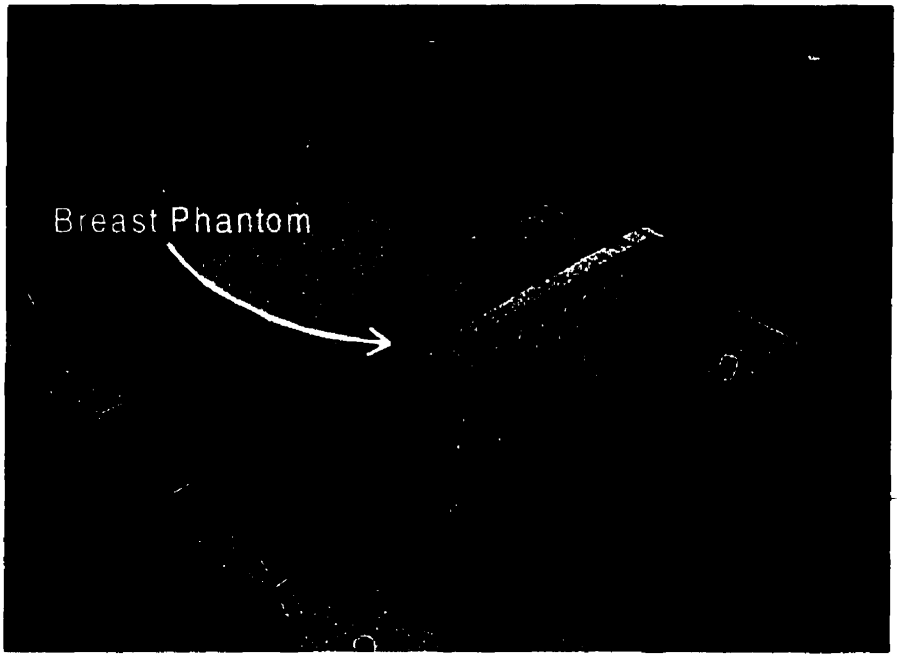

Figure 3.16: Breast equivalent phantom positioned in biopsy apparatus. The biopsy inserts are located in the medial and lateral compression frames.

A single trial involved positioning the needle tip using the MRI data so that it passed through the olive target. A localization wire then was threaded through the centre of the needle, and the

needle was withdrawn from the phantom leaving the wire in place. The accuracy of the procedure was quantified by scoring based on physical examination of the position of the wire relative to the core of the olive. This trial was repeated for a total of 24 trials, once for each of the olives in 3 phantoms. The MR sequences were slightly different then were used in the previously described targeting experiments. The phantom was scanned using a sagittal T1-weighted 2D-SPGR sequence as defined in Section 2.6.2. This sequence was used to define the position of the olive. The phantom was scanned using only one imaging sequence because that is how the breast is imaged in the clinical application of the procedure as explained in Chapter 4. This is done to speed up the procedure to ensure the lesion will remain enhanced long enough so that an MR verification scan can be obtained to validate the needle position. In the clinical case, the ability to image the breast more quickly takes precedence over the minimal accuracy improvement associated with obtaining multiple images to reduce to effects of magnetic susceptibility induced positional shift in the breast. It is believed that the amount of positional shift within homogeneous tissue such as the breast (where the magnetic susceptibility changes are minimal), is negligible compared to the shifts induced at the fiducial marker positions (where there is a large susceptibility change) [8].

The positions of the fiducials markers were determined from the first 3 imaging series; the position of the olive target was determined from the 4th imaging series. These values were entered into a computer program, which was used to calculate the required position and depth for the needle as explained in Section 2.6.3.1.1. Based on these values, the needle was positioned 1 cm past the required depth using the localization plug. A wire was threaded through the needle and the needle was removed leaving only the wire in place.

In order to determine the accuracy of the wire position, layers of agar and olive were removed with a scalpel to inspect the position of the wire visually as shown in Figure 3.17. The position of the wire relative to the core of the olive was recorded and scored. A score of 10 was assigned if the wire completely passed through part of the core, and was at a depth no greater then 15 mm from the centre of the core, and no less then 5 mm from the core. A score of 5 was assigned if the

wire passed through the olive core, but was at a depth greater then 15 mm or less than 5 mm from the core centre. A score of 2.5 was assigned if the wire passed through the olive and not the core, while a score of 0 was assigned to wire passing only through agar and missing the target completely. The ranking was based on the size of the pimento relative to the olive and the importance of positioning the localization wire at a position deeper then the lesion [9].

3.3.2.2 Results

The test was performed 24 times in 3 different phantoms, with lesions distributed throughout the biopsy volume. Of the 24 attempts, 14 scored a quality of 10, 10 scored a quality of 2.5. The average of the scores of all trials was 6.9. The distribution of these scores did not constitute a normal distribution as the scoring system imposed a maximum value on the resulting scores.

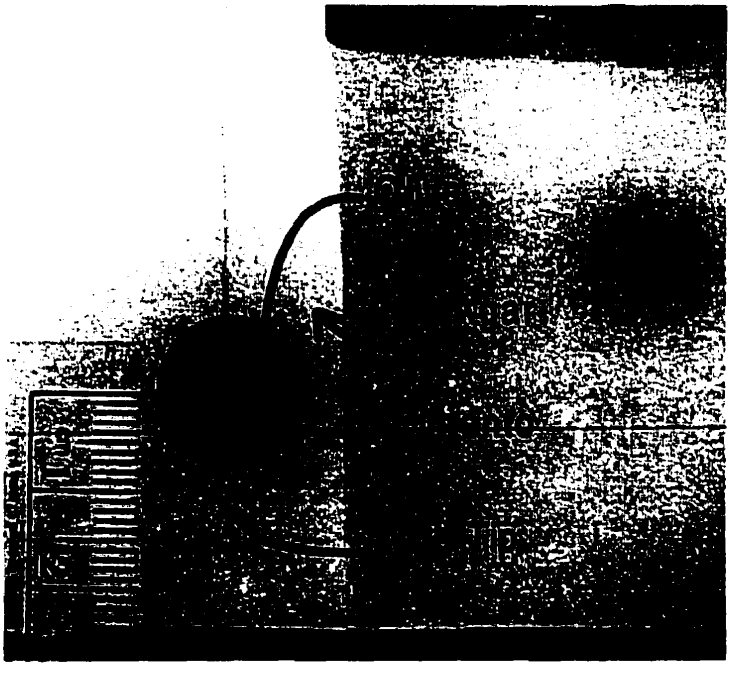

Figure 3.17: Measurement of needle localization accuracy in a phantom. The wire passes through the pimento core and is located at a position at 5 mm past the centre of the core, resulting in a score of 10 out of 10.

3.3.2.3 Conclusions

The use of the breast phantom and clinical imaging technique resulted in a more realistic version of Experiment 3.2.2. The agar concentration of the phantom was selected to be 2.5%. Preliminary testing demonstrated that this concentration of agar provided substantial amount of needle deflection. In combination with the errors identified in the associated targeting experiment, the needle missed the central core of the olive in 10 of 24 trials. Missing the core corresponds to an error, on average, that is more than 3.5 mm, where missing the olive corresponds, on average, to missing the desired position by more than 7.5 mm. These values correspond to the radius of the pimento and olive respectively.

In making comparison to the wire localization experiment performed in Section 3.2.2, an estimate of the magnitude of the needle positioning errors may be derived from these scores. Taking into consideration the average needle deviation associated with the scores based upon the size of the pimento core verses the olive; a rough estimate of the error associated with all needle placements was made. The average deviation of a needle tip associated with a score of 10 was the average of a perfect needle placement (error is 0 mm) and a maximum error for that score (error 3.5 mm). The expected error for a placement with score 10 was 1.75 mm. Using the same logic for all needle placements an expected average error was determined to be 3.3 mm. This result was larger than the average needle positioning error or 2.9 mm determined in the corresponding needle localization targeting experiment. This increased needle deviation was expected since the presence of the phantom acted to deflect the needle from its intended target.

Another feature of this experiment that differed from the targeting experiment was the method used to locate the target. The target position was determined by a set of sagittal images, instead of 3 sets of images as was done in Section 3.2.2. This resulted in anisotropic resolution where the target was defined with 1.8 mm in-plane resolution (A/P, S/I), and 4.0 mm through plane (L/R) resolution. This did not seem to affect the accuracy as all the wires were placed within 5 mm depth of the desired position. The limited effect of lesion motion may have been due to the

sharpness of the localization needle and the aggressive compression of the phantom between the plates.

This experiment lacks the needle verification sequence that would be included in the clinical application. In the clinical procedure, the needle position relative to the lesion would be verified by another imaging series before placement of the wire. Given this and the consideration of the size of surgical specimen that is removed during the surgical biopsy of the lesion, the results from this experiment indicate that the accuracy of this technique is appropriate for clinical application.

3.3.3 MR Guided Needle Biopsy

The second phantom experiment was performed to determine the accuracy of the angled core biopsy technique using a breast-tissue-equivalent phantom.

3.3.3.1 Procedure/Apparatus

The apparatus and techniques used in this experiment were identical to Experiment 3.2.3, except target was replaced by a phantom as demonstrated in Figure 3.16. A single trial involved positioning the core biopsy needle in the pre-fire position based on the MR images so that when fired, a core sample centred through the olive target would be obtained. A core biopsy rapid-fire device, otherwise known as a biopsy gun, Pro-Mag 2.2 (Manan Inc, Northbrook, Illinois) was used to obtain the core samples. A score based on the core sample obtained, was used to quantify the accuracy of the procedure. The quality of the core sample was scored with the scoring system shown in Figure 3.18. This scoring system was similar to that used in the wire localization experiment.

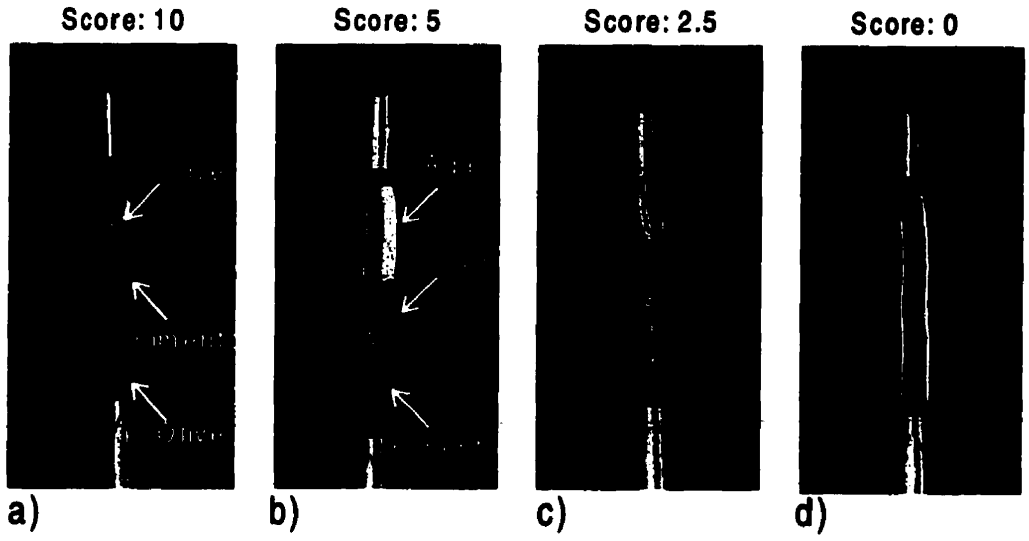

Figure 3.18: Core samples and their respective scores. a) A perfect score of 10 is obtained when a core sample contains olive on both sides of a pimento core. b) A score of 5 is obtained when a core sample contains pimento and olive on one side. c) A score of 2.5 is obtained when the core contains only olive. d) A core that contains only agar results in a score of 0.

3.3.3.2 Results

The test was performed 24 times in 3 different phantoms, with olives distributed throughout the biopsy volume. Of the 24 attempts, 18 scored a quality of 10, 2 scored a quality of 5, 3 scored a 2.5 rank, and 1 scored a 0 rank. The resulting average of these trials is a score of 8.2.

3.3.3.3 Conclusions

This experiment was a more realistic version of the targeting Experiment 3.2.3. The effects of needle deflection were evident in the trials, as the needle could actually be observed bending a slight amount as it passed though the agar gel. This was reflected in a comparison of the biopsy sample scores of targets positioned in the closer half of the phantom to targets in the farther half. The average score for all targets positioned in the closest 3 cm of the phantom was 8.5 compared to a score of 7.9 for all targets located at greater depths. The motion of the olives did not seem to be a large factor in this experiment. In an uncompressed phantom the olive tended to move in the phantom, however under compression in the biopsy device the olive was far less mobile. Whether

the degree of lesion mobility in a real breast under compression is comparable to that of the olive in the agar phantom is uncertain. Another factor that limited the effects of target motion is the use of a biopsy device with a strong mechanical throw. The strong throw of a standard biopsy device improved its cutting action. Less sharp needles, and biopsy devices with weaker throws would have a greater tendency to push the lesion out of the way, rather then pierce it. This is one of the benefits of doing the biopsy outside of the magnetic field. A biopsy device, which has been optimized for its purpose, can be used rather then one that has been compromised in order to satisfy the criteria of being non-magnetic. This benefit will most likely be apparent in real breast tissue as well. Another factor that affected the outcome of this experiment was the inaccessibility of some lesions in the regions near the biopsy insert. This issue was discussed previously, and contributed to one missed biopsy attempt in this experiment.

This system was able to achieve a high rate of successful biopsies in a breast equivalent phantom. Compared to the localization experiment, the average accuracy score was 8.2 compared to 6.9. This serves only as a general comparison because the two scoring systems used in each of these experiments were not identical. The statistical significance was determined using a non-parametric statistical test, Wilcoxon rank-sum with a large sample approximation [6]. This statistical test was used because accuracy score was based on an arbitrary scoring system that is not continuous. The Wilcoxon Rank-sum was used to test the hypothesis that the means of two independent populations are different. The *p-value* for an upper tail test was calculated to be 0.0735, which indicates that the two results are marginally statistically significant. From a practical standpoint rather than a statistical one, the two means appear to be substantially different.

The cores were sampled using only MR information such that no needle verification technique was used to validate that the needle and lesion were in the proper positions before the biopsy device was fired. The next experiment attempted to quantify if the addition of US guidance will in fact improve accuracy.

3.3.4 MR and Ultrasound Guided Needle Biopsy

The purpose of this comparative phantom experiment was to determine whether the addition of the real-time ultrasound imaging improved the accuracy of obtaining biopsy samples in a tissue equivalent phantom.

3.3.4.1 Procedure/Apparatus

Two different guidance techniques, MR-guided and MR/US hybrid guidance were used to biopsy lesions in a set of 3 different phantoms. Both techniques were performed on all the targets in the phantoms, resulting in a comparison of the quality of the core samples and a measure of the needle tip correction due to the addition of real-time US information.

The apparatus and techniques used for MR guided biopsy, were identical to those used in Experiment 3.3.3. The MR/US guided biopsy technique was presented in Chapter 2. A single trial consisted of the biopsy of a target using each guidance technique. The experiment consisted of the biopsy of all targets in a set of 6 phantoms using each guidance technique. The phantom set consisted of 2 phantoms of each agar concentration (1.0%, 2.5%, 5.0%). The quality of the core samples was the basis of comparison between the two techniques. Measurement of needle tip correction with the MR/US-guided approach quantified the impact of the ultrasound information on the pre-fire position of the biopsy needle. A biopsy sample was obtained for all targets in each phantom using both biopsy strategies.

3.3.4.1.1 MR Guided Biopsy

The phantom was imaged with the sequence used in Experiment 3.3.2 and 3.3.3, to locate the fiducial origin and the olive target centres. The apparatus was then removed from the bore of the magnet into an adjoining room as shown in Figure 3.20. The biopsy samples were acquired and scored as explained in Experiment 3.3.3.

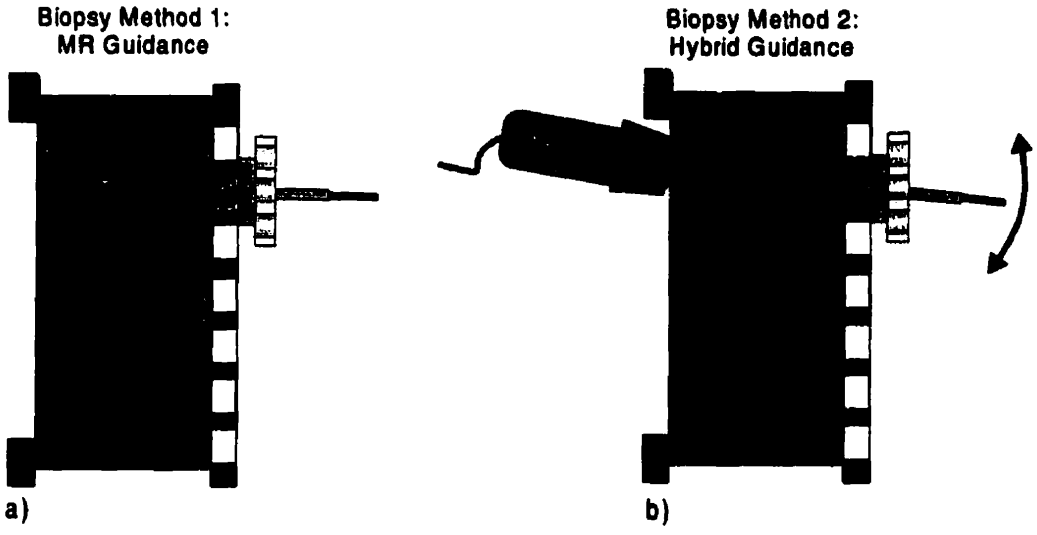

Figure 3.19: Biopsy strategies compared in this experiment. a) A biopsy was obtained for every olive target in the phantom using MR images. b) The phantom was then repositioned and a biopsy was obtained for every olive in the phantom using the MR data as an initial guide, and the US data to do fine adjustment of the needle position.

3.3.4.1.2 MR/US Guided Biopsy

For hybrid guidance biopsy, the ultrasound insert was placed in the medial compression frame while the biopsy insert was in the lateral frame. The phantom was imaged to locate the fiducial origin and the olives, and then removed from the MR magnet room into the console room. The apparatus was prepared for ultrasound imaging as depicted in Figure 3.21.

Figure 3.20: Picture of the biopsy apparatus being removed from the magnet bore. The patient bed is on wheels and can easily be undocked and removed from the MR magnet.

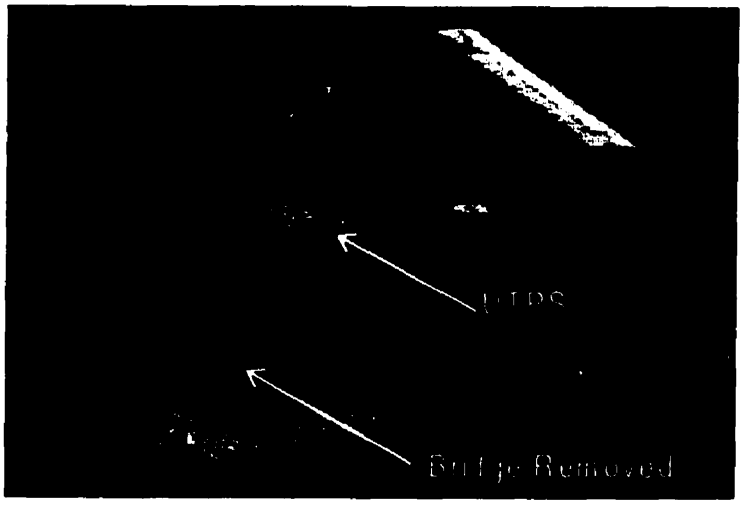

Figure 3.21: Positioning the UTPS with transducer on the medial side of the biopsy apparatus with the breast equivalent phantom in place.

The fiducial and olive positions were entered into the computer program, which determined the required core biopsy needle trajectory and the position of the ultrasound transducer. The biopsy plug was set and the US transducer positioned in the UTPS based upon the calculations. With the transducer in position, the phantom was imaged using the ATL US imaging system. The core biopsy needle was advanced into the phantom as demonstrated in Figure 3.22. The position of the US transducer and its acoustic imaging field are depicted in Figure 3.23, as well as the corresponding US images of the biopsy needle in pre-fire and post-fire positions.

The needle appeared in the US images as a hyperechoic line. As the needle progressed forward, the line approached the position indicated by the calculated ultrasound coordinates as indicated by the white cursor in Figure 3.23. In some cases, the needle trajectory could not be completely contained within the acoustic imaging plane due positioning restrictions of the transducer. In these circumstances only the tip of the needle entering the target could be visualized. The needle approach was monitored using the ultrasound information and adjustments made to the needle trajectory by loosening the collar of the biopsy plug as discussed in Section 2.6.4.2. When the needle was in the appropriate pre-fire position, the biopsy collar was tightened and the needle depth recorded. The biopsy device was then fired, post-fire position of the needle verified and

sample obtained. The biopsy plug was then put back into the goniometer and the final modified trajectory angles were recorded. The distance representing the correction of the needle tip position defined by the initial calculations, and the final needle tip position after ultrasound guided modifications was calculated for each biopsy. This is demonstrated in Figure 3.24.

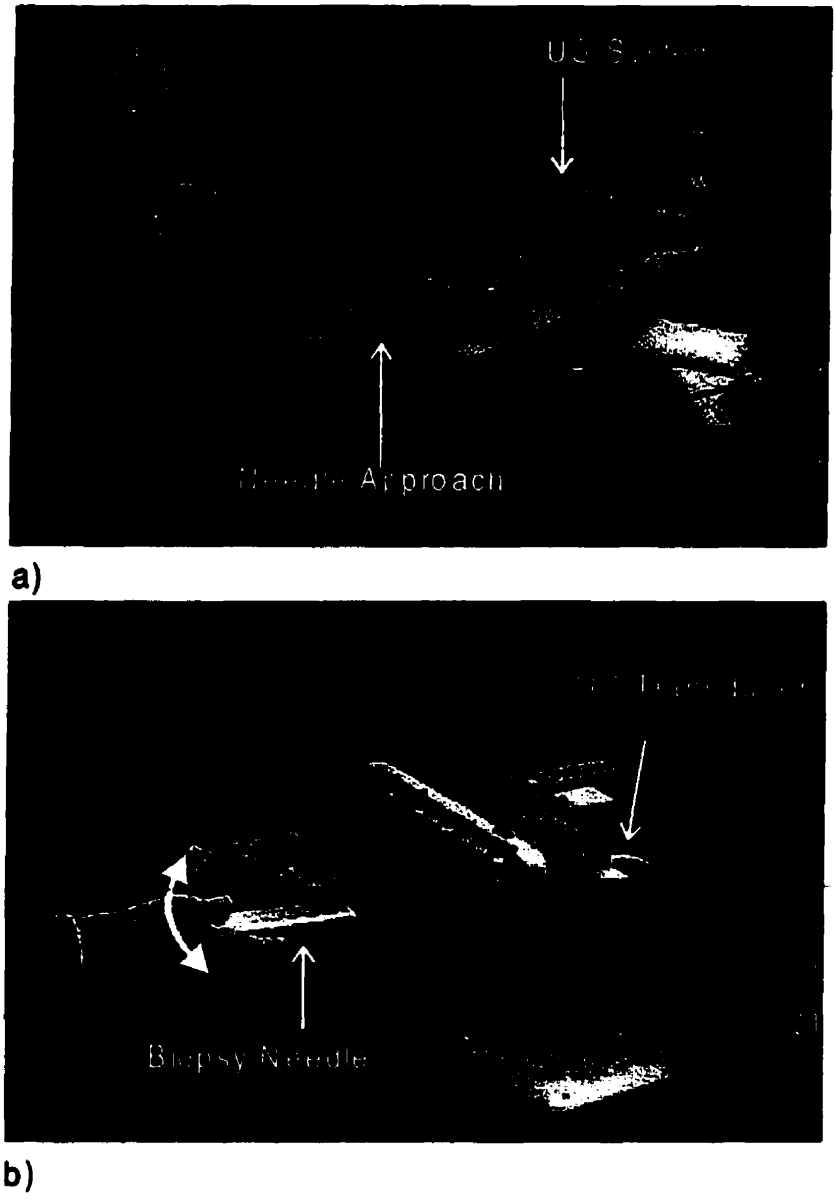

Figure 3.22: Hybrid Biopsy technique. a) With the apparatus outside of the MR magnet room, and the US system attached, the biopsy plug trajectory is set and positioned in the appropriate access window. The US images appear on the US system in real-time and are used by the radiologist to guide the needle position. b) Close up of the needle approach shows the biopsy device and the modifications in trajectory made by the radiologist.

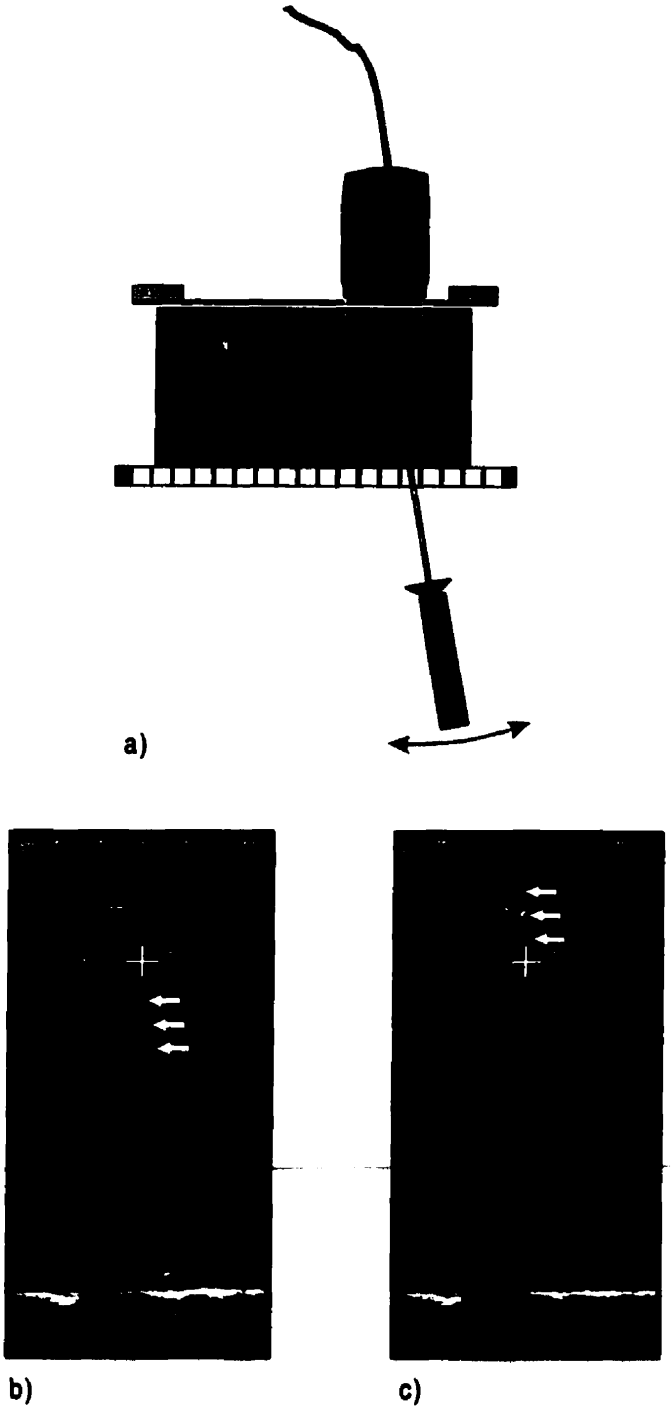

Figure 3.23: Needle guidance using US. a) Coronal view of the phantom, and the ultrasound transducer. The region enclosed in the dashed white lines corresponds to the acoustic field of the US transducer in b) and c). b) Pre-fire US image of the needle and lesion. The needle shaft appears as a bright line (identified by the three white arrowheads). c) Post-fire position of the needle. Slight modifications were made to the needle trajectory between pre and post fire. The position indicated by the cursor as calculated from the MR images, indicates the centre of the olive.

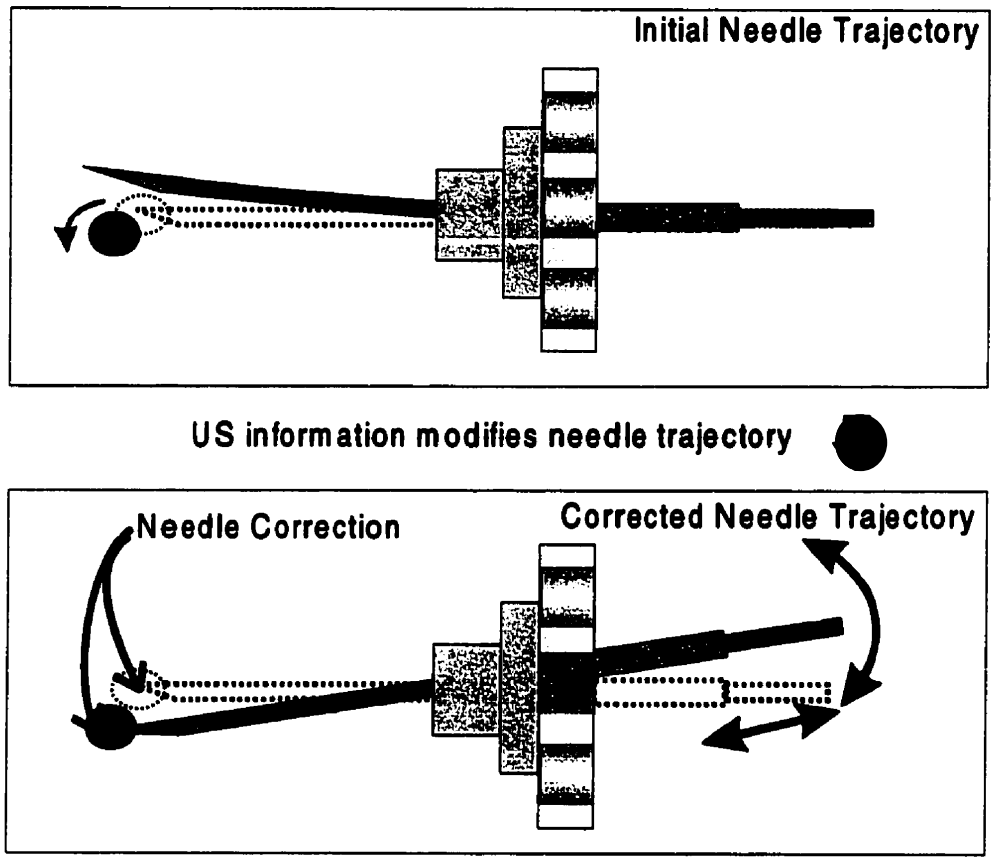

Figure 3.24: Measurement of needle correction. In the top diagram, the needle trajectory has been determined using the MR data. Upon insertion of the needle into the phantom, the needle can deflect and the lesion can move from its original position. The final position of the needle and lesion will be different from their intended positions as indicated by dashed outlines. The bottom diagram shows the final position of the needle when US information is used for needle guidance. Placing the plug into the goniometer and measuring the change in the shaft trajectory and the needle depth can determine the final corrected position of the needle.

3.3.4.2 Results

Both guidance techniques were performed resulting in a biopsy of every olive in each phantom type. A comparison of the two techniques for the different phantom types is found in Table 3.5. The first column indicates the type of phantoms, spanning 3 agar concentrations by weight (1.0%, 2.5%, 5.0%). The second column corresponds with the total number of targets sampled with each technique. The third column corresponds to the results of the MR guided biopsy strategy. The fourth and fifth columns correspond to the results of the hybrid guided biopsy strategy. The

accuracy of the biopsy strategies was quantified by averaging the core quality scores for all trials of the same phantom type. The average amount of needle correction for a particular phantom due to the real-time US information was determined by averaging the total needle correction calculated for all trials of the same phantom type.

		MR GUIDANCE	MR/US GUIDANCE	
Phantom Type	**Number of Targets**	**Average Accuracy Score out of 10**	**Average Accuracy Score out of 10**	**Average Needle Tip Correction (mm)**
1.0 % Agar	17	8.8	9.0	2.6*
2.5 % Agar	21	8.3	8.7	3.0
5.0 % Agar	21	7.4°	9.6°	3.7*

Table 3.5: Results for experiment 3.3.4, comparison of guidance techniques in a breast equivalent phantom. The symbols ° and * indicate that the pair of values is statistically different.

3.3.4.3 Conclusions

In all phantom types, the average accuracy of the hybrid biopsy strategy was better then the MR-guided biopsy. The Wilcoxon rank-sum statistical test was used for the same reasons outlined in the previous experiment to determine statistical significance of the results. A statistically significant difference ($P = 0.02275$) between the average accuracy for all biopsies obtained using MR guidance verses hybrid guidance was obtained for the 5.0% agar phantom. The same statistical analysis resulted a marginally significant difference ($P = 0.07927$), and an insignificant difference ($P = 0.41294$) for the 2.5% and 1.0% agar phantoms respectively.

As the stiffness of the phantom increased, the accuracy of the MR-guided biopsy technique tended to decrease. The average accuracy score was 8.8 in a 1.0% agar phantom, compared to only 7.4 in the 5.0% phantom yielding a marginally statistically significant difference on analysis ($P =$

0.1057). This could be attributed to the increased amount of needle deflection in the stiffer gel. A decrease in the accuracy scores was observed between the 1.0% and 2.5% agar phantoms, 8.8 verses 8.3 respectively (P=0.29460), and the 2.5% and 5.0% phantoms, 8.3 and 7.4 respectively (P=0.1922).

The decrease in accuracy scores as the phantom stiffness increased was not observed for samples obtained using the hybrid biopsy technique. The average accuracy score increased slightly from 9.0 in the 1.0% agar phantom to 9.6 in the 5.0% agar phantom (P=0.2912). The accuracy score decreased slightly from 9.0 in the 1.0% phantom to 8.7 in the stiffer 2.5% phantom (P=0.4404). A moderate increase in the accuracy scores was again evident when comparing the score of 8.7 in the 2.5% phantom to 9.6 in the 5.0% phantom (P=0.2177). From a statistical standpoint, there was no change between the accuracy scores as the phantom stiffness was increased. The improvement that was observed as the phantom stiffness increased was most likely due to the improved visibility of the needle in the stiffer phantoms, however the results do not have the statistical power to back this statement.

The average needle tip correction values tended to increase as the stiffness of the phantom increased. In the 1.0% agar phantom, the average needle tip correction was 2.6 mm, compared to the 3.7 mm in the 5.0% agar phantom (P=0.0089). This may be attributed to the increased correction required, as needle deflection became more of a factor. The average needle correction of 3.7 mm is large relative to the size of the olive core (7.0 mm diameter). That amount of correction in a stiff phantom is on the order of one half the radius of the target. The high accuracy score associated with the large amount of correction due to the US information in the stiff phantom suggests that many of these cores would be missed with MR guidance alone.

In all the phantoms the lesion mobility did not seem to be the major factor contributing to inaccurate sampling. The lesion was noted to move a slight amount in the ultrasound images when the biopsy device was fired. If lesion mobility was a major factor, we would have expected to see the accuracy of the uncorrected, MR-guided biopsy to decrease substantially in the softer

phantom. It seems that the major effect of the softer phantom was reduced needle deflection rather then increased lesion mobility, leading to an improvement in accuracy with both guidance techniques. The same factors discussed in Section 3.3.3.3, strong throw of biopsy needle and aggressive medial lateral compression contributed to the limited effect of lesion mobility.

The accuracy of the MR/US-guidance strategy depended on the ability to visualize clearly the lesion and the needle. In all cases the lesion could be registered to the ultrasound transducer and was accurately indicated by the ultrasound coordinates, z depth and x-offset. In some cases, where in-plane registration of the biopsy needle and lesion could not be accomplished due to limitations of the apparatus, the resulting biopsy samples tended to be less accurate and the procedure was more difficult. The ability to accurately register the MR and US images may present a problem in clinical application. The effects of varying velocity of sound and refraction throughout the various tissues in the breast will result in some inaccuracy in image registration. Apparent shifts of the lesion and needle in the US image and through the plane of the US transducer could make identification of the lesion and monitoring needle progression in the US image difficult. These effects are not apparent in this phantom experiment as the velocity of sound in the phantom is very near that of water, but will be apparent in real breast tissue. These issues are discussed in detail in Section 4.2.4.

The overall visibility of the needle was considered to be poor in some trials. As mentioned previously, the visualization of the needle depended on the stiffness of the agar gel, and will be different in the real breast. The optimal orientation of the needle in the US images is perpendicular to the transducer, which is not the case in this application [10]. In some cases the needle was much better visualized when it approached the lesion at an angle. A slightly different trajectory calculation strategy could be implemented so the biopsy window is selected such that the angle relative the transducer face is large. This would be a trade-off with the current restriction of selecting the shortest path to the lesion, for increased visibility of the needle.

As mentioned above, multiple factors affect the accuracy scores for a particular biopsy technique

beyond just the increased mechanical deflection of the needle due to varying the stiffness of the phantom. These multiple factors convolute the statistical results to some extent. As the stiffness of the phantom was increased, the mobility of the lesion and the visibility of the needle in the US images substantially affected the accuracy score. These multiple factors are not accounted for in the Wilcoxon rank-sum statistical analysis as presented. In order to take these factors into account the non-parametric alternative to the F-test, known as the Kruskal-Wallis test, is required [6]. A more detailed examination of the interactions between the variables affecting the accuracy of the biopsy techniques is not appropriate considering the scope of this thesis.

The accuracy of registration and biopsy needle targeting are limited by the same factors that are discussed in Experiment 3.2.3 and 3.2.4. These factors contribute to the overall accuracy of the biopsy strategies. The overall accuracy of the hybrid guidance procedure is also dependent on the ability of the operator to guide the needle to the appropriate pre-fire position based on the US images. This required some skill and training on the part of the operator and contributed to the variability associated with the accuracy results and the average needle tip correction values. The ability to infer needle position as well as updating the position of the US transducer to accommodate changes in needle trajectory was a skill that improved over time.

3.4 Summary

The phantoms developed for this experiment were a simple and reasonable approximation of a tumour in a breast, but many factors that may affect the outcome of the biopsy were not modeled. In a real breast, the needle will traverse through many interfaces of fat and fibroglandular tissue [11]. The needle will tend to deflect along the path of least resistance, so when the needle tip encounters an interface of soft fat and stiffer fibroglandular tissue, the needle will deflect in the direction of the fat [12]. Since this is a homogeneous phantom, this effect has not been modeled. Patient motion is another issue that is not addressed in this experiment, but is critically important in a clinical setting [13].

The targeting experiments presented in this Chapter (3.2.1-3.2.3), demonstrated the ideal performance of the biopsy targeting and US registration techniques. It was determined that the positioning of a localization needle, core biopsy needle, or registration of an US imaging plane, based on a set of MR images could be done accurately and consistently. Positioning of the core biopsy needle was more accurate compared to the localization needle due to the novel angulation technique developed.

The phantom Experiments (3.3.1-3.3.3) provided a more accurate test of what might occur in a real breast. This phantom was used to test the capability of the biopsy techniques and demonstrated the improvement in accuracy associated with the addition of US as a secondary guidance imaging modality. The accuracy of wire localization and core biopsy techniques were affected by the stiffness of the deflecting medium of the phantom. In order to improve the accuracy of both these methods, a verification technique would be required.

The phantom experiment comparing the US and MR guided core biopsy strategies used three different phantoms to determine how much the relative difference between the modalities changed with different stiffness of phantoms. Results showed an improvement with the addition of the US guidance. Although the phantom experiments only approximate the clinical situation, they do allow us to simulate the phenomena that occur while attempting a biopsy in real breast tissue, and provide a method to test and optimize the techniques before clinical use.

The next chapter looks at the clinical application of some of the techniques tested in this chapter and examines the phenomena that cannot be appropriately modeled using phantoms. Chapter 4 also looks into how the biopsy techniques can be improved by tackling some of the technical problems discussed as well as how this biopsy system can be integrated with other imaging and interventional technologies in novel ways.

References

1. Beese RC, Lowe S. The use of turkey breast and stuffed olives as a soft tissue model for the teaching and practice of ultrasound guided interventional procedures. *European Journal of Ultrasound*, Volume: 7, Supplement 1, February, 1998, pp. S12.

2. Kuhl CK. MRI of Breast Tumours. *European Radiology*. Volume 10, 46-58 (2000)

3. Carter D. *Interpretation of Breast Biopsies*. New York: Lippincott-Raven; 1996.

4. Liney G.P, Tozer DJ, Turnbull LW et al. Bilateral Open Breast Coil and Compatible Intervention Device. *Journal of Magnetic Resonance Imaging* 2000. 12:984-990.

5. Walton L, Hampshire A, Forster D, Kemeny A. A Phantom Study to Assess the Accuracy of Stereotactic Localization, Using T1-weighted MRI with the Leksell Stereotactic System. *Neurosurgery*. 38:170-178, 1996.

6. Applied Statistics and Probability for Engineers. D. Montgomery, Wiley & Sons Inc, 1994, Nonparametric Statistics, p803-830.

7. Rumack CM, Wilson SR, Charboneau JW. Diagnostic Ultrasound. Volume 1, Second edition, 1998, Mosby-Year book, St. Louis Missouri.

8. Sumanaweera T, Glover G, Song S, Adler J, Napel S. Characterization of Spatial Distortion in Magnetic Resonance Imaging and its implication for stereotactic surgery. Neurosurgery 1994; 35: 696-704.

9. Liberman L. Stereotactic Biopsy Technique, in "Interventional Breast Procedures", Churchill Livingston, New York, 1996.

10. Parker SH, Jobe We, Dennis MA, Stavros AT, et al. US-guided automated large-core breast biopsy. Radiology 1993; 187, 507-511.

11. Wolbarst AB. Physics for Radiologists. Prentice Hall, Toronto, 1993.

12. Problems and Pitfalls in Core Biopsy. in "A Comprehensive Approach to Stereotactic Breast Biopsy".(Fajardo LL Ed, Willison KM Ed.). Blackwell Science, Boston, 1996.

13. Liberman L. Percutaneous Imaging-Guided Core Breast Biopsy. AJR 2000; 174:1191-1199. Fisher PR,

Chapter 4

Clinical Results and Future Directions

4.1 Introduction

The previous chapter described results of experiments designed to test the accuracy of biopsy strategies presented in Chapter 2. The first section of this Chapter, 4.2, presents the results of the clinical application of some of these strategies, including wire localization (4.2.1), core biopsy (4.2.2) and MR/US registration (4.2.3). The next section, 4.3, focuses on improvements that can be made to the current apparatus to solve some of the problems presented thus far. The final segment investigates how other imaging techniques can be incorporated into the system and the potential to extend the system to applications other than biopsy.

4.2 Clinical Application – Preliminary Clinical Trials

In Chapter 3 we saw that the addition of US for needle guidance was a novel development that has demonstrated its effectiveness in improving the accuracy of acquiring biopsy samples in phantoms. Besides accuracy there are other immediate benefits afforded by this technique, mainly:

- reduced MR magnet time
- use of imaging systems for their intended purpose
- reduced procedural complexity

Reducing the required magnet time per biopsy procedure allows better throughput on MR systems. With the proposed system, the biopsy would be done outside of the magnet, requiring the magnet only for imaging purposes. This could result in a substantial cost reduction per procedure. The concept of moving the patient outside of the magnet for intervention could be extended for more time consuming MR procedures such as thermal ablation of tissue, which is considered in more detail at the end of this chapter [1,2].

Performing biopsy with hybrid guidance, by separating the function of detection and guidance, allows both imaging systems to be used for their intended purpose. MRI has demonstrated to be a highly sensitive imaging technique, while US has proven to be an effective guidance modality [3,4]. The use of ultrasound as a secondary, or adjunct imaging modality allows the possibility of improving the specificity of the procedure [5]. By simply registering the US plane to the MR detected lesion, the appearance of the lesion in US can be used to indicate its malignancy status as indicated in Chapter 1.5.2.3. This application is presented in this chapter, Section 4.2.3. Further extensions to US imaging, such as Doppler US, that have the potential to improve the specificity and sensitivity of US are also presented in Section 4.3.2 [6-7].

Performing the biopsy in an adjacent room to the MR magnet reduces the overall complexity of the procedure. The strict requirement of having non-magnetic equipment, or equipment that is not damaged by the strong magnetic field is no longer an issue. This benefit is immediately apparent when the compatible types of biopsy needles are considered. The standard biopsy needles are made of stainless steel and are much sharper and stiffer than the specialized needles developed for MRI [8]. The standard rapid-fire biopsy device fires the two biopsy needle components forward with much greater force then the comparable MR compatible systems, resulting in minimal lesion movement as the needles easily pierce the target [9].

With the expected improvement in accuracy, and the benefits previously mentioned, a strong case can be made for the clinical application of such a system. However, hybrid-guidance biopsy is a fairly complicated procedure, which effectively combines two concepts; MR-guided needle delivery, and MR/US image registration. It was decided that it would be more appropriate to perform preliminary clinical trials using the less complicated biopsy procedures; MR guided needle localization and MR guided core biopsy as well as MR/US registration separately. In fact, the need to perform biopsy on patients presenting finding suspicious on MR, and occult to other imaging modalities, expedited the development of the MR guided needle localization procedure and provided the motivation to apply this biopsy technique first.

In preparation for clinical application of all procedures, tests were performed with the senior radiologist in the SWCHSC high-risk screening study using the tissue equivalent phantom presented in Section 3.3.1. The tests demonstrated the accuracy of the techniques, and provided a means to perfect the clinical protocols that are required with an actual patient, such as patient positioning, sterile protocol and correct needle positioning.

The preliminary clinical trials for MR guided needle localization are presented in the next section whereas Sections 4.2.2 and 4.2.3 demonstrate limited clinical application of needle core biopsy, and MR/US image registration. The senior radiologist gave clinical approval for these procedures, while an ethics committee approved interventional procedures associated with the high-risk screening study.

4.2.1 MR Guided Needle Localization

The first procedure to be implemented in preliminary clinical trials was MR guided needle localization. This procedure was applied to patients in the high risk screening study at SWCHSC who had lesions detected using contrast-enhanced MRI that were occult to screening mammography and ultrasound and subsequently could not be detected retrospectively for biopsy purposes. At the time that this thesis was written, there were 5 needle localizations performed using the system and techniques presented in Chapter 3. The imaging technique used for the

procedure is outlined in Chapter 2 and a clinical case is shown in Figure 4.1.

The lesions that were localized ranged in size from 0.6 to 1.0 cm (mean 0.8 cm). They were located at various positions throughout the breast. One was medially located and required a medial biopsy approach. As far can be determined from current research literature, this was the first medial MR-guided wire localization performed. A summary of the localization procedures is found in Table 4.1 with the pathological diagnosis of the lesions. One small 0.7 cm invasive carcinoma was excised, while the rest of the findings were benign. In all cases, the appearance of the lesions in MR corresponded to the pathological findings leading us to believe that all the lesions in question were properly excised.

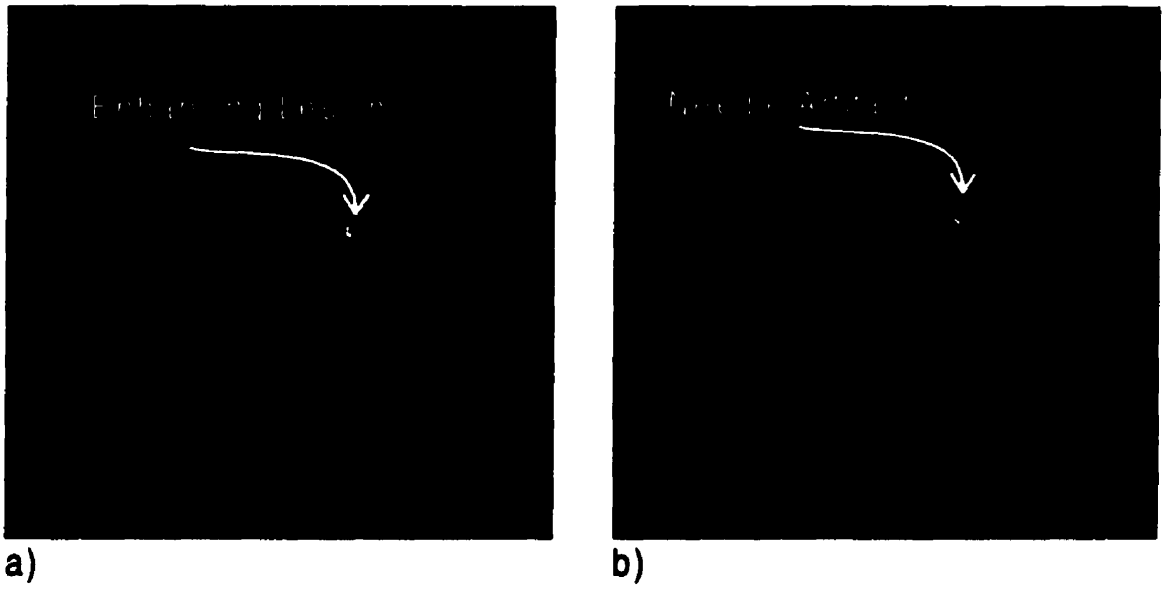

Figure 4.1: Contrast enhanced MR images acquired during a medial approach localization procedure. a) Sagittal image obtained 1-minute post contrast agent injection. The lesion was identified and the localization needle positioned based on the MR images. b) Verification MR image depicts the artifact from the localization needle relative to the lesion. The needle tip was approximately 3 mm off from the centre of the lesion.

Procedure	Approach	Lesion Size (cm)	Pathology
Localization 1	Lateral	1.0	Fibroadenoma
Localization 2	Lateral	0.7	Fibroadenoma
Localization 3	Medial	1.0	Fibrocystic disease
Localization 4	Lateral	0.6	Inflamed lymph node
Localization 5	Lateral	0.7	Invasive carcinoma

Table 4.1: Clinical Localization Results

4.2.2 MR Guided Core Biopsy

The second type of biopsy technique performed clinically was an angled approach needle core biopsy. The apparatus and techniques used were similar to the experiment performed in Section 3.2.3. This procedure was only attempted in one case. The patient who opted for this procedure presented a suspicious lesion detected with the MR bilateral screening examination and occult to other modalities. They were told of the risks and given the option to undergo a needle localization followed by an excisional biopsy, or the needle core biopsy. They selected the less invasive needle core biopsy procedure.

The procedure involved the patient lying in the apparatus with the breast containing the lesion compressed between the sterilized biopsy compression inserts. The imaging procedure involved determining the fiducial locations with a set of scouting images before the injection of contrast agent. The lesion became apparent within 80 seconds after injection of contrast agent and is depicted in the sagittal T1-weighted image shown in Figure 4.2.

Figure 4.2: MR image for core biopsy procedure. a) Fat saturated MR image demonstrates no focal enhancement prior to contrast agent injection. b) One minute after contrast agent injection, a lesion appears. This lesion corresponds to the suspicious lesion detected in screening examination, and was the target of the core biopsy procedure. The pathology indicated this lesion was stromal fibrosis, a benign condition.

The lesion and fiducial coordinates were determined from the MR console and calculations were performed to determine the needle trajectory required to intercept the lesion at multiple points. The approach selected was a medial approach in order to minimize trauma to the breast. The calculations were restricted such that all needle entry points would be made through the same incision point. A position at the centre, and 3 at the periphery were selected. The 4 biopsy plugs were set to the corresponding calculated trajectories using the goniometer, and adhered to strict sterile procedure.

The patient was removed from the magnet room, and an incision was made in the appropriate biopsy window with a scalpel. Biopsy plugs were used to guide the needle into place. The needle was positioned to the appropriate depth, the biopsy device was fired and a sample was acquired. This was repeated for all the biopsy plug trajectories in succession. The total time for the procedure was 50 minutes.

The pathology performed on the core samples indicated the lesion was stromal fibrosis. The

radiologist who performed the procedure was uncertain that the diagnosis matched what was seen in the MR images. During the procedure there had been some problems with patient motion and poor breast compression, therefore the possibility of an inaccurate core sample could not be ruled out. The patient was given the choice of undergoing a wire localization procedure to remove the lesion. The patient opted for a 6-month follow-up examination, at which time the lesion had not grown, or demonstrated any features that indicated that further clinical intervention would be required. This supported the clinical diagnosis based on the core biopsy procedure.

4.2.3 MR/US Registration

The third clinical application of the system was registration of an US scan plane to investigate the MR detected lesion. This is a segment of the entire hybrid biopsy procedure, but it may in fact demonstrate some utility as a clinical procedure independent of the needle positioning. Other than validating a component of the hybrid biopsy technique, successful registration of the US scan plane to visualize the lesion may aid in the diagnosis of whether the lesion is malignant or benign.

The patients selected for this procedure were women advised to have a follow-up MR procedure due to suspicious findings. The follow-up procedure was discussed in Chapter 1, Section 1.5.3.3 and is summarized in Table 1.1. The procedure consists of an initial T2-weighted, fast spin-echo sagittal imaging series, followed by the dynamic T1-weighted series in concert with contrast agent injection, followed by a 3D high resolution imaging series. To modify this imaging protocol for the purpose of US registration, an imaging series to detect the fiducial marker positions was added at the beginning of the protocol, while an oblique-coronal T1 weighted series was added at the end.

The patients were positioned in the apparatus with the breast of interest between the compression plates with an US insert on the side closest to the lesion and the biopsy insert on the other. The imaging sequence explained previously was used to determine the lesion and fiducial marker position. A calculation to determine the required position of the US transducer to register the

lesion was performed. The transducer position was reported as coordinates for the UTPS, and coordinates to identify the lesion in US space as described in Chapter 2. A final imaging series was obtained corresponding to the calculated angle of the US transducer. The imaging series was a coronal T1-weighted, spin-echo series with no fat suppression, and angled obliquely in the axial plane.

After this final imaging series, the patient was removed from the bore of the magnet, and rolled into the adjoining room. The UTPS was positioned on the compression frame on the same side as the US membrane insert. The cursor was positioned on the US image according to the US coordinates from the calculations. The lesion was expected to appear at the cursor position if registration was perfect. If registration was inaccurate, adjustments were made to the transducer angle and position.

This procedure was performed on a patient who presented a rim-enhancing lesion on her bilateral screening examination. The lesion was occult to other screening modalities, only detected using MRI. A rim-enhancing region believed to correspond to the previously detected lesion, appeared in the dynamic imaging series. The same location on the T2-weighted image demonstrated a focal region of bright signal indicating that this area may contain increased fluid content. This is demonstrated in Figure 4.3 where the lesion is identified in the T2-weighted and T1-weighted dynamic image.

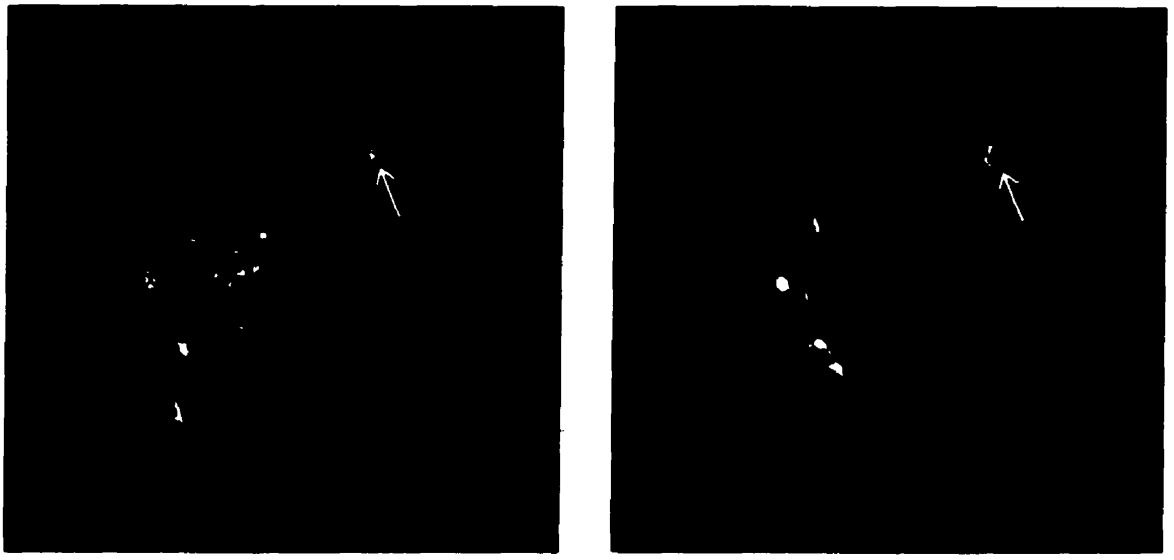

Figure 4.3: MR images from the follow-up registration experiment. a) T2 weighted fat-saturated 2D-fast-spin echo image depicts 7mm region of bright signal indicated by the white arrow. b) T1-weighted image taken 1 minute 20 seconds after gadolinium injection demonstates a 9mm region rim-enhancement around the same position as Figure a).

The woman was removed from the magnet and the transducer positioned as required. US imaging with the transducer in the calculated position did not demonstrate any obvious indications of a lesion. The transducer was scanned and repositioned 3 mm below the calculated position resulting in corresponding US image shown in Figure 4.4. The white cursor indicates the depth and offset to where the lesion should have been centred. An oval 7 mm object was identified 3 mm from the cursor. This object has well-defined boarders, some internal echogenicity, and slight posterior enhancement. The US features of this object do not correspond with the expected US features of a malignant lesion, however the US visible lesion is approximately the same size and is located at very near the expected position of the lesion based on the cursor position. The lesion was deemed to be highly suspicious based upon the MRI findings, and resulted in scheduling an MR-guided localization with excisional biopsy. The pathology indicated a 7 mm invasive carcinoma. This corresponds to the fifth localization procedure shown in Table 4.1.

Figure 4.4: Registered US image based upon MR based calculations. The solid white cursor represents the position where MR based calculations indicated the lesion to be. The dark, circular, well-circumscribed mass indicated by the measurement crosshairs was detected in the vicinity. The size of the mass, 0.67 cm corresponds well with what was seen in the MR images.

Another strategy that was initially presented in Section 2.6.3.3 was implemented in retrospect to determine whether or not the US visualized object corresponded to the MR detected lesion. The architecture of the parenchyma surrounding the lesion was used to provide valuable information to assist in locating the position of the lesion in the MR and the US images. The fat and fibroglandular interfaces were used as distinct landmarks in both imaging modalities. Using these landmarks to define the position of the lesion in MR images, and finding these landmarks in US images, can help to locate inconspicuous lesions, and validate accurate image registration.

This concept is demonstrated in Figure 4.5. Figure 4.5 a shows a coronal T1-weighted image acquired at a time over 10 minutes after contrast agent injection. It is at an oblique, coronal plane, which corresponds to the calculated position of the US transducer. The white arrow indicates the

position of the lesion, as determined by the MR coordinates. The contrast agent has washed out by this time. The white box overlaid on the MR image depicts the acoustic field of the US transducer. Figure 4.5 b is the corresponding US image, with the grayscale levels inverted to match the contrast seen in the MR image. In this image, the fat generally appears as bright signal, and the fibroglandular tissue as dark signal, corresponding to the MR image.

One of the key landmarks in this image is the fat-fibroglandular tissue interface and the corresponding "horn" of fibroglandular tissue that is indicated by three arrows on both images. This interface extends in front of the lesion seen as a dark band in both images, indicated by a pair of arrows. Using these landmarks as a reference points, the lesion position indicated by the arrowhead on the MR image, appears to correspond to the indicated lesion in the US image. This landmarking and referencing technique may prove to be a valuable method for locating lesions that are difficult to detect in the US images.

4.2.4 Clinical Application Problems

Moving the biopsy techniques from experiments to clinical application posed difficulties. The localization procedures progressed without incidence; however, the core biopsy procedure presented an unexpected challenge. Insertion of the needle into the skin required an incision to be made in-line with the needle entry point. This required the radiologist to estimate the position of the incision and monitor the entry of the needle into the skin, which proved to be difficult.

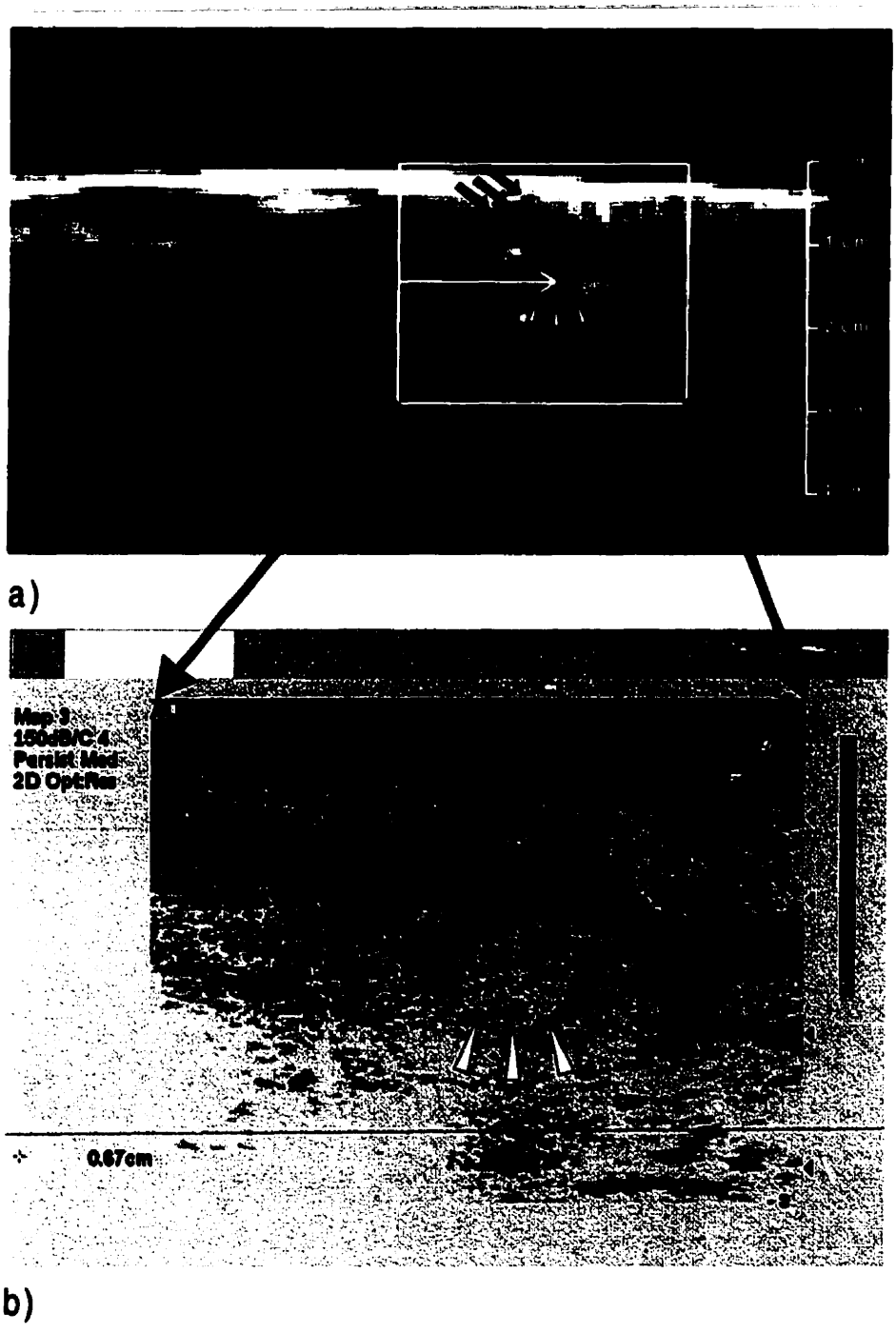

Figure 4.5: Comparison of lesion position based on native landmarks in the breast. a) An oblique coronal MR image was obtained at the position corresponding to the scan plane of the ultrasound transducer. This image is T1-weighted with no fat suppression. The bright signal corresponds to the fat in the breast, while the dark regions correspond to fibroglandular tissue. The white arrow corresponds to the centre position of the lesion as detected by MRI, while the white box corresponds to the approximate position of the US transducer imaging plane. b) The corresponding US image, which is identical to the one shown in Figure 4.4 except the grayscale intensities are inverted. The dark signal corresponds to fibroglandular tissue and the interfaces between fat and fibroglandular tissue, while the bright signal corresponds to fat. This allows us to reference the position of the lesion detected in the MR image and the US image.

The clinical MR/US registration procedure demonstrated that registration accuracy and lesion visibility in US images was compromised in a real breast compared to a phantom. Patient motion and beam deflection may have contributed to this inaccuracy. As the US beam passes through the breast, it will pass through tissues in which the speed of sound varies. The two extremes being fat and fibroglandular tissue where the speed of sound is approximately 1437 m/s and 1540 m/s respectively [10]. This change in velocity will distort the image in two ways as depicted in Figure 4.6. The US imaging system determines the depth from which echoes are reflected in the breast based on the time from the transmission of the US pulse to the time an echo is detected at the tranducer. In order to do this mean velocity of sound in the breast is assumed to be approximately 1540 m/s. All depth calculations performed in the US system are determined from this value. If the echo traverses through a region of lower velocity, the pulse will return to the transducer at a longer time interval, and the calculations will determine the echo to be located at a position deeper within the tissue than it is actually occurring. This results in a substantial mis-registration between the physical position of the structures in the breast relative to the transducer and the position of these same structures in the MR image. In the extreme case, with a solid lesion located in a breast composed mainly of fat, there would be approximately an 8% error in the axial position of the lesion. This translates to an error of approximately 2.5 mm at a depth of 3 cm in the breast. This is fairly a substantial error when considered relative to other error sources in the system. [10,11]

The other source of error is associated with refraction of the ultrasound beam at interfaces between tissue of varying velocity as shown in Figure 4.6 b. As the beam is refracted, structures deep within the tissue appear shifted laterally and axially in the images compared to their physical position. This effect is more difficult to quantify since it is dependent on the angle of the interface and the composition of the tissues. The effects of both varying velocities and beam refraction result in distortions that affect the accuracy of MR/US registration in a real breast in a way that would be difficult to predict. This source of error in US images has been investigated by numerous groups in both the breast and in other organs [12,13]. As of yet, despite attempts to correct for this phenomenon, the issue remains unresolved. A solution, limited to MR/US registered breast imaging, might emerge from the work presented in this thesis. A novel way to

use MRI information to predict how much the beam may refract and how much error may be introduced due to the fat content of the breast is presented in Section 4.3.

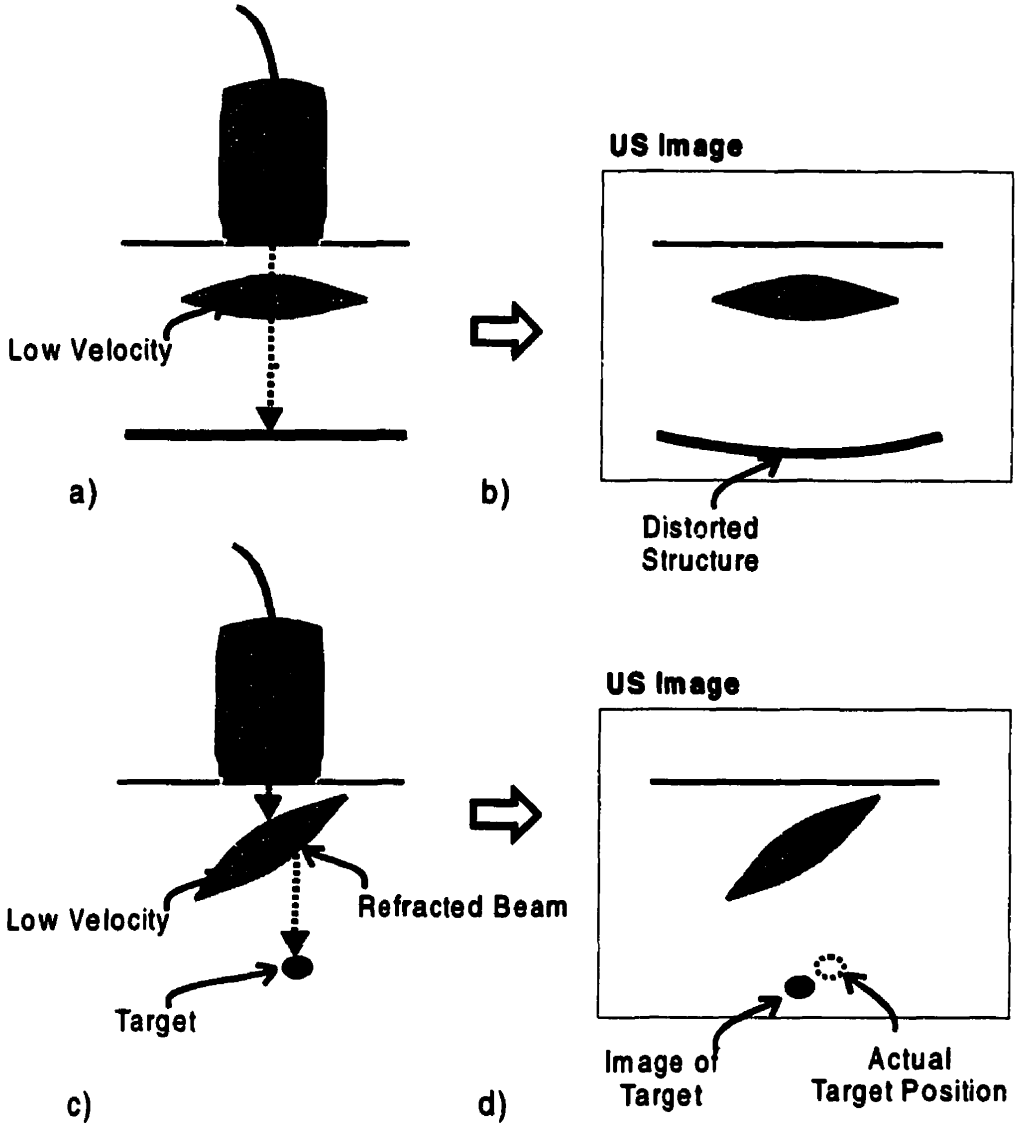

Figure 4.6: Effects of varying velocity on US images. a) Imaging through a region of different velocity results in a longer transit time for the US beam. b) This longer transit time results in axial distortion of structures in the US image. c) If the region of different velocity is non-normal to the US beam, then the beam will deflect. d) This deflection of the beam will result in structures appearing shifted in the US image resulting in a lateral distortion as well as an axial distortion and potentially mis-registration through the transducer imaging plane. These effects will result in mis-registration within breast tissue where the velocity of sound is approximately 1420 m/s compared to fibroglandular tissue (1540 m/s).

The clinical registration case also demonstrated that the visualization of the lesion in the US image could be substantially improved. A higher frequency probe would improve the resolution of the

image and help to visualize some of the finer features of the lesion better. These higher frequency transducers have limited imaging depths as discussed in Chapter 1. The penetration depth drops off as the frequency of the transducer increases [10]. This may not be a problem for registration procedures, where the transducer is positioned in a way to minimize the distance to the lesion, but may be a problem for the hybrid guided biopsy procedures. These procedures require that the biopsy needle traverse the shortest path to the lesion. It then follows that the ultrasound transducer must be positioned on the opposite side, resulting in a larger amount of tissue to be penetrated. At high frequencies, the attenuation of the breast tissue is substantial resulting in the inability to visualize adequately lesions positioned close to the biopsy approach side.

The problem of US visibility of lesions is magnified when the nature of the lesions detected using MR is considered. Many of these lesions are highly vascular, and have a high cellular content. These lesions tend not to generate the shadowing features that are often indicative of carcinomas in US images [14]. In these cases, the lesion may not be adequately visualized with standard B-scan US. Strategies that may potentially improve lesion visibility are discussed in Section 4.3.1.4.

4.3 Future Directions

A hybrid biopsy system as presented has the potential for many different applications, from improvement of surgical excision, to increasing specificity of lesion diagnosis. Improvements that can be made to this system are presented in Section 4.3.1. Ways in which various US techniques may be incorporate into such a system are presented in Section 4.3.2.

4.3.1 Improvements to Current Apparatus/Techniques

4.3.1.1 Needle Positioning

Improving the accuracy with which a needle can be positioned into the MRI detected tumour is the one of the primary motivations for the development of the hybrid biopsy system. The accuracy

depends on how well the needle is initially positioned within the breast and how well the needle tip and lesion can be visualized and their relative positions validated. More accurate needle placement would be expected if the problems outlined in the experiments of Section 3.2.2 and 3.2.3 were resolved.

Determining the extent that *gradient warp* is affecting the spatial accuracy of the images, and correcting for it in software would substantially reduce needle-positioning errors. The amount of *gradient warp* could be quantified and used to determine an appropriate offset calculation to be applied to subsequent calculations. Other groups have attempted to correct for this grad wrap with more advanced algorithmic approaches, which may also be considered [15,16].

4.3.1.2 MR/US Registration

Accurate registration of the US imaging plane, the lesion and the needle along its trajectory facilitates needle guidance. Ensuring that the lesion is defined accurately by the US space coordinates, enables the biopsy to be performed even if the lesion is not adequately visualized. The radiologist can simply guide the biopsy needle tip to the position indicated by a cursor on the US image. The corrections for *gradient warp* mentioned in the previous section and the potential redesign of the US transducer positioning apparatus would provide an improvement in registration accuracy. Further corrections for mis-registration errors associated with the US imaging system may also be addressed. The registered MR images provide an unprecedented opportunity to determine the fat and fibroglandular tissue components of the breast. Using this information to map the velocity of sound throughout the breast and using these values to calibrate the received US echo times could potentially correct for any mis-registration errors.

Development of a new transducer positioning method based upon the free-hand technique used by ultrasonographers would further provide many benefits. The ability to move the transducer in a similar manner to current US free hand technique would allow the lesion to be imaged in the ideal plane. It is well known that some lesions appear to be benign in one imaging plane, but through another plane it may appear malignant [14]. A freehand-type manipulation of the transducer

would take this into consideration. Linking the transducer position from the encoders into a computer, a program could be developed that determines the needle trajectory that corresponds to the desired transducer position such that the needle with pass through the US imaging plane into the lesion.

4.3.1.3 Needle Visualization

The visibility of the needle in the real-time US images is essential for accurate needle guidance. The strategy of orientating the needle such that it is parallel with the axis of the transducer is sub-optimal. The needle may be better visualized by calculating the needle trajectory, not simply based upon the shortest distance to the tumour, but at an angle that would provide a greater reflected signal. This strategy would result in a trade between improved needle visibility and increased tissue traversal.

Selection of the transducer type will determine how well the needle is visualized. A low frequency transducer allows better penetration of the tissue and will better depict the needle as it approaches the lesion from the contralateral side. The use of a compounding transducer, such as the SonoCT transducer [ATL Inc., Bothell, WA, USA] would provide a better depiction of the needle in the breast [17].

The ability to visualize adequately the needle may present a problem in real breast tissue. A better model of breast tissue using turkey breast as the body of the phantom can be used to test needle visualization [18]. With this model, the aforementioned approaches to improve needle visualization can be tested.

4.3.1.4 Lesion Visualization

The visualization of the lesion in US images may be a significant problem when applied clinically as indicated in Section 4.2.4. The lesion may be better visualized with proper selection of the transducer and with use of advanced US imaging functions. A higher frequency transducer may

allow visualization of subtle indicators that may help identify the lesion, such as hypoechoic regions or areas of shadowing [15]. The implementation of US imaging functionalities such as Doppler imaging will be discussed in Section 4.3.2 in order to detect lesions that are not evident due to their acoustical properties [6]. Another method that may have potential to improve the ability to identify the lesion in the US image involves investigating new ways in which the MR and US data can be combined.

The incorporation of the US and MR data has been presented in a relatively simple manner thus far. Positioning the cursor in the US image based upon the MR calculations was useful for identifying the lesion in the clinical case presented in Section 4.2.3. In that same case, the use of the MR image to guide the search for the lesion in the US image was performed retrospectively. The use of the oblique-coronal MR image to determine corresponding breast features requires some effort. The inversion of the grayscale in the US image aided in the identification of common MR and US features. This image modification may not be appropriate to the real-time US images therefore it may be more convenient to enhance the MR images to match the US data. Implementation of a technique that can merge the information pertaining to the position of the lesion and the surrounding landmark features of the breast in the US image would aid in lesion identification.

Consider the following strategy: The MRI data could be downloaded from the MR system database to a stand-alone PC after the MR imaging procedure has been completed. The MR data consists of MR images demonstrating the fat and fibroglandular tissue of the breast as shown in Figure 4.5 a), as well as the dynamic enhancement information as demonstrated in Figure 4.3 b). This data could be combined and reformatted to match the orientation of the US transducer. The reformatting technique could be linked with the encoder position of the US transducer and perform a reformatting calculation of the MR images. The two sets of MR data, registered to the position of the transducer would provide both architectural information and contrast enhancement information as demonstrated in Figure 4.7. Attempts could also be made to enhance the features of the MR image to match the US image, such as edge detection. Enhancement of the edges in the direction of the acoustical beam propagation corresponds to the US signal generated by the

reflections at interfaces between fat and fibroglandular tissue. The details pertaining to how this image reformatting and image enhancement would be implemented are not presented.
This image registration method would aid in the determination of the lesion position in the US images, as well as provide an interesting comparison to US blood flow imaging techniques. These techniques are discussed in detail in the following section.

4.3.2 Extension of Ultrasound Technology

The ability of US to image blood flow using Doppler imaging techniques has the potential to improve many aspects of the system. The ability to detect the lesion based upon blood flow signal will aid in obtaining accurate biopsy samples, improve the ability to determine whether the lesion is malignant or benign without biopsy, and provide a tool to examine the nature the microvasculature of these MRI detected lesions.

4.3.2.1 Doppler Ultrasound

Doppler US provides information about blood flow in a specified region. The technique is based upon the Doppler shift phenomenon in which flow information can be derived from the measured shift in frequency of an US wave reflected from a moving target. In most current US imaging systems this flow information is transposed onto the B-scan US image so that flow signal can be associated with anatomical structures. Doppler imaging has been successfully applied to clinical breast imaging in many different variations offering unique advantages [19].

The use of color Doppler (CD) and power Doppler (PD) has been used to visualize the neovascularization characteristic of malignancies in the breast. Color Doppler US, which is generally based on mean Doppler frequency shift, has demonstrated to be an effective technique to differentiate complex cysts from solid masses based upon the absence of flow signal [20]. Power Doppler US is a more sensitive technique for low flow signals in the breast and has gained popularity in breast applications. The use of power Doppler in some studies has shown overlap in the vascularity of malignant and benign lesions [21], while other groups have demonstrated 68%

sensitivity and 95% specificity using the presence of penetrating vessels as an indication for malignancy [22].

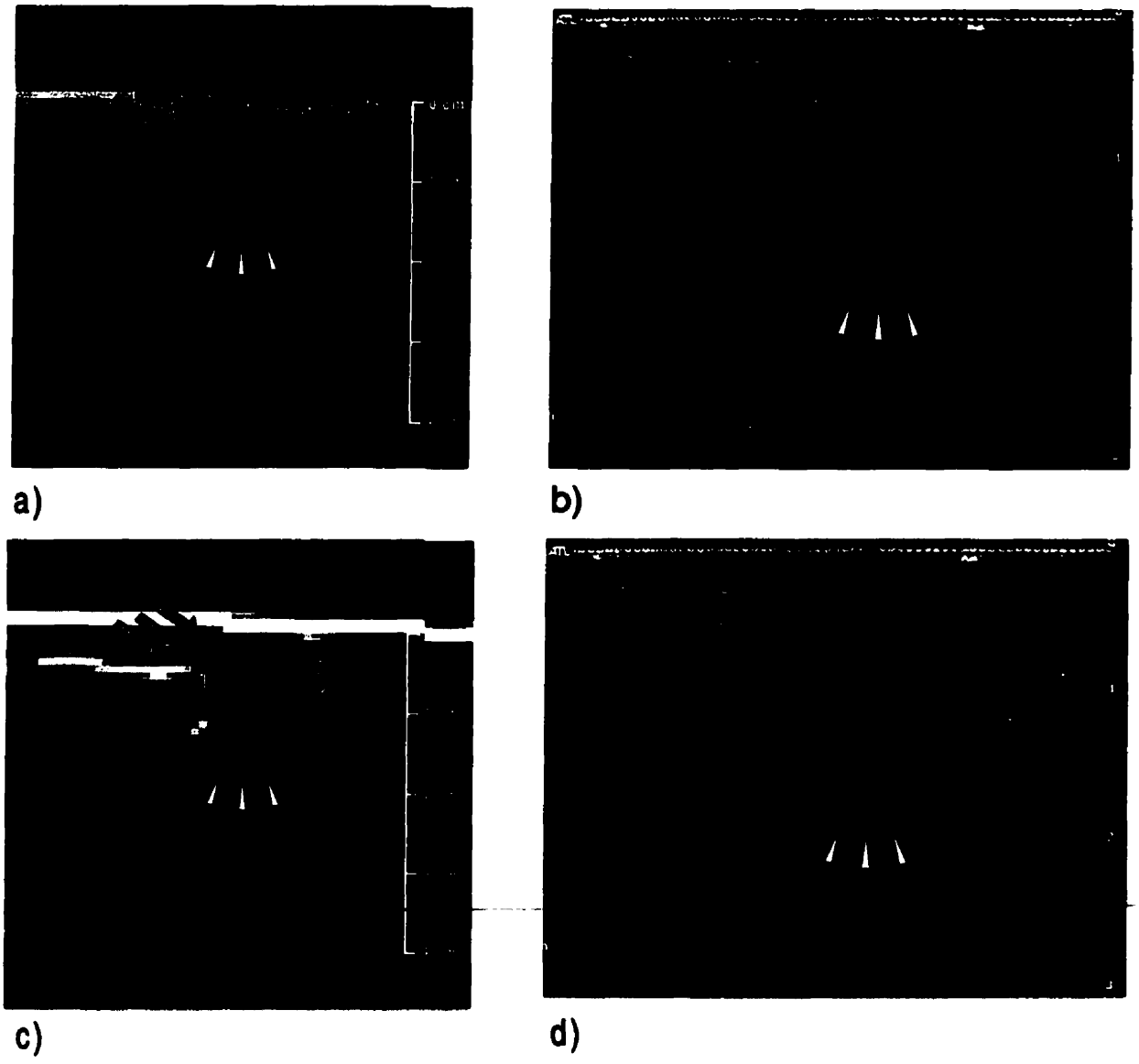

Figure 4.7: Various methods of MR and US Registration and depiction of lesion enhancement. a) Oblique-Coronal MR image corresponding to US transducer position in Figure b). This image is a spin-echo image that was shown previously, shown here only for comparison. b) US image with lesion depicted with white arrowheads. Two landmarks are defined in image a) and b) with a grouping of three arrows. c) The edge information from Figure a) has been enhanced, and the dynamic contrast-enhanced data has been superimposed (red). This image would depict the landmarks and the lesion in one image that would provide a better comparison to the US image. d) A simulation of what a power Doppler spectrum might look like in this case. The red depicts the blood flow that might be expected around the periphery of the lesion. A comparison of Figure c) and d) would provide a clinically useful representation of lesion enhancement and blood flow in the respective imaging modalities.

Power Doppler has also been shown to be effective technique to guide the biopsy of both in-situ and invasive breast tumours [23]. The application of Power Doppler to enhance visualization of the lesion for US guided biopsy in the context of this thesis may be appropriate. An example of how this might enhance visualization of the lesion in the clinical registration case is presented in Figure 4.7 d). Here we see the blood signal (red) overlaid on the grayscale B-scan image. If the lesion is not visualized in B-scan image based on the grayscale image then targeting the region of increased blow flow may result in an accurate biopsy. The use of the blood flow signal to detect the lesion is actually more closely related to how it would be detected in the screening protocol. The lesion is initially detected based upon the contrast enhancement in a dynamic MRI protocol, and it should follow that the US blood flow signal would be more indicative of lesion presence than the acoustical properties detected with B-scan grayscale US imaging.

4.3.2.2 Microbubble Contrast Agent

In some cases, the Doppler signals in lesions are difficult to detect either due to the small size of the tumour vessels, or the small Doppler shift [24]. Recently developed microbubble US contrast agents have been shown to enhance the echo strength in small vessels [25,26,27]. Intravenous injection of the contrast agent introduces microbubbles into the blood that act as scattering particles.

These contrast agents have been used to enhance lesion visualization in Power and Color Doppler ultrasound imaging. Substantial increases in sensitivity have been demonstrated in some of the available literature. One such clinical breast Power Doppler US study reported an increase in sensitivity from 36% to 95% after contrast agent injection [26]. The use of contrast agents in Color Doppler imaging has allowed improvements in the sensitivity and specificity of breast lesions by improved visualization of the vascular patterns and timing of the transit of the contrast bolus [25,26,27].

The ability of US to detect blood flow and corresponding use of contrast agents will no doubt improve the effectiveness of US detection and diagnosis of breast lesions. It seems reasonable that

these concepts can be used in conjunction with the hybrid biopsy technique presented in this thesis.

4.3.3 Further Extensions of System

4.3.3.1 Investigate Breast Tumour Microvasculature

The ability to register MR and US data accurately may act as a research tool enabling an accurate comparison of how these imaging modalities visualize the tumour microvasculature. The technique proposed in Section 4.3.1.4 that would merge the modified architectural and contrast enhancement imaging information on a single image registered to the corresponding US real-time image offers an interesting comparison to US Doppler imaging. The enhancement depicted in the MR image is primarily due to the permeability of the microvasculature, whereas the Doppler US with and without contrast agent, demonstrates lesion blood flow [3,6,28]. Characterizing MR and US contrast agent kinetics using enhancement curves is an active area of research [3,25,29]. A comparison of MR and US contrast enhancement curves for a lesion in the same conformation within the same clinical protocol can provide a novel tool to examine pharamcokinetics.

4.3.3.2 Placement of Surgical Markers

A hybrid guidance biopsy system may also be used in a slightly different manner. Instead of removal of a tissue sample, a small marker may be placed into the breast to define the centre and the extent of an MR detected tumour. If the marker is visible in another modality, such as US, then the possibility exists of using these markers as guides for surgical resection with intraoperative US guidance. This application would be a simple extension of the current biopsy platform.

4.3.3.3 Guidance for Minimally Invasive Therapies

The platform for delivery of a needle to a point in space can also be extended to therapeutic applications. Fiber optic lasers, radio frequency heating, or high frequency US probes that are used for tissue ablation could also be accurately positioned into an MR-detected tumour. Further applications involving complete removal of the cancerous tissue in sections or local injection of chemotherapeutic agents may also be considered. Placement of tissue ablation, tissue removal or chemical injection probes guided by MR and US, as presented in this thesis, allows the procedure to be done outside of the magnet room. Using US to monitor the procedure could result in substantial savings in the MR magnet costs associated with these procedures.

Whether the system presented in this thesis is used to guide biopsy needles accurately, provide insight into imaging of tumour microvasculature, or allow currently impractical minimally invasive therapies to be used clinically, it is clear that accurate image registration resulting in true hybrid imaging has the potential to improve breast cancer care.

References

1. Lufkin RB, ed. *Interventional MRI.* St.Louis:Mosby, **1999**:315-319.

2. Jolesz F. Interventional and Intraoperative MRI: A General Overview of the Field. JMRI 1998; 8, 3-6.

3. Kuhl CK. MRI of Breast Tumors (review article). European Radiology 2000; 10:46-58.

4. Jackson VP. Breast Sonography. *Breast Disease.* 10(3,4) (1998) pp. 55-66.

5. Zonderland HM, Coerkamp EG, Hermans J, et al. Diagnosis of Breast Cancer: Contribution of US as an Adjunct to Mammography. Radiology 1999; 213:413-422.

6. Rizzatto G, Chersevani R. Breast Ultrasound and new technologies. *European Journal of Radiology.* 1998; 27 S242-S249.

7. S Raza, J.K. Baum. Solid Breast Lesions: Evaluation with Power Doppler US. *Radiology.* 1997, 203:164-168.

8. Jolesz FA, Morrison PR, Koran SJ, et al. Compatible Instrumentation for Intraoperative MRI: Expanding Resources. JMRI 1998; 8:8-11.

9. Fisher PR, Problems and Pitfalls in Core Biopsy. in "A Comprehensive Approach to Stereotactic Breast Biopsy".(Fajardo LL Ed, Willison KM Ed.). Blackwell Science, Boston, 1996.

10. Foster SF, D'Astous FT. Frequency Dependence of Ultrasound Attenuation and Backscatter in Breast Tissue. *Ultrasound in Med & Biol.* Vol 12, No.10, pp. 795-808, 1986.

11. Wolbarst AB. Physics for Radiologists. Prentice Hall, Toronto, 1993.

12. Lockwood GF, Foster FS, Hunt JW. A Ray Tracing Method For Calculating The Speed of Sound in a Nonparallel Layered Model Using Pulse Echo Ultrasound. *Ultrasonic Imaging.* Vol 11, pp 106-118, 1989.

13. Kishell EK, Foster FS, Connor T, Khodai M, Harasciewicz, Hunt JW. Clinical Performance of a Cone/Annular Array Ultrasound Breast Scanner. *Ultrasound in Med & Biol.* Vol 16, No.4, pp. 361-374, 1990.

14. Stravos TA, Thickman D, Rapp CL, Dennis MA, Parker SH, Sisney GA. Solid Breast Nodules: *Radiology* 1995; 196:123-134

15. Sumanaweera T, Glover G, Song S, Adler J, Napel S. Quantifying MRI Geometric Distortion

in Tissue. MRM 1994; 31:40-47.

16. Langlois S, Desvignes M, Constans JM, Revenu M. MRI Geometric Distortion: A Simple Approach to Correcting the Effects of Non-Linear Gradient Fields. JMRI 1999; 9:821-831.

17. SonoCT case studies at web address http://www.atl.com/ATLSonoCT/sonoctcasestudies/sp_breast.asp.

18. Beese RC, Lowe S. The use of turkey breast and stuffed olives as a soft tissue model for the teaching and practice of ultrasound guided interventional procedures. *European Journal of Ultrasound*, Volume: 7, Supplement 1, February, 1998, pp. S12.

19. Rumack CM, Wilson SR, Charboneau JW. Diagnostic Ultrasound. Volume 1, Second edition, 1998, Mosbey-Year book, St. Louis Missouri.

20. Fornage BD. Role of Color Doppler imaging in differentiating between psuedocystic malignant tumors and fluid collections. J Ultrasound Med 1995; 14:125-128.

21. Birdwell RL, Ikeda Dm, et al. Preliminary experience with Power Doppler imaging of solid breast masses. AJR 1997; 169:703-707.

22. S Raza, J.K. Baum. Solid Breast Lesions: Evaluation with Power Doppler US. *Radiology*. 1997, 203:164-168.

23. W.L. Teh, A.R.M. Wilson, A.J. Evans, H. Burrell, S.E. Pinder, I.O. Ellis. Ultrasound Guided Core Biopsy of Suspicious Mammographic Calcifications Using High Frequency and Power Doppler Ultrasound. Clinical Radiology. 2000; 55, 390-394.

24. Rumack CM, Wilson SR, Charboneau JW. Diagnostic Ultrasound. Volume 1, Second edition, 1998, Mosbey-Year book, St. Louis Missouri.

25. S. Huber, T. Helbich, J. Kettenbach, W. Dock, I. Zuna, S. Delorme. Effects of a Microbubble Contrast Agent on Breast Tumors: Computer-assisted Quantitative Assessment with Color Doppler US-Early Experience. Radiology. 1998; 208:485-489.

26. W.K. Moon, J.G. Im, D Noh, M C Han. Nonpalpable Breast Lesions: Evaluation with Power Doppler US and a Microbubble Contrast Agent – Initial Experience. *Radiology*. 2000; 217:240-246.

27. R.P. Kedar, D. Cosgrove, V.R. McCready, J.C. Bamber, E.R. Carter, Microbubble Contrast Agent for Color Doppler US: Effect on Breast Masses. *Radiology*. 1996; 198:679-686.

28. Buadu LD, Murakami J, Murayama S, et al. Breast Lesions: Correlation of Contrast Medium Enhancement Patterns on MR Images with Histopathologic Findings and Tumor Angiogenesis. Radiology 1996; 200:639-649.

29. Kuhl CK, Mielcareck P, Klaschik S, et al. Dynamic Breast MR Imaging: Are signal intensity time course date useful for differential diagnosis of enhancing lesions? Radiology 1999; 211:101-110.